Published in final edited form as:
Compr Physiol. ; 2: 675–709. doi:10.1002/cphy.c100081.

Structure and composition of pulmonary arteries, capillaries and veins

Mary I. Townsley
Departments of Physiology and Medicine and Center for Lung Biology University of South Alabama Mobile, Alabama 36688

Abstract

The pulmonary vasculature is comprised of three anatomic compartments connected in series: the arterial tree, an extensive capillary bed, and the venular tree. Although in general this vasculature is thin-walled, structure is nonetheless complex. Contributions to structure (and thus potentially to function) from cells other than endothelial and smooth muscle cells as well as those from the extracellular matrix should be considered. This review is multifaceted, bringing together information regarding 1) classification of pulmonary vessels, 2) branching geometry in the pulmonary vascular tree, 3) a quantitative view of structure based on morphometry of the vascular wall, 4) the relationship of nerves, a variety of interstitial cells, matrix proteins, and striated myocytes to smooth muscle and endothelium in the vascular wall, 5) heterogeneity within cell populations and between vascular compartments, 6) homo- and heterotypic cell-cell junctional complexes, and 7) the relation of the pulmonary vasculature to that of airways. These issues for pulmonary vascular structure are compared, when data is available, across species from human to mouse and shrew. Data from studies utilizing vascular casting, light and electron microscopy, as well as models developed from those data, are discussed. Finally, the need for rigorous quantitative approaches to study of vascular structure in lung is highlighted.

Keywords

pulmonary circulation; pulmonary endothelium; microcirculation; vascular smooth muscle; extracellular matrix

The architecture of the normal pulmonary vasculature is engineered to ensure a high compliance, low resistance network that provides an extensive surface area for gas exchange. As in systemic vascular beds, the pulmonary vasculature is composed of three vascular compartments connected in series: arteries, capillaries and veins. Rather than define pulmonary conduit or microvessels based on an arbitrary selection of diameter ranges, extra-alveolar arteries or veins are subclassified based on structural features such as the presence and number of elastic lamina and the degree of muscularity (58, 115). The relationship of the pulmonary vasculature to surrounding lung tissue provides additional context for compartmentalization. Pulmonary vessels can be divided into 1) those external to (pre-acinar) vs those within the respiratory acinus of the lung (intra-acinar), 2) those external to (extra-alveolar) vs those within the alveolar compartment, and 3) those upstream of (pre-capillary) vs those distal to the alveolar capillary bed (post-capillary). Intra-acinar vessels are associated with respiratory bronchioles, alveolar ducts and alveolar walls, i.e., airways involved in gas exchange. Extra-alveolar vessels are tethered to lung parenchyma and

Correspondence to: Mary I. Townsley.
Contact Information Phone: 251-460-6815 mtownsley@southalabama.edu.

distend and/or lengthen with lung inflation (48, 173). In contrast, the diameter of capillaries that populate the alveolar septal walls tends to decrease with lung inflation (37, 94, 183).

Morphometric approaches have been used to quantitate the fraction of overall anatomic lung volume (which includes lung tissue, intravascular volume and intra-airway volume) which can be defined as either parenchyma or non-parenchyma (124). The parenchyma includes vessels < 20-25 μm in diameter, predominantly capillaries, whereas non-parenchymal structures include vessels and airways which exceed 20-25 μm in diameter. On average parenchyma comprises 84% of lung anatomic volume (range 77-87%) (84, 87, 125, 175, 244, 245, 300, 343), leaving a relatively small fraction of lung volume for extra-alveolar structures, including extra-alveolar blood vessels. The proportion of parenchyma appears to be well conserved, from 85% in human lung (84) to 86% in mouse lung (87). The walls of extra-alveolar vessels comprise only ~15 % of total non-parenchymal volume, whereas the vascular lumen and other structures such as airways contribute 41 and 44%, respectively (351). Cells in the alveolar septal wall contribute only 5% to parenchymal volume (300), the remainder comprised of air and blood volume.

Despite the relatively thin wall in the adult pulmonary vasculature, structure can nonetheless be complex. Vascular smooth muscle cells, various other contractile cells including fibroblasts, intermediate cells, pericytes, and striated cardiac myocytes (in some species), endothelium, nerves, mast cells, and interstitial macrophages populate the vascular wall to varying degrees in each compartment. The interstitial matrix includes collagens and elastin as the predominant non-cellular structural elements, as well as fibronectin, glycosaminoglycans and proteoglycans. Airway and alveolar epithelial cells are clearly not components of the pulmonary circulation per se. Nonetheless, proximity of the vasculature to the epithelium in terminal airways and alveoli set the stage for potential crosstalk that might impact vascular function. This review will focus on the structure and ultrastructure of the pulmonary vasculature in mature mammals, with perspective on the comparative aspects of structure and on heterogeneity in structure between compartments.

Arteries

On entering the lung, the major conduit arteries and their paired airways course through the center of the lobe from the hilus to the pleural surface. The bronchovascular bundles coursing along this axial pathway are typically constrained by a common adventitial sheath (133, 187, 202). In cow, pig, and sheep lung, the bronchovascular bundle includes pulmonary veins (152, 186, 187, 203, 254). In contrast, in smaller mammals - monkey, dog, cat, rabbit, guinea pig and rat - pulmonary veins follow a course independent of the airway-artery bundle (186, 187). In both horse and human lung, a mixed pattern is evident. In the distal lung, pulmonary arteries, airways and veins form a common bundle in these species, while in more proximal lung regions pulmonary veins diverge from the airway-artery bundle to take a separate path to the hilus (186, 187). Lymphatic vessels, which lie within the adventitial sheaths of bronchovascular bundles, are easily apparent when the adventitial interstitium is expanded with edema fluid (8, 271).

Branching in the arterial tree

The conventional axial pathway of the pulmonary arterial tree courses from the lung hilus to the peripheral lung pleural border. Conventional branches leave the parent arterial segment of the axial path at an oblique angle coincident with airway branching. In addition to this conventional pathway, supernumerary arteries exit the parent pulmonary artery at a 90-degree angle, unaccompanied by an airway branch (58, 67, 115, 119, 250, 275). The diameter of these supernumerary branches can be quite small compared to that of the parent pulmonary artery. In rat lung, supernumerary arteries frequently are ~1/10th the diameter of

the parent conventional artery (115). Though there is some species-dependent variation, the number of supernumerary vessels tends to increase as the arterial tree branches into the respiratory acinus (58, 67, 115, 250, 275). In the pre-lobular region of the human lung, Reid reported 1.4-fold more supernumerary arteries than conventional arteries. However, within the respiratory acinus, the ratio rises to nearly 4 (250). Although Hislop and Reid noted a nearly one-to-one ratio for the total number of supernumerary and conventional arteries along the axial pathway in rat lung, more of the supernumerary arteries clustered toward the distal end of the axial pathway (115). In bovine lung, Shaw and colleagues identified 6-8 supernumerary arteries for each conventional artery near the hilus, with a slight increase towards the lung periphery (275). The large number of supernumerary arteries in this species was attributed to the degree of lobulation. Additional considerations include differences in lung mass and resultant differences in the length of the axial pathway: 15-20 cm in bovine lung vs 4 cm in rat lung (150).

The ordered branching of the pulmonary arterial tree has been extensively studied in human lung, as well as in other mammalian species. The most common approach has utilized vascular casts (80, 119, 127, 135, 176, 286, 346, 348). However, x-ray contrast arteriograms (75, 121) and more recently computed tomography (27, 150, 212) have been employed. Extensive vascular branching, with contributions from both conventional and supernumerary branches, leads to the three-dimensional space-filling pattern observed with contrast arteriograms and via other imaging modalities. **Figure 1** shows x-ray images of the barium gelatin-filled pulmonary arterial vasculature in human, pig and rat lung (141, 252, 254). Although the axial pulmonary arteries are evident in these images, the borders of larger arteries can be obscured by background haze due to extensive filling of small peripheral branches that are < 200 μm (141). Similar three-dimensional space-filling images have been obtained from computed tomography of human, rat and mouse lung (27, 149, 150, 259).

To investigate the ordered branching of the pulmonary arterial (or venous) tree in a quantitative fashion, the whole of the network is considered as a confluent system of vessels categorized by orders (counting from the lung periphery) or generations (counting from the lung hilus) (118). One key difference in outcomes between these two strategies arises from the fact that the diameter of supernumerary arteries can be substantially smaller than that of the parent conventional artery segment, even in pre-acinar segments of the arterial tree. As a result, pulmonary artery branches of any given diameter, e.g., 50 μm branches, can be distributed over a wide range of generations. As a result of this asymmetry in branching in the pulmonary vascular tree, the use of orders rather than generations is particularly applicable (118).

Strahler ordering begins with the smallest distal extra-alveolar branches. Order number increases when two branches of the same order meet. Using a Strahler ordering system, Singhal *et al.* and Horsfield evaluated resin casts of the proximal and distal pulmonary vasculature in human lung (119, 286). The integrated data from these studies (119) suggests that the human pulmonary arterial tree is comprised of 17 branch orders, from the main pulmonary artery (order 17) with a diameter of ~ 30 mm to more than 72 million order 1 arteries which range in diameter from 10-15 μm. In a subsequent study Huang *et al.* evaluated casts of two human lungs using a diameter-modified Strahler ordering system. In contrast to the ordering utilized by Horsfield and colleagues, the diameter-modified system adds an additional rule. When two branches of the same order meet, order number increases only if the diameter of the proximal parent segment exceeds that of either distal branch by a specified fractional amount. The resulting data from this study documents 15 orders in the pulmonary arterial tree. Order 1 arteries have an average diameter of 20 μm, whereas the diameter of order 15 pulmonary arteries (average 14.8 mm) is similar to that of order 16 pulmonary arteries in Horsfield's study (127). A summary of the data regarding branching in

the pulmonary arterial (and venous) vascular tree is provided in **Table 1**. In contrast to the 15-17 orders of pulmonary artery branches in human lung, in smaller mammals such as dog, cat or rat, the pulmonary arterial tree is comprised of only 11-12 orders (80, 127, 135, 348). As would be expected, the number of distal order 1 branches decreases with body mass. For example, in dog and rat lung the number of order 1 branches is estimated to be ~1 and 3 log orders less, respectively, than that in human lung. Regardless, the diameter of these distal pre-capillary order 1 branches is remarkably similar from human to rat lung. The use of generations to evaluate branching yields substantially different results. For example, 22 generations of pulmonary arteries have been identified in pig lung. The average diameter (0.85 ± 0.29 mm) and length (4.5 ± 3.6 mm) of generation 21 arteries in pig lung (mean ± SD) (176) are roughly equivalent to average data for order 10 arteries in human lung (119, 286). However, the large variance in these measures for any generation highlights the limitation in using such data to elucidate geometric patterning in the arterial tree.

Overall, there is significant diversity among species with respect to the absolute diameter of hilar pulmonary arteries, the number of Strahler orders, and the number of terminal order 1 branches predicted by Strahler ordering (**Table 1**). Nonetheless, the aggregate data obtained from analyses of branching orders yield additional information that demonstrate the remarkable preservation of some features in arterial branching patterns. For example, the log-linear plot of mean diameter for any order relative to order number produces a linear relationship, where the antilog of the slope defines the diameter ratio. In essence this term predicts the average proportional increase in vessel diameter moving from one distal order to the next order up the arterial tree. Despite the markedly different lung mass in human, compared to smaller mammals, the diameter ratio is fairly well preserved from human lung to pig, dog, cat and rat lung. Across these species, the diameter ratio averages 1.65 ± 0.11 (mean ± SD), which means that on average arterial diameter increases 65% with each new branch order. A similar strategy can be used to determine length and branching ratios, which average 1.58 ± 0.14 and 3.43 ± 0.26, respectively. These data predict that the length of arterial segments increases nearly 60% with each successive order. In contrast, the number of branches increases more than 3-fold with each successive order moving from the hilus to the lung periphery.

The adventitia of the arterial wall

The adventitial surface of vessels in the bronchovascular bundle is tethered to the surface of the adjacent airway on one face and to alveolar septal networks on other aspects. **Figure 2** illustrates these relationships in pulmonary arteries from human and rat lung. In larger pre-acinar arteries, the volume of tissue in the interface between the airway and the artery, including submucosal glands (see **Figure 2A**, human lung), the bronchial vasculature and lymphatics, tends to uncouple these conducting airways and vessels from mechanical distending forces exerted by lung parenchyma during lung expansion (323). However, in smaller intra-acinar extra-alveolar arteries (and veins), where more of the artery circumference is tethered to alveolar septal walls and adventitial volume is decreased (**Figure 2B**, rat lung), there is more effective mechanical coupling of arteries to the distal lung parenchyma. As a result of such tethering, intra-acinar extra-alveolar arteries (and veins) distend and/or lengthen with lung inflation (48, 145, 173). Electron micrographs of distal pulmonary arteries from rat and mouse lung (**Figure 3**) effectively highlight the close apposition of the arterial adventitia to the airway epithelium in more distal arteries. The pulmonary artery from rat lung shown in **Figure 3A** is of comparable caliber to that shown in the light micrograph in **Figure 2B**, with multiple smooth muscle cell layers in the media. Note that the adventitial structure in this artery, with matrix fibers, fibroblasts and innervation, appears to be shared between this part of the artery perimeter and the adjacent airway. The accompanying image from a more distal artery in mouse lung shows that the

basal aspect of the airway epithelial layer may be only a few microns distant from the media or vascular endothelium in the wall of some intra-acinar arteries (**Figure 3B**).

In general, the adventitia of pulmonary arteries is loosely organized, comprised of extracellular matrix, fibroblasts or other interstitial cells, a vasa vasorum, and a neuronal network. In rat lung, the vasa vasorum may extend to arteries as small as 100 μm in diameter (187, 228). Both elastin and collagen fiber bundles can be observed in the arterial adventitia (**Figure 3A**). Via light or transmission microscopy, elastin fibers in the wall of extra-alveolar vessels appear to be unrelated to elastin networks in the distal alveolar compartment. However, recent work from Toshima and colleagues provides a different perspective (308). These investigators utilized selective maceration of fixed human and rat lung, along with scanning electron microscopy to visualize the elastin and collagen fiber networks in human lung. Elastic fibers in the outermost lamina of small vessels of human lung are seen to be continuous with elastin fibers in alveolar septal walls (**Figure 4**). This network, along with a similarly interconnected network for collagen (not shown), continues through to the pleural surface. This continuum in the fiber matrix scaffold of the lung contributes to overall stability of the distal lung, as well as to functional mechanical coupling of parenchymal volume to extra-alveolar vessel diameter (48, 145, 173, 336).

Fibroblasts that sparsely populate the adventitia of pulmonary arteries (50, 195, 196, 200, 202) play an important role in fibrogenesis. These interstitial cells contribute to the synthesis of interstitial matrix molecules including collagens, fibronectin and proteoglycans, and appear to remain associated with the fiber matrix in the arterial wall (336). Although fibroblasts play an important role in elastin synthesis during lung development, it is not clear that the capacity for elastogenesis is retained by fibroblasts in the adult lung (61, 336). Using the accumulation of D-aspartate and carbon dating, Shapiro and colleagues concluded that the elastin network of human lung parenchyma is metabolically stable: the inferred age of lung elastin correlated well with the age of the subject (274). Mackay *et al.* reported an extensive analysis of collagen and elastin content in extralobar pulmonary arteries from autopsy specimens of human lung. In young adults, hydroxyproline content (reflectively primarily of collagen, but inclusive of some elastin content) represented ~40% of the total dry weight (172). Based on histologic measures in young adults, collagen was found to occupy ~16% of the artery wall, decreasing to ~10% in arteries from individuals > 80 years of age. In contrast, elastin content in the arterial wall does not change over the same time span, a result consistent with the elastin stability documented by Shapiro and colleagues. Nonetheless, the distensibility of the pulmonary artery in human lung does decrease with age (28). In contrast to the relative stability of the elastin network, the collagen fiber network in lung is much more dynamic. In rabbit lung, 5-9% of lung collagen is newly synthesized each day (20, 166), and further, ~50-60% of that newly synthesized collagen is incorporated into the collagen fibrillar network (20, 165, 185). In rat lung, the overall collagen synthesis rate decreases rather dramatically with age, from 13% at one month of age to 1% per day at 24 months. In contrast, the rate of degradation of newly synthesized collagen increases from 28% to 62% over the same time frame (182). While these values are based on collagen synthesis and turnover for the lung as a whole, regular turnover in collagen content of the vascular wall is likely as well. Total collagens, including the major fibrillar collagens types I and III, contribute ~15-20% to total dry mass in human lung (31, 165, 306). Morphometric measures of collagen content, assessed as a volume fraction or percentage of total wall area, range from 15-45% in the main pulmonary artery of human and rat lung (15, 199, 261). Several excellent reviews provide much more detail regarding the biochemistry of extracellular matrix in blood vessels and the lung (31, 49, 61, 324).

Fibroblasts are stellate cells that possess a prominent nucleus, well-developed Golgi and rough endoplasmic reticulum, and multiple long, thin cytoplasmic extensions (333). The

diameter at the nucleus averages ~2.8 μm, while cell volume of fibroblasts has been estimated at 1600 μm^3 (196, 336). In rat hilar pulmonary arteries, fibroblasts have been variously reported to appear with a frequency of 2-17 per 100 μm length (195, 196). Mast cells, with characteristic basophilic cytoplasmic granules, can also be found in the adventitia and/or perivascular space surrounding pulmonary arteries. Mast cell granules store numerous mediators, including proteases, proteoglycans, and chemotactic factors, to name a few (339). Mast cells are characterized in part by expression of either tryptase (mucosal mast cells) or both tryptase and chymase (connective tissue mast cells). Although the mucosal type dominates in most of the human lung, extra-alveolar vessels have both mucosal and connective tissue types in a 1:1 or 2:1 ratio (10, 11). In the main pulmonary artery in rat, mast cells represent only ~1% of total cell number (312). The density of perivascular mast cells in small pulmonary arteries (< 260 μm) is not consistent across species. The density is highest in dog and guinea pig lung (5-7/mm^2), less in pig, calf and sheep lung (2-3/mm^2), and least in rat lung (0.2-1.5/mm^2) (211, 314).

Innervation—Innervation to the pulmonary vasculature is predominantly derived from branches originating in the vagus and cervicothoracic sympathetic nerves, including adrenergic, cholinergic and sensory fibers. The pulmonary trunk receives innervation from the right cardiac recurrent nerve, with branches forming an adventitial nerve plexus (321). An extensive neural plexus at the lung hilus contains parasympathetic ganglia and postganglionic sympathetic fibers derived from thoracic sympathetic ganglia (14). Fibers project from this perihilar nerve plexus to form an adventitial perivascular nerve network, in which the more superficial fibers contain several axons and are wrapped in Schwann cells (14, 163, 257, 293). Deeper in the adventitia and at the adventitia-media border, networks are often comprised of single fibers with periodic varicosities (257, 321). In some species, including pig, dog, cat and rat, occasional fibers penetrate into the media of the artery wall (64, 70, 144, 158, 178). Though innervation density can vary substantially among species, in general adrenergic innervation is more extensive than cholinergic fiber density (14).

Neuronal fibers in the pulmonary vasculature have been characterized using light microscopy and immunostaining, as well as by electron microscopy. Adrenergic fibers are identified by expression of enzymes required by norepinephrine (NE) synthesis, including tyrosine hydroxylase (TH) and dopamine-β- hydroxylase (DβH) (7, 99, 171, 178). Similarly, expression of choline acetyltransferase (ChAT, required for acetylcholine synthesis), the vesicular acetylcholine transporter (VAChT), or acetylcholinesterase (AChase) which degrades acetylcholine have all been used in immunostaining strategies to identify cholinergic neurons in pulmonary arteries (65, 99, 158, 327). While identification of expression in neurons is based not only on positive staining but also on cell morphology, it is also important to note that ACh and ChAT can be synthesized in non-neuronal cells (243, 340). Thus, use of probes for the vesicular transporter VAChT may yield more specific information regarding cholinergic innervation (243).

In addition to norepinephrine and acetylcholine, neuronal fibers in the pulmonary arteries express an array of neuropeptides, including neuropeptide Y (NPY), vasoactive intestinal peptide (VIP), substance P (SP), and calcitonin gene related peptide (CGRP). In some cases, neuropeptides are co-expressed in postganglionic autonomic fibers with NE or ACH (e.g., NPY and VIP, respectively), while others are expressed in sensory neurons (24, 90, 258, 316). Some neurons in lung expressing CGRP have been definitively shown by retrograde dye transfer to be sensory afferent fibers (237). However not all CGRP neurons may be sensory in nature. Nohr *et al.* found that CGRP and SP were frequently co-expressed with neuronal ChAT in monkey lungs (222), and suggested the possibility that these neuropeptides might modulate cholinergic transmission. A final player in neurotransmission

is the relatively new candidate nitric oxide generated from neuronal nitric oxide synthase. The synthase is commonly detected by NADPH diaphorase immunoreactivity (96, 316).

Ultrastructural characteristics, i.e., the size, granularity and electron density of vesicles within axonal varicosities and terminals, have been used in the identification of nerve fibers (22, 70, 71, 73, 128, 158, 197, 198). Adrenergic fibers possess both large and small dense core vesicles, containing chromogranins and neuropeptide Y, while the latter contain norepinephrine and ATP. In cholinergic fibers, the majority of vesicles are agranular, though a few large granular vesicles may be found. However, cholinergic fibers and those of the non-adrenergic non-cholinergic system may be difficult to discriminate on an ultrastructural basis (89). The autonomic neuroeffector junction and general features of autonomic neuropeptides in the vasculature have been recently reviewed (23, 90).

Given this background, innervation in the pulmonary vasculature can be put into context. Pulmonary arteries display considerable diversity in the pattern and type of innervation, depending upon the species, and in some cases, artery size. Autonomic fibers, either adrenergic or cholinergic in nature, are common. Adrenergic innervation of pulmonary arteries has been documented in human, monkey, pig, guinea pig, ferret, and rat lung (7, 64, 99, 171, 178, 256). Cholinergic innervation of pulmonary arteries has also been documented in cat, rabbit, and guinea pig lung (65, 99, 158). Allen *et al.* (7) found expression of TH as well as NPY in proximal pulmonary arteries in human lung, indicative of sympathetic adrenergic innervation. Often the distribution is limited to varicosities through the adventitia. In dog, monkey and rat lung, the neural network is particularly dense at pulmonary artery branch points (64, 70). In small pulmonary arteries, VIP is expressed in addition to TH and NPY. Sheppard *et al.* (277) similarly found NPY expressed within fine varicosities, although this transmitter is limited to the adventitia of pulmonary arteries in human lung. In rat and monkey lung, utilizing a fluorescent histochemical method, El-Bermani *et al.* (64) found adrenergic neurons to form varicose plexes in the arterial wall adventitia which penetrated into the media. Other studies in rat lung have reported sparse adrenergic innervation, characterized by non-varicose fibers in the adventitia, with varicose plexes extending into the media (64). In Wistar rats, Ricci *et al.* (256) found sparse varicose networks of adrenergic neurons in the adventitia of pulmonary arteries, particularly around the vasa vasorum, while fibers entering the media were rare.

Muscular and partially muscular arteries maintain significant innervation, even within the respiratory acinus. In human lung, small bundles of non-myelinated axons wrapped in a Schwann cell coat can be observed at the border between the media and adventitia (201, 293). Varicosities contain agranular, and dense core vesicles, ranging in size from 50-75 nm (201). This neural network extends to small intra-acinar pulmonary arteries (293), and thus can be observed in the adventitial cuff of small pulmonary arteries near the insertion of alveolar septal walls (201). Haberberger and colleagues (99) conducted a broad survey in guinea pig lung, assessing innervation according to vessel diameter and neurotransmitter type. These data support the maintenance of cholinergic (ChAT) and adrenergic (TH) neurons, as well as those expressing substance P, quite distal into the pulmonary arterial tree, to arteries as small as 50 μm in diameter. In contrast, neurons expressing NADPH diaphorase (a neuronal nitric oxide synthase) were predominantly observed in more proximal arteries > 350 μm in diameter. In addition to autonomic innervation, blood vessels in the lung are innervated by other neurons expressing neuropeptides typical of the non-adrenergic non-cholinergic system. In addition to substance P, blood vessels in lung express neuropeptide Y, vasoactive intestinal peptide, and calcitonin gene related peptide with moderate frequency (316). Coexpression of neuropeptide Y and vasoactive intestinal peptide with small molecular weight amine transmitters in sympathetic and cholinergic neurons is common. The appearance of substance P and calcitonin gene related peptide are indicative

of sensory neurons present in the vascular wall (316). In some cases, nerves can be observed within the adventitia distally to the alveolar septal capillary wall (71, 73, 334), though in part these nerves may be sensory in nature (197). Nerves expressing tyrosine hydroxylase indicative of sympathetic adrenergic fibers, as well as those expressing neuropeptide Y and more rarely substance P, can be observed in pulmonary arteries at the level of the alveolar duct (7).

The arterial media

The composition of the wall, as well as the contribution of each layer to total wall thickness, varies from the proximal pulmonary artery trunk to the smallest extra-alveolar arteries. However, classification of pulmonary arteries is based on two characteristics of the medial layer: the presence of elastic lamina and the degree of muscularity. Thus, arteries are identified as elastic, transitional (with features of both elastic and muscular arteries), muscular, partially-muscular or non-muscular arteries. In elastic arteries, numerous elastic lamina are interspersed throughout the media of the vessel wall. The largest conduit pulmonary arteries in humans or dogs are the predominant elastic arteries in these species (202). In the main pulmonary artery trunk of adults living at sea level, elastic lamina are not aligned in parallel, nor are the lamina of uniform thickness as in the aorta (112). Rather, elastin fibers are short, relatively thin and interspersed with collagen and smooth muscle cells (**Figure 5**). Smaller elastin fibers branch to interconnect larger lamina organized around the circumference of the media (105, 263). In lung of adult humans, for example, pulmonary arteries down to ~ 2 mm in diameter possess 4 or more clear elastic lamina (**Figure 5A**). Note that since discontinuities appear, the elastic lamina do not form complete bounding layers. Elliott and Reid reported that elastic pulmonary arteries are found from the main pulmonary artery trunk through the proximal half of the axial arterial pathway (67, 250). In contrast, in rat lung even the main pulmonary artery trunk has only 1-3 elastic lamina, that average 0.57 ± 0.57 μm in thickness (196). Based on the few number of lamina, the main pulmonary artery in rat should be considered a muscular artery (115, 194). Overall, elastin contributes 24 ± 5% and 15 ± 1% to total wall area in the main pulmonary artery in human and rat lung, respectively (15, 261). In the hilar pulmonary arteries, medial thickness can range between 380 – 630 μm in human lung vs < 20 μm in rat lung (132, 172). The relative volume of smooth muscle within the media of elastic arteries is highlighted by that occupied by α-smooth muscle actin-positive cells (Figure 5B). However, significant extracellular matrix, including elastin and collagen separates bundles of smooth muscle cells in the media of these hilar arteries; collagen deposition is shown in Figure 5C. In contrast to the loosely organized elastic lamina in adults, the aortic type of lamellar structure is found in the pulmonary artery trunk in individuals less than 9 years of age (263). However, in high altitude natives the aortic type of lamellar structure persists in adults (28, 264). Similar organization is observed in yaks and llamas adapted to high altitude (62, 111).

Larger elastic pulmonary arteries in which the media is comprised of multiple layers of elastic lamina and smooth muscle cells gradually give rise to smaller muscular arteries. As diameter decreases, the media becomes more clearly delineated by single internal and external elastic lamina. In human and rat pulmonary arteries less than 1 mm in diameter, single internal and external laminae are apparent (115). In small distal pulmonary arteries, the lamina may begin to further fragment and may eventually disappear. In rat distal pulmonary arteries, the internal elastic lamina fragments (50), while the external lamina is lost in rabbit pulmonary arteries (301). Throughout much of the pulmonary arterial tree, the internal elastic lamina is characterized by frequent gaps, which enable endothelial projections into the media and facilitate myo-endothelial communication (50, 103, 133). Gap frequency is not constant however. In human lung, an average of 3.2 gaps are observed

per 100 μm length of the internal lamina in arteries > 100 μm in diameter. This number nearly doubles in arteries < 100 μm in diameter, where 5.6 gaps/100 μm are found (5).

The contribution of the media to wall thickness, as well as the distribution of muscular, partially muscular and non-muscular arteries within the respiratory acinus, is compared in **Table 2**. The data shown include two related measures commonly utilized to characterize medial thickness: the absolute thickness and the % medial thickness. The latter is calculated as [(2 × medial thickness) × 100/external diameter]. Additional data regarding medial thickness for pre-acinar vessels is provided for comparison. In aggregate, these data illustrate a key message, i.e., that the measure of medial thickness in any one sized artery depends upon the experimental techniques used for lung fixation. One technique, instillation of barium gelatin into the pulmonary arterial tree under a fixed pressure, followed by airway fixation, yields a standardized approach to morphometric assessment of the pulmonary arterial wall. A further benefit is that since the gelatin does not penetrate into the alveolar capillary network, small pulmonary arteries can be readily differentiated from small veins in the distal acinus. With such methodology, medial thickness of large arteries in rat, macaque, dog, pig and human lung ranges between 1-3% of external diameter, increasing to ~5-10% in smaller arteries with external diameter less than 100 microns (52, 115, 254, 276, 285). However, this consistent proximal-to-distal decrement in medial thickness is absent in lungs fixed by immersion or by airway instillation of fixative (but without gelatin in the vasculature). As a result, the % medial thickness measured with these preparations varies little between large and small arteries (see **Table 2**) and exceeds that measured when gelatin infusion is included in the preparation (227). Data varies regarding the contribution of muscular pulmonary arteries to total artery number within the respiratory acinus in human lung. Based on measurements provided by Snow and colleagues, ~10% of intra-acinar pulmonary arteries are completely muscular (289). In contrast, Haworth and Hislop reported that in adolescents, ~73% of pulmonary arteries adjacent to alveolar ducts are completely muscular (108). More quantitative data are available for other species. For example, in sheep, 39 to 56 % of arteries adjacent to respiratory bronchioles are muscular (193, 235). In rat the frequency with which muscular arteries are found adjacent to respiratory bronchioles is substantially less, ranging from 4-10% in most reports (2, 115, 140). Muscular arteries can be found as far distal as the alveolar wall in the dog, rabbit and rat lung, albeit with low frequency (52, 132, 204, 227).

As the arterial tree branches into the respiratory acinus, partially muscular and non-muscular arteries appear adjacent to respiratory bronchioles and alveolar ducts. In partially muscular arteries, smooth muscle cells do not provide complete coverage around the circumference of the vessel wall. Further, the vascular smooth muscle cells begin to give way to intermediate cells and pericytes. The gradual loss of musculature along the pulmonary vascular tree is shown conceptually in **Figure 6** (252). In human lung, partially muscular arteries can be found over a wide range of diameters, from 35 to 228 μm. Non-muscular arteries in human lung may be as large as ~120 μm in diameter (276). Further diversity is apparent when assessing the diameter of pulmonary arteries at one location in the arterial tree. For example, in canine lung, non-muscular arteries ranging from 100- 200 μm in diameter may be found, albeit infrequently, adjacent to alveolar ducts (202). At the level of the alveolar duct in dog or rat lung, 10-26% of arteries are partially muscular (52, 115). While medial thickness is often assessed by evaluating short-axis cross sections of pulmonary arteries, the impact of partial smooth muscle cell coverage is better appreciated in long-axis sections (**Figure 7**). From this view, smooth muscle cells clearly do not provide a complete wrap around the vessel wall in some arteries, leaving segments of the wall without any musculature (**Figure 7A**). Thus, these vessels are classified as partially muscular. With respect to orientation, medial smooth muscle cells in human pulmonary arteries are oriented around the circumference of the vessel wall, typically with their long axes perpendicular to the

longitudinal axis of the vessel (**Figures 2B** and **7A**). However, in rat lung pulmonary arteries, a spiral coat of smooth muscle cells can appear (194, 251) as seen in **Figure 7B**. In these small arteries, the impact of smooth muscle contraction on vascular diameter (and resistance to flow) may be offset to some extent by shortening of the long axis of the vessel segment. Finally, the aggregate data provided in **Table 2** emphasize the conclusion that the degree of muscularity in pulmonary arteries cannot be predicted based either on the proximity of the artery to any particular airway structure or on vascular diameter.

Heterogeneity within the arterial media may arise from one of several factors, including varying smooth muscle cell phenotype. Phenotypic diversity of smooth muscle cells has been identified within the media of large conduit pulmonary arteries. In the bovine pulmonary artery, distinct subpopulations of smooth muscle cells can be identified in the outer versus the inner layers of the media. In particular, cells clustering around the media-intima border appear to lack typical smooth muscle cell markers and have scant myofibrils while those at the outer edge of the media may express smooth muscle α-actin but lack smooth muscle myosin and calponin (12, 76, 297). Further, in rat lung, a spirally-oriented or oblique layer of smooth muscle arises in muscular arteries external to the conventional circumferential layer, resulting in a thickened vascular wall (194). These thick-walled oblique muscular arteries range in diameter from 680 μm down to 40-80 μm (194, 200). Medial thickness in this type of muscular artery can exceed 30% of wall thickness and smooth muscle can occupy up to 88% of total wall area (194). In pulmonary arteries adjacent to alveolar ducts of rat lung, only the oblique layer of smooth muscle may remain. Thick-walled oblique pulmonary arteries have not been observed in human lung (115, 194). Finally, there is heterogeneity within the media of intra-acinar arteries. Specifically, the density of contractile myofilaments and anchoring dense bodies in arterial smooth muscle cells decreases in smaller diameter distal vessels. Using careful microdissection and step-wise sectioning of the pulmonary arterial tree in rat lung (50), Davies and colleagues determined that as muscularization of pulmonary arteries decreases, transition or "intermediate" cells can be identified in partially muscular arteries at the level of the alveolar duct. These intermediate cells lack myofibrils and dense bodies, but appear to be distinct from pericytes (50, 137).

Throughout the pulmonary arterial tree, the thin intima consists of a non-fenestrated monolayer of endothelial cells lining the vessel lumen, as well as a sub-endothelial interstitium that extends to the internal elastic lamina. Intimal thickness in human lung ranges from 1-16% of total wall thickness (33, 101) or ~15% of wall area (174). In dog and rat lung, intimal thickness averages ~1-2% of wall thickness, irrespective of overall vessel diameter (153, 154). In rat intra-acinar pulmonary arteries, the absolute thickness of the intima averages 1.8 ± 0.2 and 2.0 ± 0.2 μm (mean ± SE) in muscular and thick-walled oblique arteries, decreasing to 0.9 ± 0.2 and 0.6 ± 0.1 μm in partially muscular and non-muscular arteries, respectively (200). By comparison, the endothelium per se comprises ~50% of the total intimal thickness in these same segments of rat lung. In proximal pulmonary arteries, endothelial cells are elongated and rather spindle-shaped, with their long axis parallel to the flow path (4, 98, 103, 110, 233, 284, 333). As a result, elongated imprints of endothelial nuclei are observed on vascular corrosion casts of the arterial tree (4, 98, 273). In rat lung, the length of these spindle-shaped endothelial cells in small pulmonary arteries averages 21.9 ± 1.0 μm, but is substantially less and relatively uniform in thick-walled oblique (13.0 ± 0.7 μm), partially muscular (15.0 ± 1.0 μm), and non-muscular arteries (13.8 ± 0.6 μm) (194). Thus, only 5-6 endothelial cells are found along a 100 μm linear path towards the periphery in small intra-acinar pulmonary arteries (137).

The ultrastructure of endothelial cells, smooth muscle cells and fibroblasts in the arterial wall is shown in **Figures 8-10**. The oval nuclei of endothelial cells lining the vessel luminal

face are oriented parallel to the flow path and occupy much of the cellular volume. Smooth endoplasmic reticulum comprises 9% of cytoplasmic volume in rat pulmonary artery endothelial cells, whereas less volume is occupied by vesicles (5%), mitochondria (4%) and caveoli (4%) and the occasional microtubule (260). These organelles are not necessarily constrained to the perinuclear space, and may appear quite close to intercellular junctions (**Figure 8**). Vesicle diameter in pulmonary artery endothelium averages ~65 nm, while vesicular density ranges between 110-130/μm^3 of endothelial volume (54). Rough endoplasmic reticulum (RER) is evident in the endothelium, irrespective of the vascular compartment, although the RER sits in closer proximity to the apical plasma membrane in pulmonary artery endothelium compared to that in capillary endothelium (155). Weibel-Palade bodies, cylindrical rod-shaped organelles in vascular endothelium which sequester von Willebrand factor and P-selectin (338), are present throughout the pulmonary arterial tree in human, pig, rabbit and cat lung (83, 103, 188, 195, 200, 255, 354). In rat pulmonary arteries, the frequency of Weibel-Palade bodies decreases from the hilum to the periphery, from 10-25 to 5-10 per endothelial cell, respectively (195, 200). Zhou and colleagues documented the presence of Weibel-Palade bodies in small pre-capillary arteries in human, rat and mouse lung (354). In contrast, Sobin and Chen did not find these structures in 10-40 μm pulmonary arteries in rat lung (290). Endothelial cells lining the vessel luminal face are connected by well-organized tight junctions (265, 270), contributing to the integrity of the endothelial barrier (**Figure 8A**). The inter-endothelial junctions may contain specialized gap junctions, evidenced by a length of very electron dense segment of closely apposed membranes. An enlarged view of the junction shown in **Figure 8A** is provided in **Figure 8B**. The Golgi network (**Figure 8C**) is relatively rare, occupying less than 0.5% of cell volume (260). Vascular smooth muscle cells in the pulmonary artery wall (**Figure 9**) possess numerous myofibrils (myofilaments) that align with the long axis of the cell and attach via dense bodies to the plasma membrane (**Figure 9A)**. The "bundling" of myofilaments is more apparent when the smooth muscle cell is sectioned perpendicular to its long axis (**Figure 9B**). The parallel array of myofilaments in a bundle is best resolved at higher magnification (**Figure 9C**). Dense bodies are numerous but small, occupying only 5.2 ± 0.5% of cell volume. In contrast, in rat hilar pulmonary arteries, Meyrick and Reid determined that myofilaments comprised 38.2 ± 1.3% of cytoplasmic volume in smooth muscle (196). Mitochondria, ribosomes, smooth endoplasmic reticulum and vesicles are present in similar proportions, averaging 5.2-7.8% of the cellular volume, while RER and Golgi apparatus occupy less volume (3.2 and 1.2%, respectively). Mitochondria, RER and Golgi cluster around the nucleus of smooth muscle cells. Fibroblasts (**Figure 9A**) in the arterial adventitia possess an extensive network of rough endoplasmic reticulum and long cytoplasmic extensions. While fibroblasts are not bounded by a basement membrane, they are closely associated with collagen bundles and elastin in the vascular wall interstitium. The stellate nature and extensive cytoplasmic projections of adventitial fibroblasts are better appreciated in **Figure 10**, from edematous mouse lung.

Intercellular junctions in the arterial wall

Cell-cell tethering and communication contribute to structural integrity and functional signaling in the vascular wall. Homotypic junctions are found in both the intima and the media of the pulmonary vasculature (205, 269). The tight junctions connecting endothelial cells are critical to the integrity of the endothelial monolayer in the pulmonary vasculature. Under normal conditions, tight junctions limit (but do not completely prevent) transfer of fluid, proteins and other constituents of blood to the interstitium (231, 236, 266, 269, 304, 305). Freeze-fracture studies have elucidated the organization of the junctional strands and provided ultrastructural evidence for the presence of gap junctions in arterial and venous endothelium (265, 349). As shown in the freeze-fracture images in **Figure 11**, junctional strands appear as rows or particles (or grooves on the complementary face). Tight junction

strand density appears to be highest in arterial endothelium (2-7 strands per junction), compared to that in pulmonary capillaries (1-3 strands) and veins (1-5 strands, not shown) (265). With freeze-fracture, gap junctions can be identified as tightly packed arrays of particles embedded within the junctional complex (53, 265, 269). Numerous large inter-endothelial cell gap junctions are expressed in larger intra-acinar arteries, whereas in non-muscular arteries gap junction frequency is lower (265). Using immunogold or immuno-fluorescence labeling, co-expression of connexins 37, 40 and 43 can be observed within inter-endothelial cell tight junctions of the main pulmonary artery in rat lung (160, 345). Freeze-fracture has also been used to document gap junctions between pulmonary arterial smooth muscle cells in the guinea pig lung (77). Occasionally, gap junctions can be observed via transmission electron microscopy in mouse lung (see **Figure 9D**). Heterocellular junctions are also common in pulmonary arteries. These myoendothelial junctions allow bi-directional signaling between vascular smooth muscle and endothelial cells in extra-alveolar vessels. Varying morphologies for myoendothelial junctions are evident in rat and mouse pulmonary arteries (**Figure 12**). Either endothelial or smooth muscle cells (or both) project through 0.5-1 μm focal discontinuities in the internal elastic lamina (50, 205, 326). Several reports have suggested that myoendothelial junctions occur less frequently in pulmonary artery than in pulmonary veins (202, 255, 288). In canine lung, Michel and colleagues quantified the density of myoendothelial junctions in pulmonary arteries less than 300 μm in diameter (205). In this size range ~2 junctions are observed per 100 μm of basal lamina, whereas the density is ~5-7/100 μm in capillaries and veins. Despite this apparent gradient across the pulmonary circulation, the frequency of myoendothelial junctions in pulmonary arteries does not correlate with arterial diameter (205).

Capillaries

Several anatomic features of pulmonary capillaries provide a starting point for discussion of capillary structure: the origin of capillary networks from pre-capillary arteries, spatial heterogeneity in capillary network density, and overall capillary loading in the alveolar septal wall. Despite the ordered branching pattern in the pulmonary arterial tree, pulmonary capillaries do not consistently emerge from the most distal pulmonary artery branches. A number of other patterns have been observed for the relationship of arteries to capillaries (119, 240, 247, 249, 295, 323). As illustrated in **Figure 13**, precapillary vessels may branch at right angles from a small (30 μm) parent artery then give rise to a capillary network or alternatively a small artery may abruptly end in a capillary network. Further, in human and rat lung, extra-alveolar pulmonary arteries 100 μm or more in diameter may give rise directly to capillary networks (119, 137). These latter networks supply respiratory bronchioles (119).

Network structure

The ratio of intra-acinar pulmonary arteries to alveoli has been estimated using light microscopy, counting both arteries and alveoli within a planar area, and typically reported as the number of arteries/100 alveoli. The ratio ranges from 2.1 in human lung (116), 3.2-3.7 in sheep (193, 235), 3.3-4.3 in rat (115, 132, 167), and 2.0-6.9 in mouse (17, 102, 192, 282, 350). Estimates of artery-to-alveoli ratios based on the number of order 1 pulmonary arteries derived from vascular casting (see **Table 1**) and morphometric measures of alveolar number yield more variable data, likely due to the margin of error in projecting the number of small precapillary arteries. For example, given the estimates in human lung of 51-72 million order 1 pulmonary arteries (120, 127) and 300 million alveoli (114), a ratio ranging between 17-24 arteries/100 alveoli can be projected. Similar projections for cat and rat lung yield ratios of 4.1 and 0.3, respectively (131, 135, 355). Ratios based on light microscopy may be more

predictive of the in situ relationship. Nonetheless, these data together provide support for the notion that pulmonary arteries supply capillary networks across numerous alveoli.

Vascular corrosion casting has elucidated spatial heterogeneity in the density of pulmonary capillary networks (3, 26, 82, 97, 272, 283, 353). Examples of such heterogeneity in rat lung vascular casts are shown in **Figure 14**. Capillary networks adjacent to bronchovascular bundles and in the subpleural network are comprised of long tubular segments (**Figures 14A** and **B**, respectively), similar in organization to those capillary networks seen in many systemic vascular beds. In contrast, shorter capillary segments are present in the much more dense capillary networks which occupy alveolar septal walls (**Figure 14C**). Overall capillary loading or capillary density in the septal compartment in lung can be estimated by the ratio of total capillary volume (V_C) to total alveolar surface area (S_A) (86, 334). Based on data provided by Gehr *et al.* in their comprehensive assessment of scaling in the respiratory system (86), the V_C/S_A ratio increases from 1.18 in mouse lung to 1.24, 1.43, and 1.49 in rat, dog and human lung, respectively. These data suggest that the alveolar capillary network is somewhat more dense, i.e. occupies more of the alveolar septal wall, in larger mammals. However, even in rat lung capillaries have been estimated to cover 86 ± 10% (mean ± SD) of the alveolar surface, but covere less (73 ± 9%) of the pleural surface (272).

Length-diameter relationships in pulmonary capillary networks, as well as the overall path length from artery to vein through the capillary network, have been extensively investigated. Morphometric measures of capillary volume and capillary endothelial surface area in human lung predict an average capillary radius of 3.15 μm, translating to an average capillary diameter of 6.3 μm (218). Based on direct measurements accumulated from casts of the pulmonary vasculature or from transmission electron microscopy, average capillary diameter ranges from ~ 5-8 μm (6, 21, 37, 94, 97, 161, 255, 272, 291, 302). In a large survey utilizing light microscopy of fixed dog and rat lung, capillary diameters range between 3 and 13 μm in both the subpleural and intra-acinar capillary networks. However, the frequency distribution of diameter at these locations differs. As a result, the average diameter of subpleural vessels exceeds that of intra-acinar capillaries by 20-30% (94, 161, 283). Measures of capillary diameter need to be interpreted in context of the state of perfusion and lung inflation. Both intravascular and transpulmonary pressures are clearly recognized to impact dimensions of capillaries, as well as those of extra-alveolar vessels (13, 91, 94, 183, 184, 313). For example, in perfusion-fixed rabbit lung, Ciurea and Gil fixed zonal conditions by varying lung inflation pressure as well as pulmonary arterial and venous pressures. Under these conditions, they documented that capillary diameter increased from 4.9 ± 3.5 μm in zone 1, to 6.9 ± 2.7 and 7.6 ± 3.5 μm (mean ± SD) in zones 2 and 3, respectively. Note that despite substantial distension from zone 1 to 3, the variance in diameter remained similar across zones.

As noted earlier, small distal pulmonary arteries appear to supply numerous alveoli. Further, numerous septal walls may separate a pulmonary artery inflow point and the pulmonary vein which provides outflow. The path length for flow through the alveolar capillary network from artery to vein has been estimated to range from 250-850 μm in several mammalian species (95, 210, 296). In lungs from 20 g mice, total capillary length (estimated from capillary surface density and weighted capillary diameter) averages 1.13 ± 0.13 km (159). Mühlfeld and colleagues have highlighted the limitations in assessment of capillary length, considering this the least robust measure of network geometry. They note that in human lung, the aggregate capillary length estimated from direct measures of capillary profiles yields an average of 6950 ± 3108 km, whereas that derived from the volume/capillary surface area ratio averaged 2746 ± 722 km (218).

Morphometry of the septal wall

Regardless of whether the alveolar capillary network is considered to be a sheet of interconnecting capillary segments or a network of short tubes, the wall of each capillary segment/tube is comprised of only a few thin, squamous endothelial cells (91, 155, 333, 334). The capillary is surrounded by an interstitial compartment, delimited primarily by alveolar type I epithelial cells with the occasional type II cell. In cross-sections of alveolar capillaries visualized by transmission electron microscopy, portions of only 2-3 endothelial cells are evident (60, 155). Using quantitative morphometric approaches, capillary endothelial cells have been documented to comprise 30-50% of the total cell population in the alveolar septal wall (**Table 3**). In human lung, Crapo and colleagues reported that endothelial cells contributed 30% to the total cell number within the septal wall in the human lung (44). The relative number of endothelial cells in non-human primates ranges from 36-39% of total septal wall cell number (38, 45, 47), while in rodents endothelial cells may contribute as much as 46-50% to the total (47, 109).

Total alveolar surface area, capillary volume and the harmonic mean thickness of the alveolar septal barrier all scale with body mass in adult mammals, albeit with markedly different slopes. The harmonic mean thickness is weighted more towards the thin side of the septal barrier and so is thought to better relate to the resistance of the barrier to gas exchange (334). The allometric log-log relationships of alveolar surface area, capillary surface area and capillary volume to body mass have slopes ranging from 0.92 to 1.0 (86), meaning that these indices of alveolar structure scale proportionately with body mass. Based on morphometric assessments using electron microscopy, total capillary surface area has been estimated to range from 124 cm^2 in mouse lung to 4,500 cm^2 in rat lung, 3.5 -4.2 m^2 in rabbit lung, up to 126-130 m^2 in human lung (13, 84, 159, 218, 244, 334, 342). Since specific endothelial surface area (~ 1100 μm^2 per cell) is relatively well conserved across species (**Table 3**) (44, 45, 100, 109), the increase in total capillary surface area reflects an increase in total endothelial number. In contrast, the slope of the harmonic mean thickness-to-body mass relationship is only 0.05 (86), supporting the conclusion that the thickness of the alveolar septal gas exchange barrier is better conserved across species. In comparison to the harmonic mean thickness, the arithmetic mean thickness is derived from the volume-to-surface area ratio. As such, the arithmetic mean thickness provides overall barrier dimensions, without any particular sampling bias for the thin or thick side of the septal wall.

Measures of endothelial, interstitial and epithelial thickness in the septal wall are arithemetic mean measures (**Table 3**). The endothelial and epithelial layers each contribute roughly one-third to the overall wall thickness, with the remaining 40% residing in the interstitial space. The cellular and non-cellular components of the alveolar septal wall interstitium are not distributed uniformly. On the “thin” side of the septal wall, shown in **Figure 15,** along a fold in the septal wall the basement membrane of the endothelium appears in places to be essentially fused with that of the alveolar type I epithelial cell (156, 318), though micrographs obtained at higher magnification can resolve distinct lamina (55, 318, 334). Both the endothelium and the type I epithelium on the thin side are demonstrably attenuated (55, 155, 310, 334) compared with their counterparts on the thick side of the septal wall, comprising an efficient gas-exchange barrier (334). Further, endothelial thickness is markedly attenuated over 10-14% of the endothelium surface in intra-acinar alveolar capillaries, decreasing to only 20-30 nm (55, 57). As a consequence, most organelles are excluded from the endothelial cell periphery on the thin side of the septal wall. In contrast, the “thick” side of the septal wall is occupied by prominent endothelial cell nuclei and the bulk of the septal wall interstitium, which includes cellular and matrix elements.

In addition to the degree of attenuation and resultant restriction of organelles to the perinuclear space, capillary endothelial cells display other features which make the

endothelium in this compartment unique compared to that in extra-alveolar vessels (82, 155, 226, 298, 299). First, the surface glycocaylx in capillary endothelium is distinct from that in extra-alveolar vessels. In rat lung, capillary endothelium binds *Griffonia simplicifolia*, a lectin that specifically interacts with α-galactose in surface glycoproteins. In contrast, pulmonary artery endothelium binds *Helix pomatia*, a lectin that interacts with α- and β-*N*-acetyl-galactosamine (82, 155). Second, although Weibel-Palade bodies are commonly expressed in endothelium of extra-alveolar vessels, Zhou and colleagues did not find Weibel-Palade bodies in capillary endothelium of human, rat or mouse lung (354). In contrast, Meyrick and Reid reported rare Weibel-Palade bodies in capillary endothelium from rat lung (200). Third, although endothelial cells throughout the pulmonary vasculature are joined by tight junctions (see **Figure 11**), the organization of junctional complexes in capillary endothelium appears different from that in extra-alveolar vessels (265, 266, 329, 349). For example, in mouse lung, tight junctions in the capillary endothelial barrier tend to possess only 1-3 junctional strands, fewer than observed in arterial or venous endothelium (265-267). However, an extensive study in normal and edematous canine lung found that qualitative assessment of junctional strand morphology does not necessarily provide information that correlates in a predictable way with the functional state of capillary endothelium (330). Nonetheless, in human lung, the complexity of tight junctions - i.e., strand density - is increased at the lung base, where intravascular pressures are higher, compared to the apex (349). Further, while the large gap junctions characteristic of endothelial junctions in extra-alveolar arteries and veins are missing from capillary endothelium, small gap junctions can occasionally be found in capillary inter-endothelial cell junctional complexes (265). An additional unique feature has been elucidated by three-dimensional reconstruction of serial sections through junctions between adjacent capillary endothelial cells in guinea pig lung (329). A ~ 27 nm gap appears between the plasma membrane of two adjacent endothelial cells, a finding at odds with the very low hydraulic conductivity in the lung microvascular barrier (63, 232). However, a third adjoining endothelial cell forms a flap overlaying the borders of the remaining two cells. The junctional strands within this flap run parallel (rather than perpendicular) to the plane of the overlying cell (329). It is conceivable that this organization in the lung capillary bed provides some protection against transendothelial fluid movement with increased intravascular pressure, as the increased hydrostatic force could lead to relative “sealing” of this junctional complex. Finally, although cross-sections of only 2-3 endothelial cells may be apparent in transmission electron micrographs of lung capillaries (155), the location of their junctional complexes does not appear to be random. Walker *et al.* noted in rabbit and mouse lung that up to 80% of tight junctions were situated at the interface between the thick and the thin sides of the septal wall (328). Placement of junctions preferentially at this location (arrowheads, **Figures 16A** and **B**) should provide some measure of structural stability, as the increased mass of surrounding tissue (rather than air or blood as on the thin side of the septal wall) would likely minimize the distensibility of this segment of the capillary wall.

The septal interstitium

Despite its small volume, the alveolar septal wall interstitium is populated by a variety of cells. Roughly 30-50% of interstitial volume is occupied by cells, including fibroblasts, pericytes, macrophages, and mast cells (25, 333). Overall, interstitial cells represent roughly 30-40% of total cell number in the septal wall (38, 43, 44, 46). While the presence of edema fluid in the septal wall and resultant “cuffing” of capillaries is not normal, consequent expansion of the septal wall interstitium does allow clear visualization of interstitial cells within the thin sections of the wall (Figure 16). Fibroblasts and pericytes, the contractile cells in the septal wall interstitium, have been variously proposed to play a role in regulation of interstitial compliance and capillary blood flow (25). Though neither fibroblasts nor

pericytes express smooth muscle heavy chain myosin, both cell types do possess cytoplasmic actin filaments (147). On the other hand, pericytes can express α-smooth muscle actin (146). As in the wall of extra-alveolar vessels, fibroblasts in the alveolar septal wall associate with the fiber matrix scaffold. The morphology of alveolar interstitial fibroblasts is similar to that of adventitial fibroblasts found in pulmonary arteries. The cell bodies of the interstitial fibroblasts are located in the thick side of the alveolar septal wall or in corner sections at the junctions of alveolar walls. Long cytoplasmic extensions (**Figure 16A**) of these cells penetrate into the thin interstitial spaces separating endothelial cells from the epithelial cells on the alveolar surface (137). In immature rodent lungs, the proportion of fibroblasts in the alveolar septal wall averages ~ 50% of the total cell population, but decreases to ~ 20% in the adult (148). Irrespective of age, nearly half of the total fibroblast population in the septal wall contains lipid droplets, which may be decorated with glycogen (148). The lipid droplets primarily contain triglycerides, although cholesterol esters, free fatty acids and cholesterol may be present as well (248). These lipid-containing fibroblasts (**Figure 16B**) are thought to play an important role in surfactant synthesis in type II cells via crosstalk with hormonal signaling from the type II cell and resultant shuttling of triglycerides back to type II cells (248). As with fibroblasts in extra-alveolar arteries, septal wall fibroblasts possess abundant rough endoplasmic reticulum and prominent Golgi. Actin filaments are arranged in compact, parallel bundles, which in the lipid-containing fibroblasts attach to the plasma membrane at dense bodies (146, 148). Alveolar interstitial fibroblasts, with or without lipid droplets, participate in synthesis of matrix proteins including collagen, and in some cases elastin (146, 148, 317, 336).

While pericytes have been found to be more numerous near alveolar septal wall convergence points (146), cell bodies of pericytes can also be situated in the “posts” or thick sections of interstitium between capillaries (335). Pericytes can be identified in part due to their thin cytoplasmic processes that intercalate between the endothelial cell and its basement membrane (113, 287, 335). In addition, the cytoplasmic actin filaments in pericytes tend to be aligned near the face of the cytoplasmic process that abuts the capillary endothelium (335). While pericytes are relatively rare in the septal wall of rat lung and absent in the shrew, they can be frequently observed in human, dog and guinea pig lung (335). In rabbit and mouse lung, ~40% of pericyte profiles lie adjacent to an endothelial cell tight junction (328).

In rabbit lung, Gil and McNiff (92) identified an additional interstitial “boundary” cell situated near the insertion of alveolar septa into the adventitial sheath of extra-alveolar vessels. They postulated, based on its location in the septal wall, that this cell might provide a delimiting barrier between the interstitial compartments in the septal wall and extra-alveolar vessels. Although the boundary cell was not identified as an interstitial fibroblast, the morphology is similar in that thin cytoplasmic projections from the cell body of the boundary cell penetrate back into the septal wall. Finally, macrophages and mast cells are commonly observed in the alveolar septal wall. In the septal wall of rat lung, 3-12% of interstitial cells are macrophages (32, 43, 46, 100). The mucosal type of mast cell, i.e., that expressing tryptase, is dominant in the alveolar septal wall, comprising ~90% of the mast cell population in this compartment (10, 11, 339). The mucosal type mast cell is small, with granules of varying size (339).

Von Hayek documented finely branching neural networks on the pleural surface of human lung that extended towards alveoli (323). However, while nerve fibers can be observed within the alveolar septal wall with electron microscopy, the frequency is low. In human lung, nerve endings are only rarely observed (7, 73). Similarly, innervation within the septal wall is rare in dog, rat, and mouse lung (71, 129, 198). Importantly, neuronal fibers immunoreactive for tyrosine hydroxylase, indicative of sympathetic innervation, have not

been found in human lung. In contrast, the neuropeptides CGRP and SP can be identified in the alveolar septal wall of cow, dog, cat, guinea pig, ferret, rat and hamster lung. Although expression is sparse in some cases, the presence of these neuropeptides suggests the possibility that the neuronal fibers observed with electron microscopy may be sensory in nature (171, 221, 223, 332).

Finally, although endothelium comprises the capillary wall per se, inter-cellular junctions may connect capillary endothelium to other cellular constituents of the alveolar septal wall. Electron micrographs of rat and mouse lung provide some evidence for close cell-cell contact within the septal wall. **Figure 17** includes higher magnification images of the boxed sections from **Figure 16**, showing a loose connection between a fibroblast and the type I alveolar epithelium (**Figure 17A**), tight junctions between the type I and type II alveolar epithelium (**Figure 17B**), and an interface between a fibroblast and the capillary endothelium (**Figure 17C**). Similar intercellular junctions, including inter-epithelial cell gap junctions, have been demonstrated in alveolar septal wall of human lung (287, 349). Finally, in canine lung, myoendothelial junctions occur between capillary endothelium and pericytes, with a density averaging 4 per 100 μm of basal lamina (205). Walker and colleagues utilized serial sectioning of human and rabbit lung and three-dimensional reconstructions to elucidate the extent of heterotypic intercellular communication in the alveolar septal wall (287, 328). They found that single fibroblasts in the septal interstitium contact capillary endothelium, as well as pericytes and alveolar epithelial cells. In human lung, opportunity for such physical interaction between fibroblasts and Type II epithelial cells is provided by gaps in the Type II cell basal lamina, averaging ~1 μm in width, which occur beneath ~50% of these cells (287). Fibroblasts access other cells in the septal wall through similar apertures in their basal lamina. A model of the septal wall network developed from reconstruction of serial sections in human lung is shown in **Figure 18** (287).

As shown in **Figure 16B**, collagen and elastin deposition is particularly dense at the tips of the alveolar septa in the adult lung, where these fibers provide structural support to the entrance ring of the alveolus (191). Although bundles of collagen and elastin fibers in the septal interstitium are clearly apparent in such transmission electron micrographs, the fibrous matrix scaffold in the septal wall is more complex and interconnected with networks in extra-alveolar vessels and the pleura, as previously discussed (see **Figure 4**). Both collagen and elastin fibers coalesce into rich bundles surrounding the entrance to the alveolus, then disperse into finer networks through the septal wall (308). Collagen bundles in the rat alveolar septal walls shift from a “wave-like” appearance to straight bundles when lungs are inflated prior to fixation (308). A morphometric assessment of collagen and elastin volume density in the alveolar septal wall of canine lung provides additional quantitative evidence. For both collagen and elastin, the volume density of these extracellular matrix proteins at the septal crest was 2- to 2.5-fold higher than that in the remainder of the septal wall (229). Collagen and elastin volume fractions in the alveolar parenchyma as a whole increase with body mass, as does the thickness of these bundles in the septal wall (190, 191, 229). Interstitial thickness within the alveolar septal barrier **(Figure 19**), as well as the relative contribution of collagen and elastin, also scales with body size and alveolar volume in adult mammals (72, 85, 175, 191, 334, 352). However, the slope of the relationship for these thickness measures to body size is quite shallow. Thus, although interstitial thickness in the alveolar septal wall increases ~5.2-fold from mouse to human lung, this should be taken in context of the > 3 log order difference in body mass.

Veins

Vascular corrosion casting has been utilized to investigate the branching pattern in the pulmonary venous tree in human, pig, dog, and cat lung (79, 120, 347, 355). For the most

part, the number and caliber of order 1 veins emerging from the capillary bed mirror the characteristics of order 1 arteries (**Table 1**). Fewer orders of veins appear in human lung, where multiple extra-pulmonary veins drain blood flow into the left atrium. Note that the diameter of the largest, order 15 pulmonary veins in humans is less than half that of the main pulmonary artery. Nonetheless, diameter, length and branching ratios are similar to those determined for the arterial tree. As previously discussed, characterization of branching patterns in the pulmonary vascular tree via enumeration of generations leads to a markedly different result, i.e., 22 generations of veins in pig lung vs 15 in human and 11 in dog or rat lung.

The structure of small intra-pulmonary veins continues to show some similarities to that of small arteries: a thin intima, a smooth muscle-containing media in larger diameter veins, and an adventitia containing a vasa vasorum, nerves and bundles of collagen or elastin fibers. The density of myoendothelial junctions is similar to that observed in pulmonary arteries (205). However, there are notable differences. Unlike the oval or elliptical shape of endothelial cell nuclei in pulmonary arteries, those in pulmonary veins are polygonal or round (3, 273, 333). In contrast to large pulmonary arteries in human and dog lung, large pulmonary veins are muscular rather than elastic in nature (202) and pulmonary veins possess an indistinct or absent internal elastic lamina (81, 255). Little quantitative data is available which evaluates muscularity in pulmonary veins (see **Table 2**). However, when vessels from the same animal are compared, the media of pulmonary veins is demonstrably thinner that that of comparably sized arteries (202, 279, 311). Michel evaluated quantitative structural differences in canine lung, finding that the media of pulmonary veins contributes on average 33-60% less to the thickness of the vessel wall, compared to that in pulmonary arteries (202). We obtained similar results in canine lung: both wall thickness and medial thickness in intrapulmonary veins >400 μm in diameter were ~50% less than that in pulmonary arteries in the same size range (311). In general, pulmonary veins contain more extracellular matrix and less smooth muscle than pulmonary arteries (136, 162). Notably, the collagen content of human pulmonary veins is substantially higher than that in pulmonary arteries at any age (172). Further, human pulmonary veins can exhibit intimal thickening with age, in the absence of any cardiopulmonary disease (325). In addition, the complete circumferential wrap of smooth muscle that defines a muscular vessel does not appear to extend as far distally in the venous tree, at least in some species, compared to that in the arterial tree. In sheep, pulmonary veins less than 125 μm in diameter are not muscular, whereas in dog and rat lung muscular veins less than 100 μm in diameter can occasionally be observed (126, 136, 202).

The pulmonary venous myocardium

In some species, one additional distinction between intrapulmonary veins and arteries is the inclusion of sleeves of striated cardiac myocytes covering the wall of the intrapulmonary veins. Pulmonary myocardial sleeves develop from primordial myocardium in the dorsal atrial wall (9, 208, 213, 292). The gene expression pattern of the pulmonary venous myocardium appears similar to that of atrial cardiac muscle (143). In both, myocytes are connected extensively by desmosomes and intercalated discs, which are sites of connexin expression (320, 344). In rat extra- and intrapulmonary pulmonary veins, similarity to atrial myocardium extends to the expression of atrial natriuretic peptide in dense granules within a subset of pulmonary myocardial cells (164, 294, 309). Although this review focuses on the normal pulmonary vasculature, it is worth noting that the pulmonary venous myocardium can hypertrophy, such as with dilated cardiomyopathy in humans (16) or genetic knockout of heme oxygenase-2 in mice (1). Further, granules containing atrial natriuretic peptide appear in the myocardium of smaller pulmonary veins after myocardial infarction in rats (164).

Though not the first report of intrapulmonary striated musculature, Karrer evaluated the ultrastructural features of the contractile elements in these cells in the pulmonary veins of mice (151). Subsequently the presence of cardiac myocytes in the wall of intrapulmonary veins has been noted in squirrel, rat, marmoset and shrew lung (19, 68, 69, 157, 206). The wall of large intrapulmonary veins from rat lung (**Figure 20**) includes the endothelium, scant smooth muscle, and abundant striated myocytes. The pulmonary myocardium can be oriented in a circumferential or longitudinal pattern (or both), but may not necessarily be organized as a complete sleeve around the circumference of the vein (216). Further, when multiple layers exist, they are much more loosely organized than are layers of smooth muscle cells in pulmonary arteries. In extra-pulmonary veins, the myocardium is overlaid with an extensive adventitial capillary network (106). However, capillaries can be distributed within the myocardium as well, as seen in rat lung (**Figure 20**).

Fibroblasts, along with other interstitial cells, can be present in pulmonary veins (see **Figure 20**). In this section from rat pulmonary vein, a fibroblast with long cytoplasmic extensions is interposed between the smooth muscle and myocardial layers, bounded by densely packed collagen on one face and the cardiac myocyte on the other. Interstitial cells with some structural similarities to the interstitial cells of Cajal (pacemaker cells found in the wall of the gastrointestinal track (331)) are also present (88). These interstitial Cajal-like cells are multipolar pyramidal-shaped cells that possess very thin, attenuated processes similar to those displayed by fibroblasts (88, 214). The processes track in close proximity to nerve bundles, cardiac myocytes and adventitial capillaries (**Figure 20B**). However, unlike lung interstitial fibroblasts, these interstitial Cajal-like cells are not contractile (104). The interstitial Cajal-like cells have been proposed to serve as an interconnecting cell linking other cellular components in the vascular wall (88, 177, 239). Whether these Cajal-like cells in pulmonary veins actually serve as pacemakers is not clear.

In most large mammals, including human and dog, myocardial sleeves extend as much as 10-20 mm from the left atrial wall into the large extra-pulmonary veins (107, 117, 216, 219, 220, 320). While sleeve length in pulmonary veins from some other large mammals, e.g., sheep, horse, and pig, appears similar to that in human, 30-40 mm sleeves can be found in pulmonary veins of cattle (220). There are no reports of pulmonary myocardium extending to the intra-pulmonary veins in lungs of large mammals, including humans. In contrast, in rat, squirrel, and mouse lung (19, 151, 170, 206, 216, 230), striated myocytes can be observed in pulmonary veins as small as ~ 30-40 μm in diameter. With light microscopy, the myocardial sleeve in small pulmonary veins of rat or mouse lung can appear similar to smooth muscle in the media of the vascular wall, unless smooth muscle-specific probes are utilized (107, 206). Light and transmission electron microscopy images of a pulmonary vein (~ 100 μm in internal diameter) from the same block of rat lung highlight this issue (**Figure 21**). One m sections of lung blocks fixed and embedded for electron microscopy typically show more cellular detail than do the thicker sections utilized for traditional light microscopy. Nonetheless, the media in this vein is thickened but otherwise does not appear unusual. However, images from the same block collected via electron microscopy identify only an endothelial cell monolayer and a media composed of a striated cardiac myocyte.

Some striated myocytes have ultrastructural characteristics similar to those of nodal pacemaker cells (179) or specialized conducting fibers (36). For example, in extra-pulmonary veins, P cells and Purkinje cells can be present, which act as specialized conducting cells (234). P cells lack intercalated disks and possess only a few unorganized contractile elements at the cell periphery. In contrast, the Purkinje cells have an abundant, well-organized contractile apparatus, and are connected via intercalated disks and desmosomes. Despite the presence of potential pacemaker cells in venous myocardium, intrinsic pacemaker activity has not been documented. However, when the myocardial cells

are activated, conduction of electrical impulses is facilitated by ultrastructural features of the pulmonary venous myocardium and the surrounding cells (**Figure 22**). In these images from pulmonary veins in rat and mouse lung, demosomes are apparent which provide a lateral tight junction between myocardial cells (**Figure 22A**). Further, intercalated discs connect myocytes end-to-end (**Figure 22B**). Both connexin 40 and 43 are expressed at the cell borders of striated myocytes isolated from canine pulmonary vein (344). In some veins the myocardium overlays a smooth muscle layer, and interfaces can occasionally be seen which appear to have the potential as junctional complexes with smooth muscle (**Figure 22C**). Finally, proximity of the venous myocardium to autonomic nerve fibers (**Figure 22D**) could facilitate neural control. Functional studies of ion channel expression, electrophysiology, and tone development in pulmonary veins suggest significant contribution of cardiac myocytes to tone (29, 35, 36, 41, 142, 189, 206). For example, in isolated 100 m intrapulmonary veins from rat, the myocardial layer contributes significantly to tone (206). Further, focal activation of the pulmonary venous myocardium can lead to propagation of electrical activity. Impulse conduction velocity in pulmonary veins from rats and mice has been estimated to range between 0.4-1.2 m/s (30, 230). A combined light and scanning EM study of intra-pulmonary veins in rat lung (106) yielded a model of the small partially muscular and muscular vein (**Figure 23**), reminiscent of the model for pulmonary arteries (**Figure 6**), except for the presence of the striated myocardium in the former.

Venous sphincters

On a final note, sphincter-like structures have been identified in small pulmonary veins of mouse, rat and cattle using scanning EM of vascular casts. Some evidence suggests that highly vasoreactive bands of vascular smooth muscle bulge into the lumen of the vein, providing focal points of increased resistance to flow (3, 4, 233). The pulmonary venous myocardium has been suggested to provide the anatomic construct of the sphincters reported in pulmonary veins (206). This notion has some merit for rat and mouse lung, where the venous myocardium extends to very small vessels (151, 170, 206, 216, 230). However, based on histologic evidence to date documenting the limited extension of the venous myocardium into the intra-pulmonary venous network (220), the myocardium is not likely to account for post-capillary venous sphincters in cattle.

Innervation of pulmonary veins

Innervation of pulmonary veins is predominantly limited to the adventitia, where neuronal fibers form a varicose network (7). Nonetheless, penetration of neuronal fibers into the media does occur (7, 64, 256). As in the pulmonary arterial compartment, extension of the adventitial neuronal network to small veins is common (99, 144, 277, 293). While some degree of innervation persists distally to 50-100 μm veins, there are far fewer autonomic and substance P-containing neurons compared to similar sized arteries (99). In human and rat pulmonary veins, autonomic nerve bundles within the adventitia are enclosed by Schwann cells (106, 230, 303). Depending upon the species, nerve fibers in pulmonary veins express enzymes and transmitters characteristic of adrenergic neurons (7, 64, 99, 256). NPY, a neuropeptide frequently co-expressed in adrenergic neurons, Substance P and NADPH diaphorase-containing neurons are also present (7, 99, 277). In human, dog and cat pulmonary veins VIP is also expressed (59). While neuronal fibers in pulmonary veins can project into the myocardial layer (see **Figures 20** and **22**) and have been observed to lie in close proximity (~150 nm in some cases) to the musculature of pulmonary veins (70), specialized junctions between nerves and the pulmonary myocardium have not been observed (230). At the root of pulmonary veins in humans, where myocardial sleeves are relatively short, additional nerve fibers project from epicardial ganglia into the myocardial sleeve and even into the subendothelial layer (319).

Conclusions

The pulmonary vascular wall per se comprises a relatively small fraction of the overall anatomic volume in the adult lung. Nonetheless, wall structure is richly varied in composition throughout the pulmonary circulation from artery to vein. Future studies on lung vascular structure in health and disease should seek to apply rigorous quantitative approaches. The utilization of unbiased quantitative morphometric approaches to assessment of lung vascular (and airways) structure is critical, not only for documenting characteristics of normal features, but also for investigating the impact of disease and/or disease models in experimental animals (123, 124, 130, 217, 225, 337). While such techniques have long been applied to study of the alveolar septal wall, their consistent application to quantitation of structure in extra-alveolar vessels will allow better comparison across studies. In addition to assessment of lung vascular structure per se, stereological approaches are also applicable to quantitation of subcellular structures and labeling patterns for nanoparticles or immunogold particles (181, 224).

Acknowledgments

Research support was provided by grants from the National Heart Lung and Blood Institute: HL067461, HL066299, and HL081851. The assistance of Drs. Judy King and Diego Alvarez with electron microscopy, as well as discussion regarding structure, is appreciated.

References

1. Adachi T, Ishikawa K, Hida W, Matsumoto H, Masuda T, Date F, Ogawa K, Takeda K, Furuyama K, Zhang Y, Kitamuro T, Ogawa H, Maruyama Y, Shibahara S. Hypoxemia and blunted hypoxic ventilatory responses in mice lacking heme oxygenase-2. Biochem Biophys Res Commun. 2004; 320:514–522. 10.1016/j.bbrc.2004.05.195 S0006291X04012100 [pii]. [PubMed: 15219859]
2. Aguirre JI, Morrell NW, Long L, Clift P, Upton PD, Polak JM, Wilkins MR. Vascular remodeling and ET-1 expression in rat strains with different responses to chronic hypoxia. Am J Physiol Lung Cell Mol Physiol. 2000; 278:L981–987. [PubMed: 10781429]
3. Aharinejad S, Bock P, Lametschwandtner A, Firbas W. Scanning and transmission electron microscopy of venous sphincters in the rat lung. Anat Rec. 1992; 233:555–568. 10.1002/ar.1092330410. [PubMed: 1626715]
4. Aharinejad S, Egerbacher M, Nourani F, Bock P, Friederici C, Schraufnagel DE. Pulmonary venous sphincters in cattle. Anat Rec. 1996; 246:356–363. 10.1002/(SICI)1097-0185(199611)246:3<356::AID-AR6>3.0.CO;2-W [pii] 10.1002/(SICI)1097-0185(199611)246:3<356::AID-AR6>3.0.CO;2-W. [PubMed: 8915457]
5. Aiello VD, Gutierrez PS, Chaves MJ, Lopes AA, Higuchi ML, Ramires JA. Morphology of the internal elastic lamina in arteries from pulmonary hypertensive patients: a confocal laser microscopy study. Mod Pathol. 2003; 16:411–416. 10.1097/01.MP.0000067685.57858.D7. [PubMed: 12748246]
6. Alexander IG, Ritchie BC, Maloney JE. Scanning electron microscopy of pulmonary alveolar capillary vessels. Thorax. 1973; 28:222–227. [PubMed: 4731118]
7. Allen KM, Wharton J, Polak JM, Haworth SG. A study of nerves containing peptides in the pulmonary vasculature of healthy infants and children and of those with pulmonary hypertension. Br Heart J. 1989; 62:353–360. [PubMed: 2686736]
8. Alvarez DF, King JA, Weber D, Addison E, Liedtke W, Townsley MI. Transient receptor potential vanilloid 4-mediated disruption of the alveolar septal barrier: a novel mechanism of acute lung injury. Circ Res. 2006; 99:988–995. 01.RES.0000247065.11756.19 [pii] 10.1161/01.RES.0000247065.11756.19. [PubMed: 17008604]
9. Anderson RH, Brown NA, Moorman AF. Development and structures of the venous pole of the heart. Dev Dyn. 2006; 235:2–9. 10.1002/dvdy.20578. [PubMed: 16193508]

10. Andersson CK, Mori M, Bjermer L, Lofdahl CG, Erjefalt JS. Alterations in lung mast cell populations in patients with chronic obstructive pulmonary disease. Am J Respir Crit Care Med. 2010; 181:206–217. 200906-0932OC [pii] 10.1164/rccm.200906-0932OC. [PubMed: 19926870]
11. Andersson CK, Mori M, Bjermer L, Lofdahl CG, Erjefalt JS. Novel site-specific mast cell subpopulations in the human lung. Thorax. 2009; 64:297–305. thx.2008.101683 [pii] 10.1136/thx.2008.101683. [PubMed: 19131451]
12. Arciniegas E, Graterol A, Sanchez F. Characterization of nonmuscle cells present in the intima of normal adult bovine pulmonary artery. Anat Rec. 2000; 258:262–268. 10.1002/(SICI)1097-0185(20000301)258:3<262::AID-AR5>3.0.CO;2-7 [pii]. [PubMed: 10705346]
13. Bachofen H, Wangensteen D, Weibel ER. Surfaces and volumes of alveolar tissue under zone II and zone III conditions. J Appl Physiol. 1982; 53:879–885. [PubMed: 7153122]
14. Barnes PJ, Liu SF. Regulation of pulmonary vascular tone. Pharmacol Rev. 1995; 47:87–131. [PubMed: 7784481]
15. Ben Driss A, Devaux C, Henrion D, Duriez M, Thuillez C, Levy BI, Michel JB. Hemodynamic stresses induce endothelial dysfunction and remodeling of pulmonary artery in experimental compensated heart failure. Circulation. 2000; 101:2764–2770. [PubMed: 10851216]
16. Benedek I, Hintea T, Toganel R. Myocardial fibres in pulmonary veins--possible compensatory factor in dilated cardiomyopathy. Rom J Intern Med. 1998; 36:175–181. [PubMed: 10822514]
17. Beppu H, Ichinose F, Kawai N, Jones RC, Yu PB, Zapol WM, Miyazono K, Li E, Bloch KD. BMPR-II heterozygous mice have mild pulmonary hypertension and an impaired pulmonary vascular remodeling response to prolonged hypoxia. Am J Physiol Lung Cell Mol Physiol. 2004; 287:L1241–1247. 10.1152/ajplung.00239.2004 00239.2004 [pii]. [PubMed: 15286002]
18. Berendsen PB, Ritter AB, DeFouw DO. An ultrastructural morphometric comparison of the peripheral with the hilar air-blood barrier of dog lung. Anat Rec. 1984; 209:535–540. 10.1002/ar.1092090413. [PubMed: 6476419]
19. Best PV, Heath D. Interpretation of the appearances of the small pulmonary blood vessels in animals. Circ Res. 1961; 9:288–294.
20. Bishop JE, Guerreiro D, Laurent GJ. Changes in the composition and metabolism of arterial collagens during the development of pulmonary hypertension in rabbits. Am Rev Respir Dis. 1990; 141:450–455. [PubMed: 1689130]
21. Burbach JA, Waltz WF, Goodman BE, Schlenker EH. Structural abnormalities underlying alveolar hypoventilation and fluid imbalance in the dystrophic hamster lung. Anat Rec. 1999; 256:321–333. 10.1002/(SICI)1097-0185(19991101)256:3<321::AID-AR9>3.0.CO;2-3 [pii]. [PubMed: 10521788]
22. Burnstock G. Autonomic neuromuscular junctions: current developments and future directions. J Anat. 1986; 146:1–30. [PubMed: 3319994]
23. Burnstock G. Non-synaptic transmission at autonomic neuroeffector junctions. Neurochem Int. 2008; 52:14–25. S0197-0186(07)00074-5 [pii] 10.1016/j.neuint.2007.03.007. [PubMed: 17493707]
24. Burnstock G. Purinergic cotransmission. Exp Physiol. 2009; 94:20–24. expphysiol.2008.043620 [pii] 10.1113/expphysiol.2008.043620. [PubMed: 18723580]
25. Burri PH. Cellular components of the alveolar unit. Curr Probl Clin Biochem. 1983; 13:11–22. [PubMed: 6653141]
26. Burri PH, Tarek MR. A novel mechanism of capillary growth in the rat pulmonary microcirculation. Anat Rec. 1990; 228:35–45. 10.1002/ar.1092280107. [PubMed: 2240600]
27. Burrowes KS, Hunter PJ, Tawhai MH. Anatomically based finite element models of the human pulmonary arterial and venous trees including supernumerary vessels. J Appl Physiol. 2005; 99:731–738. 01033.2004 [pii] 10.1152/japplphysiol.01033.2004. [PubMed: 15802366]
28. Castillo Y, Kruger H, Arias-Stella J, Hurtado A, Harris P, Heath D. Histology, extensibility, and chemical composition of pulmonary trunk in persons living at sea-level and at high altitude in Peru. Br Heart J. 1967; 29:120–128. [PubMed: 6018312]
29. Cha TJ, Ehrlich JR, Zhang L, Chartier D, Leung TK, Nattel S. Atrial tachycardia remodeling of pulmonary vein cardiomyocytes: comparison with left atrium and potential relation to

arrhythmogenesis. Circulation. 2005; 111:728–735. 01.CIR.0000155240.05251.D0 [pii] 10.1161/01.CIR.0000155240.05251.D0. [PubMed: 15699259]

30. Challice CE, Wilkens JL, Chohan KS. Electrical impulse conduction in pulmonary veins. Biophys J. 1974; 14:901–904. S0006-3495(74)85957-6 [pii] 10.1016/S0006-3495(74)85957-6. [PubMed: 4433676]
31. Chambers, RC.; Laurent, GJ. Collagens.. In: Crystal, RG.; West, JB.; Barnes, PJ.; Weibel, ER., editors. The lung: Scientific foundations. Lippincott-Raven Publishers; Philadelphia: 1997. p. 709-727.
32. Chang LY, Overby LH, Brody AR, Crapo JD. Progressive lung cell reactions and extracellular matrix production after a brief exposure to asbestos. Am J Pathol. 1988; 131:156–170. [PubMed: 2833103]
33. Chazova I, Loyd JE, Zhdanov VS, Newman JH, Belenkov Y, Meyrick B. Pulmonary artery adventitial changes and venous involvement in primary pulmonary hypertension. Am J Pathol. 1995; 146:389–397. [PubMed: 7856750]
34. Chen YF, Feng JA, Li P, Xing D, Zhang Y, Serra R, Ambalavanan N, Majid-Hassan E, Oparil S. Dominant negative mutation of the TGF-β receptor blocks hypoxia-induced pulmonary vascular remodeling. J Appl Physiol. 2006; 100:564–571. 00595.2005 [pii] 10.1152/japplphysiol.00595.2005. [PubMed: 16223981]
35. Cheung DW. Electrical activity of the pulmonary vein and its interaction with the right atrium in the guinea-pig. J Physiol. 1981; 314:445–456. [PubMed: 7310698]
36. Chou CC, Nihei M, Zhou S, Tan A, Kawase A, Macias ES, Fishbein MC, Lin SF, Chen PS. Intracellular calcium dynamics and anisotropic reentry in isolated canine pulmonary veins and left atrium. Circulation. 2005; 111:2889–2897. CIRCULATIONAHA.104.498758 [pii] 10.1161/CIRCULATIONAHA.104.498758. [PubMed: 15927973]
37. Ciurea D, Gil J. Morphometry of capillaries in three zones of rabbit lungs fixed by vascular perfusion. Anat Rec. 1996; 244:182–192. 10.1002/(SICI)1097-0185(199602)244:2<182::AID-AR6>3.0.CO;2-3 [pii] 10.1002/(SICI)1097-0185(199602)244:2<182::AID-AR6>3.0.CO;2-3. [PubMed: 8808393]
38. Coalson JJ, King RJ, Winter VT, Prihoda TJ, Anzueto AR, Peters JI, Johanson WG Jr. O_2- and pneumonia-induced lung injury. I. Pathological and morphometric studies. J Appl Physiol. 1989; 67:346–356. [PubMed: 2759963]
39. Coflesky JT, Jones RC, Reid LM, Evans JN. Mechanical properties and structure of isolated pulmonary arteries remodeled by chronic hyperoxia. Am Rev Respir Dis. 1987; 136:388–394. [PubMed: 3619198]
40. Coulombe PA, Cote MG. Application of linear integration in the morphometric study of mild and severe pulmonary alveolar injury. Exp Mol Pathol. 1988; 48:77–96. [PubMed: 3335253]
41. Coutu P, Chartier D, Nattel S. Comparison of Ca^{2+}-handling properties of canine pulmonary vein and left atrial cardiomyocytes. Am J Physiol Heart Circ Physiol. 2006; 291:H2290–2300. 00730.2005 [pii] 10.1152/ajpheart.00730.2005. [PubMed: 16798822]
42. Cowan KN, Heilbut A, Humpl T, Lam C, Ito S, Rabinovitch M. Complete reversal of fatal pulmonary hypertension in rats by a serine elastase inhibitor. Nat Med. 2000; 6:698–702. 10.1038/76282. [PubMed: 10835689]
43. Crapo JD, Barry BE, Foscue HA, Shelburne J. Structural and biochemical changes in rat lungs occurring during exposures to lethal and adaptive doses of oxygen. Am Rev Respir Dis. 1980; 122:123–143. [PubMed: 7406333]
44. Crapo JD, Barry BE, Gehr P, Bachofen M, Weibel ER. Cell number and cell characteristics of the normal human lung. Am Rev Respir Dis. 1982; 125:740–745. [PubMed: 7091881]
45. Crapo JD, Hayatdavoudi G, Knapp MJ, Fracica PJ, Wolfe WG, Piantadosi CA. Progressive alveolar septal injury in primates exposed to 60% oxygen for 14 days. Am J Physiol. 1994; 267:L797–806. [PubMed: 7810684]
46. Crapo JD, Marsh-Salin J, Ingram P, Pratt PC. Tolerance and cross-tolerance using NO2 and O2 II. Pulmonary morphology and morphometry. J Appl Physiol. 1978; 44:370–379. [PubMed: 632178]

47. Crapo JD, Young SL, Fram EK, Pinkerton KE, Barry BE, Crapo RO. Morphometric characteristics of cells in the alveolar region of mammalian lungs. Am Rev Respir Dis. 1983; 128:S42–46. [PubMed: 6881707]
48. Culver BH, Butler J. Mechanical influences on the pulmonary microcirculation. Annu Rev Physiol. 1980; 42:187–198. 10.1146/annurev.ph.42.030180.001155. [PubMed: 6996579]
49. Davidson JM. Biochemistry and turnover of lung interstitium. Eur Respir J. 1990; 3:1048–1063. [PubMed: 2289553]
50. Davies P, Burke G, Reid L. The structure of the wall of the rat intraacinar pulmonary artery: an electron microscopic study of microdissected preparations. Microvasc Res. 1986; 32:50–63. 0026-2862(86)90043-9 [pii]. [PubMed: 3736448]
51. Davies P, Maddalo F, Reid L. Effects of chronic hypoxia on structure and reactivity of rat lung microvessels. J Appl Physiol. 1985; 58:795–801. [PubMed: 3980385]
52. Davies P, McBride J, Murray GF, Wilcox BR, Shallal JA, Reid L. Structural changes in the canine lung and pulmonary arteries after pneumonectomy. J Appl Physiol. 1982; 53:859–864. [PubMed: 7153121]
53. Davies PF, Olesen SP, Clapham DE, Morrel EM, Schoen FJ. Endothelial communication. State of the art lecture. Hypertension. 1988; 11:563–572. [PubMed: 2455686]
54. DeFouw DO. Structural heterogeneity within the pulmonary microcirculation of the normal rat. Anat Rec. 1988; 221:645–654. 10.1002/ar.1092210210. [PubMed: 3414986]
55. DeFouw DO. Vesicle numerical densities and cellular attenuation: comparisons between endothelium and epithelium of the alveolar septa in normal dog lungs. Anat Rec. 1984; 209:77–84. 10.1002/ar.1092090110. [PubMed: 6731872]
56. DeFouw DO, Chinard FP. Variations in cellular attenuation and vesicle numerical densities in capillary endothelium and type I epithelium of isolated, perfused dog lungs after acute severe edema formation. Microvasc Res. 1983; 26:15–26. [PubMed: 6310353]
57. DeFouw DO, Shumko JZ. Pulmonary microcirculation: differences in endothelia of subpleural and alveolar capillaries. Microvasc Res. 1986; 32:348–358. [PubMed: 3796307]
58. deMello, DE.; Reid, LM. Arteries and veins.. In: Crystal, RG.; West, JB.; Weibel, ER.; Barnes, PJ., editors. The lung: scientific foundations. Lippincott-Raven; Philadelphia: 1997. p. 1117-1127.
59. Dey RD, Shannon WA Jr. Said SI. Localization of VIP-immunoreactive nerves in airways and pulmonary vessels of dogs, cat, and human subjects. Cell Tissue Res. 1981; 220:231–238. [PubMed: 7296630]
60. Dornan JC, Meban C. The capillary plexus in the gas exchange zone of human neonatal lung: an ultrastructural study. Thorax. 1985; 40:787–792. [PubMed: 4060099]
61. Dunsmore SE, Rannels DE. Extracellular matrix biology in the lung. Am J Physiol. 1996; 270:L3–27. [PubMed: 8772523]
62. Durmowicz AG, Hofmeister S, Kadyraliev TK, Aldashev AA, Stenmark KR. Functional and structural adaptation of the yak pulmonary circulation to residence at high altitude. J Appl Physiol. 1993; 74:2276–2285. [PubMed: 8335557]
63. Effros RM, Parker JC. Pulmonary vascular heterogeneity and the Starling hypothesis. Microvasc Res. 2009; 78:71–77. S0026-2862(09)00088-0 [pii] 10.1016/j.mvr.2009.03.004. [PubMed: 19332080]
64. El-Bermani AW. Pulmonary noradrenergic innervation of rat and monkey: a comparative study. Thorax. 1978; 33:167–174. [PubMed: 96545]
65. El-Bermani AW, Bloomquist EI, Montvilo JA. Distribution of pulmonary cholinergic nerves in the rabbit. Thorax. 1982; 37:703–710. [PubMed: 7157224]
66. El-Bizri N, Wang L, Merklinger SL, Guignabert C, Desai T, Urashima T, Sheikh AY, Knutsen RH, Mecham RP, Mishina Y, Rabinovitch M. Smooth muscle protein 22α-mediated patchy deletion of *Bmpr1a* impairs cardiac contractility but protects against pulmonary vascular remodeling. Circ Res. 2008; 102:380–388. CIRCRESAHA.107.161059 [pii] 10.1161/CIRCRESAHA.107.161059. [PubMed: 18079409]
67. Elliott FM, Reid L. Some new facts about the pulmonary artery and its branching pattern. Clin Radiol. 1965; 16:193–198. [PubMed: 14324878]

68. Endo H, Kurohmaru M, Nishida T, Hattori S, Hayashi Y. Cardiac musculature of the intrapulmonary vein in the musk shrew. J Vet Med Sci. 1992; 54:119–123. [PubMed: 1558874]
69. Endo H, Mifune H, Maeda S, Kimura J, Yamada J, Rerkamnuaychoke W, Chungsamarnyart N, Ogawa K, Kurohmaru M, Hayashi Y, Nishida T. Cardiac-like musculature of the intrapulmonary venous wall of the long-clawed shrew (Sorex unguiculatus), common tree shrew (Tupaia glis) and common marmoset (Callithrix jacchus). Anat Rec. 1997; 247:46–52. 10.1002/(SICI)1097-0185(199701)247:1<46::AID-AR7>3.0.CO;2-D [pii]. [PubMed: 8986302]
70. Fillenz M. Innervation of pulmonary and bronchial blood vessels of the dog. J Anat. 1970; 106:449–461. [PubMed: 4193092]
71. Fillenz M. Innervation of pulmonary capillaries. Experientia. 1969; 25:842. [PubMed: 5348547]
72. Forrest JB, Weibel ER. Morphometric estimation of pulmonary diffusion capacity. VII. The normal Guinea pig lung. Respir Physiol. 1975; 24:191–202. [PubMed: 1179048]
73. Fox B, Bull TB, Guz A. Innervation of alveolar walls in the human lung: an electron microscopic study. J Anat. 1980; 131:683–692. [PubMed: 7216905]
74. Fracica PJ, Caminiti SP, Piantadosi CA, Duhaylongsod FG, Crapo JD, Young SL. Natural surfactant and hyperoxic lung injury in primates. II. Morphometric analyses. J Appl Physiol. 1994; 76:1002–1010. [PubMed: 8005838]
75. Frey U, Hislop A, Silverman M. Branching properties of the pulmonary arterial tree during pre- and postnatal development. Respir Physiol Neurobiol. 2004; 139:179–189. 10.1016/j.resp.2003.09.010 S1569904803002465 [pii]. [PubMed: 15123001]
76. Frid MG, Moiseeva EP, Stenmark KR. Multiple phenotypically distinct smooth muscle cell populations exist in the adult and developing bovine pulmonary arterial media in vivo. Circ Res. 1994; 75:669–681. [PubMed: 7923613]
77. Fry GN, Devine CE, Burnstock G. Freeze-fracture studies of nexuses between smooth muscle cells. Close relationship to sarcoplasmic reticulum. J Cell Biol. 1977; 72:26–34. [PubMed: 401506]
78. Fung YC, Sobin SS, Tremer H, Yen MR, Ho HH. Patency and compliance of pulmonary veins when airway pressure exceeds blood pressure. J Appl Physiol. 1983; 54:1538–1549. [PubMed: 6874475]
79. Gan RZ, Tian Y, Yen RT, Kassab GS. Morphometry of the dog pulmonary venous tree. J Appl Physiol. 1993; 75:432–440. [PubMed: 8376295]
80. Gan RZ, Yen RT. Vascular impedance analysis in dog lung with detailed morphometric and elasticity data. J Appl Physiol. 1994; 77:706–717. [PubMed: 8002518]
81. Gao Y, Raj JU. Role of veins in regulation of pulmonary circulation. Am J Physiol Lung Cell Mol Physiol. 2005; 288:L213–226. 288/2/L213 [pii] 10.1152/ajplung.00103.2004. [PubMed: 15640520]
82. Gebb S, Stevens T. On lung endothelial cell heterogeneity. Microvasc Res. 2004; 68:1–12. 10.1016/j.mvr.2004.02.002 S0026286204000329 [pii]. [PubMed: 15219415]
83. Gebrane-Younes J, Drouet L, Caen JP, Orcel L. Heterogeneous distribution of Weibel-Palade bodies and von Willebrand factor along the porcine vascular tree. Am J Pathol. 1991; 139:1471–1484. [PubMed: 1750513]
84. Gehr P, Bachofen M, Weibel ER. The normal human lung: ultrastructure and morphometric estimation of diffusion capacity. Respir Physiol. 1978; 32:121–140. [PubMed: 644146]
85. Gehr P, Erni H. Morphometric estimation of pulmonary diffusion capacity in two horse lungs. Respir Physiol. 1980; 41:199–210. [PubMed: 7433781]
86. Gehr P, Mwangi DK, Ammann A, Maloiy GM, Taylor CR, Weibel ER. Design of the mammalian respiratory system. V. Scaling morphometric pulmonary diffusing capacity to body mass: wild and domestic mammals. Respir Physiol. 1981; 44:61–86. [PubMed: 7232887]
87. Geiser M, Zimmermann B, Baumann M, Cruz-Orive LM. Does lack of Cftr gene lead to developmental abnormalities in the lung? Exp Lung Res. 2000; 26:551–564. [PubMed: 11076312]
88. Gherghiceanu M, Hinescu ME, Andrei F, Mandache E, Macarie CE, Faussone-Pellegrini MS, Popescu LM. Interstitial Cajal-like cells (ICLC) in myocardial sleeves of human pulmonary veins. J Cell Mol Med. 2008; 12:1777–1781. JCMM444 [pii] 10.1111/j.1582-4934.2008.00444.x. [PubMed: 18671760]

89. Gibbins IL. Lack of correlation between ultrastructural and pharmacological types of non-adrenergic autonomic nerves. Cell Tissue Res. 1982; 221:551–581. [PubMed: 6276003]

90. Gibbins IL, Morris JL. Pathway specific expression of neuropeptides and autonomic control of the vasculature. Regul Pept. 2000; 93:93–107. S0167011500001816 [pii]. [PubMed: 11033057]

91. Gil J. The normal lung circulation. State of the art. Chest. 1988; 93:80S–82S. [PubMed: 3277820]

92. Gil J, McNiff JM. Interstitial cells at the boundary between alveolar and extraalveolar connective tissue in the lung. J Ultrastruct Res. 1981; 76:149–157. [PubMed: 7299895]

93. Gil J, Silage DA, McNiff JM. Distribution of vesicles in cells of air-blood barrier in the rabbit. J Appl Physiol. 1981; 50:334–340. [PubMed: 7204207]

94. Glazier JB, Hughes JM, Maloney JE, West JB. Measurements of capillary dimensions and blood volume in rapidly frozen lungs. J Appl Physiol. 1969; 26:65–76. [PubMed: 5762878]

95. Godbey PS, Graham JA, Presson RG Jr. Wagner WW Jr. Lloyd TC Jr. Effect of capillary pressure and lung distension on capillary recruitment. J Appl Physiol. 1995; 79:1142–1147. [PubMed: 8567555]

96. Guembe L, Villaro AC. Histochemical demonstration of neuronal nitric oxide synthase during development of mouse respiratory tract. Am J Respir Cell Mol Biol. 1999; 20:342–351. [PubMed: 9922227]

97. Guntheroth WG, Luchtel DL, Kawabori I. Functional implications of the pulmonary microcirculation. An update. Chest. 1992; 101:1131–1134. [PubMed: 1555432]

98. Guntheroth WG, Luchtel DL, Kawabori I. Pulmonary microcirculation: tubules rather than sheet and post. J Appl Physiol. 1982; 53:510–515. [PubMed: 7118671]

99. Haberberger R, Schemann M, Sann H, Kummer W. Innervation pattern of guinea pig pulmonary vasculature depends on vascular diameter. J Appl Physiol. 1997; 82:426–434. [PubMed: 9049720]

100. Haies DM, Gil J, Weibel ER. Morphometric study of rat lung cells. I. Numerical and dimensional characteristics of parenchymal cell population. Am Rev Respir Dis. 1981; 123:533–541. [PubMed: 7015935]

101. Hale KA, Ewing SL, Gosnell BA, Niewoehner DE. Lung disease in long-term cigarette smokers with and without chronic air-flow obstruction. Am Rev Respir Dis. 1984; 130:716–721. [PubMed: 6497154]

102. Hales CA, Kradin RL, Brandstetter RD, Zhu YJ. Impairment of hypoxic pulmonary artery remodeling by heparin in mice. Am Rev Respir Dis. 1983; 128:747–751. [PubMed: 6226226]

103. Hall SM, Haworth SG. Normal adaptation of pulmonary arterial intima to extrauterine life in the pig: ultrastructural studies. J Pathol. 1986; 149:55–66. 10.1002/path.1711490111. [PubMed: 3723227]

104. Harhun MI, Pucovsky V, Povstyan OV, Gordienko DV, Bolton TB. Interstitial cells in the vasculature. J Cell Mol Med. 2005; 9:232–243. 009.002.02 [pii]. [PubMed: 15963246]

105. Harris P, Heath D, Apostolopoulos A. Extensibility of the human pulmonary trunk. Br Heart J. 1965; 27:651–659. [PubMed: 5829747]

106. Hashizume H, Tango M, Ushiki T. Three-dimensional cytoarchitecture of rat pulmonary venous walls: a light and scanning electron microscopic study. Anat Embryol (Berl). 1998; 198:473–480. [PubMed: 9833686]

107. Hassink RJ, Aretz HT, Ruskin J, Keane D. Morphology of atrial myocardium in human pulmonary veins: a postmortem analysis in patients with and without atrial fibrillation. J Am Coll Cardiol. 2003; 42:1108–1114. S0735109703009185 [pii]. [PubMed: 13678939]

108. Haworth SG, Hislop AA. Pulmonary vascular development: normal values of peripheral vascular structure. Am J Cardiol. 1983; 52:578–583. 0002-9149(83)90030-9 [pii]. [PubMed: 6613881]

109. Hayatdavoudi G, O'Neil JJ, Barry BE, Freeman BA, Crapo JD. Pulmonary injury in rats following continuous exposure to 60% O_2 for 7 days. J Appl Physiol. 1981; 51:1220–1231. [PubMed: 6457819]

110. Heath D, Smith P. The pulmonary endothelial cell. Thorax. 1979; 34:200–208. [PubMed: 483185]

111. Heath D, Smith P, Williams D, Harris P, Arias-Stella J, Kruger H. The heart and pulmonary vasculature of the llama (Lama glama). Thorax. 1974; 29:463–471. [PubMed: 4854860]

112. Heath D, Wood EH, Dushane JW, Edwards JE. The structure of the pulmonary trunk at different ages and in cases of pulmonary hypertension and pulmonary stenosis. J Pathol Bacteriol. 1959; 77:443–456. [PubMed: 13642192]
113. Hirschi KK, D'Amore PA. Pericytes in the microvasculature. Cardiovasc Res. 1996; 32:687–698. 0008636396000636 [pii]. [PubMed: 8915187]
114. Hislop A, Reid L. Development of the acinus in the human lung. Thorax. 1974; 29:90–94. [PubMed: 4825556]
115. Hislop A, Reid L. Normal structure and dimensions of the pulmonary arteries in the rat. J Anat. 1978; 125:71–83. [PubMed: 632217]
116. Hislop A, Reid L. Pulmonary arterial development during childhood: branching pattern and structure. Thorax. 1973; 28:129–135. [PubMed: 4731102]
117. Ho SY, Cabrera JA, Tran VH, Farre J, Anderson RH, Sanchez-Quintana D. Architecture of the pulmonary veins: relevance to radiofrequency ablation. Heart. 2001; 86:265–270. [PubMed: 11514476]
118. Horsfield K. Axial pathways compared with complete data in morphological studies of the lung. Respir Physiol. 1984; 55:317–324. [PubMed: 6739988]
119. Horsfield K. Morphometry of the small pulmonary arteries in man. Circ Res. 1978; 42:593–597. [PubMed: 639181]
120. Horsfield K, Gordon WI. Morphometry of pulmonary veins in man. Lung. 1981; 159:211–218. [PubMed: 7289655]
121. Horsfield K, Thomas M. Morphometry of pulmonary arteries from angiograms in chronic obstructive lung disease. Thorax. 1981; 36:360–365. [PubMed: 7314005]
122. Howell K, Preston RJ, McLoughlin P. Chronic hypoxia causes angiogenesis in addition to remodelling in the adult rat pulmonary circulation. J Physiol. 2003; 547:133–145. 10.1113/jphysiol.2002.030676 2002.030676 [pii]. [PubMed: 12562951]
123. Hsia CC, Hyde DM, Ochs M, Weibel ER. How to measure lung structure--what for? On the "Standards for the quantitative assessment of lung structure". Respir Physiol Neurobiol. 2010; 171:72–74. S1569-9048(10)00062-5 [pii] 10.1016/j.resp.2010.02.016. [PubMed: 20206304]
124. Hsia CC, Hyde DM, Ochs M, Weibel ER. An official research policy statement of the American Thoracic Society/European Respiratory Society: standards for quantitative assessment of lung structure. Am J Respir Crit Care Med. 2010; 181:394–418. 181/4/394 [pii] 10.1164/rccm.200809-1522ST. [PubMed: 20130146]
125. Hsia CC, Johnson RL Jr. Further examination of alveolar septal adaptation to left pneumonectomy in the adult lung. Respir Physiol Neurobiol. 2006; 151:167–177. S1569-9048(06)00032-2 [pii] 10.1016/j.resp.2006.01.013. [PubMed: 16563882]
126. Hu LM, Jones R. Injury and remodeling of pulmonary veins by high oxygen. A morphometric study. Am J Pathol. 1989; 134:253–262. [PubMed: 2521773]
127. Huang W, Yen RT, McLaurine M, Bledsoe G. Morphometry of the human pulmonary vasculature. J Appl Physiol. 1996; 81:2123–2133. [PubMed: 8941537]
128. Hung KS, Hertweck MS, Hardy JD, Loosli CG. Electron microscopic observations of nerve endings in the alveolar walls of mouse lungs. Am Rev Respir Dis. 1973; 108:328–333. [PubMed: 4720694]
129. Hung KS, Hertweck MS, Hardy JD, Loosli CG. Innervation of pulmonary alveoli of the mouse lung: an electron microscopic study. Am J Anat. 1972; 135:477–495. 10.1002/aja.1001350404. [PubMed: 4637867]
130. Hyde DM, Tyler NK, Plopper CG. Morphometry of the respiratory tract: avoiding the sampling, size, orientation, and reference traps. Toxicol Pathol. 2007; 35:41–48. 770780166 [pii] 10.1080/01926230601059977. [PubMed: 17325971]
131. Hyde DM, Tyler NK, Putney LF, Singh P, Gundersen HJ. Total number and mean size of alveoli in mammalian lung estimated using fractionator sampling and unbiased estimates of the Euler characteristic of alveolar openings. Anat Rec A Discov Mol Cell Evol Biol. 2004; 277:216–226. 10.1002/ar.a.20012. [PubMed: 14983516]
132. Ilkiw R, Todorovich-Hunter L, Maruyama K, Shin J, Rabinovitch M. SC-39026, a serine elastase inhibitor, prevents muscularization of peripheral arteries, suggesting a mechanism of

monocrotaline-induced pulmonary hypertension in rats. Circ Res. 1989; 64:814–825. [PubMed: 2495195]

133. Jaenke RS, Alexander AF. Fine structural alterations of bovine peripheral pulmonary arteries in hypoxia-induced hypertension. Am J Pathol. 1973; 73:377–398. [PubMed: 4357176]
134. Jiang Y, Dai A, Li Q, Hu R. Hypoxia induces transforming growth factor-β1 gene expression in the pulmonary artery of rats via hypoxia-inducible factor-1α. Acta Biochim Biophys Sin (Shanghai). 2007; 39:73–80. [PubMed: 17213961]
135. Jiang ZL, Kassab GS, Fung YC. Diameter-defined Strahler system and connectivity matrix of the pulmonary arterial tree. J Appl Physiol. 1994; 76:882–892. [PubMed: 8175603]
136. Johnson JE, Perkett EA, Meyrick B. Pulmonary veins and bronchial vessels undergo remodeling in sustained pulmonary hypertension induced by continuous air embolization into sheep. Exp Lung Res. 1997; 23:459–473. [PubMed: 9267799]
137. Jones R. Ultrastructural analysis of contractile cell development in lung microvessels in hyperoxic pulmonary hypertension. Fibroblasts and intermediate cells selectively reorganize nonmuscular segments. Am J Pathol. 1992; 141:1491–1505. [PubMed: 1466406]
138. Jones R, Jacobson M, Steudel W. α-Smooth-muscle actin and microvascular precursor smooth-muscle cells in pulmonary hypertension. Am J Respir Cell Mol Biol. 1999; 20:582–594. [PubMed: 10100989]
139. Jones R, Kirton OC. Lung microvessel injury from peritoneal abscesses and gram-negative bacteremia. Microvasc Res. 1996; 52:84–100. S0026-2862(96)90046-1 [pii] 10.1006/mvre.1996.0046. [PubMed: 8812762]
140. Jones R, Zapol WM, Reid L. Oxygen toxicity and restructuring of pulmonary arteries--a morphometric study. The response to 4 weeks' exposure to hyperoxia and return to breathing air. Am J Pathol. 1985; 121:212–223. [PubMed: 2932915]
141. Jones R, Zapol WM, Reid L. Pulmonary artery remodeling and pulmonary hypertension after exposure to hyperoxia for 7 days. A morphometric and hemodynamic study. Am J Pathol. 1984; 117:273–285. [PubMed: 6238536]
142. Jones SA, Yamamoto M, Tellez JO, Billeter R, Boyett MR, Honjo H, Lancaster MK. Distinguishing properties of cells from the myocardial sleeves of the pulmonary veins: a comparison of normal and abnormal pacemakers. Circ Arrhythm Electrophysiol. 2008; 1:39–48. 1/1/39 [pii] 10.1161/CIRCEP.107.748467. [PubMed: 19808392]
143. Jones WK, Sanchez A, Robbins J. Murine pulmonary myocardium: developmental analysis of cardiac gene expression. Dev Dyn. 1994; 200:117–128. 10.1002/aja.1002000204. [PubMed: 7919499]
144. Kadowitz PJ, Knight DS, Hibbs RG, Ellison JP, Joiner PD, Brody MJ, Hyman AL. Influence of 5- and 6-hydroxydopamine on adrenergic transmission and nerve terminal morphology in the canine pulmonary vascular bed. Circ Res. 1976; 39:191–199. [PubMed: 181163]
145. Kalk J, Benjamin J, Comite H, Hutchins G, Traystman R, Menkes H. Vascular interdependence in postmortem human lungs. Am Rev Respir Dis. 1975; 112:505–511. [PubMed: 1200485]
146. Kapanci, Y.; Gabbiani, G. Contractile cells in pulmonary alveolar tissue.. In: Crystal, RC.; West, JB.; Barnes, PJ.; Weibel, ER., editors. The lung: Scientific foundations. Lippincott-Raven Publishers; Philadelphia: 1997. p. 697-707.
147. Kapanci Y, Ribaux C, Chaponnier C, Gabbiani G. Cytoskeletal features of alveolar myofibroblasts and pericytes in normal human and rat lung. J Histochem Cytochem. 1992; 40:1955–1963. [PubMed: 1333502]
148. Kaplan NB, Grant MM, Brody JS. The lipid interstitial cell of the pulmonary alveolus. Age and species differences. Am Rev Respir Dis. 1985; 132:1307–1312. [PubMed: 3000236]
149. Karau KL, Johnson RH, Molthen RC, Dhyani AH, Haworth ST, Hanger CC, Roerig DL, Dawson CA. Microfocal X-ray CT imaging and pulmonary arterial distensibility in excised rat lungs. Am J Physiol Heart Circ Physiol. 2001; 281:H1447–1457. [PubMed: 11514318]
150. Karau KL, Molthen RC, Dhyani A, Haworth ST, Hanger CC, Roerig DL, Johnson RH, Dawson CA. Pulmonary arterial morphometry from microfocal X-ray computed tomography. Am J Physiol Heart Circ Physiol. 2001; 281:H2747–2756. [PubMed: 11709444]

151. Karrer HE. The striated musculature of blood vessels. I. General cell morphology. J Biophys Biochem Cytol. 1959; 6:383–392. [PubMed: 14404587]

152. Kay JM. Comparative morphologic features of the pulmonary vasculature in mammals. Am Rev Respir Dis. 1983; 128:S53–57. [PubMed: 6881709]

153. Kim H, Yung GL, Marsh JJ, Konopka RG, Pedersen CA, Chiles PG, Morris TA, Channick RN. Endothelin mediates pulmonary vascular remodelling in a canine model of chronic embolic pulmonary hypertension. Eur Respir J. 2000; 15:640–648. [PubMed: 10780753]

154. Kim H, Yung GL, Marsh JJ, Konopka RG, Pedersen CA, Chiles PG, Morris TA, Channick RN. Pulmonary vascular remodeling distal to pulmonary artery ligation is accompanied by upregulation of endothelin receptors and nitric oxide synthase. Exp Lung Res. 2000; 26:287–301. [PubMed: 10923246]

155. King J, Hamil T, Creighton J, Wu S, Bhat P, McDonald F, Stevens T. Structural and functional characteristics of lung macro- and microvascular endothelial cell phenotypes. Microvasc Res. 2004; 67:139–151. 10.1016/j.mvr.2003.11.006 S002628620300116X [pii]. [PubMed: 15020205]

156. Kistler GS, Caldwell PR, Weibel ER. Development of fine structural damage to alveolar and capillary lining cells in oxygen-poisoned rat lungs. J Cell Biol. 1967; 32:605–628. [PubMed: 6034481]

157. Klavins JV. Demonstration of striated muscle in the pulmonary veins of the rat. J Anat. 1963; 97:239–241. [PubMed: 14033309]

158. Knight DS, Ellison JP, Hibbs RG, Hyman AL, Kadowitz PJ. A light and electron microscopic study of the innervation of pulmonary arteries in the cat. Anat Rec. 1981; 201:513–521. 10.1002/ar.1092010308. [PubMed: 7305032]

159. Knust J, Ochs M, Gundersen HJ, Nyengaard JR. Stereological estimates of alveolar number and size and capillary length and surface area in mice lungs. Anat Rec (Hoboken). 2009; 292:113–122. 10.1002/ar.20747. [PubMed: 19115381]

160. Ko YS, Yeh HI, Rothery S, Dupont E, Coppen SR, Severs NJ. Connexin make-up of endothelial gap junctions in the rat pulmonary artery as revealed by immunoconfocal microscopy and triple-label immunogold electron microscopy. J Histochem Cytochem. 1999; 47:683–692. [PubMed: 10219060]

161. Kwon KY, Park KK, Chang ES. Scanning electron microscopic study of capillary change in bleomycin-induced pulmonary fibrosis. J Korean Med Sci. 1991; 6:234–245. [PubMed: 1723279]

162. LaBourene JI, Coles JG, Johnson DJ, Mehra A, Keeley FW, Rabinovitch M. Alterations in elastin and collagen related to the mechanism of progressive pulmonary venous obstruction in a piglet model. A hemodynamic, ultrastructural, and biochemical study. Circ Res. 1990; 66:438–456. [PubMed: 2297812]

163. Laitinen, LA.; Laitinen, A. Neural system.. In: Crystal, RC.; West, JB.; Weibel, ER.; Barnes, PJ., editors. The lung: scientific foundations. Lippincott-Raven; Philadelphia: 1997. p. 1107-1116.

164. Larsen TH, Saetersdal T, Rumyantsev PP. Striated myocytes and atrial specific granules in the pulmonary veins of chronically infarcted rat hearts. Res Exp Med (Berl). 1987; 187:225–236. [PubMed: 3616140]

165. Laurent GJ. Lung collagen: more than scaffolding. Thorax. 1986; 41:418–428. [PubMed: 3024347]

166. Laurent GJ. Rates of collagen synthesis in lung, skin and muscle obtained in vivo by a simplified method using [^{3}H]proline. Biochem J. 1982; 206:535–544. [PubMed: 7150261]

167. Le Cras TD, Fernandez LG, Pastura PA, Laubach VE. Vascular growth and remodeling in compensatory lung growth following right lobectomy. J Appl Physiol. 2005; 98:1140–1148. 00479.2004 [pii] 10.1152/japplphysiol.00479.2004. [PubMed: 15516366]

168. Littler CM, Wehling CA, Wick MJ, Fagan KA, Cool CD, Messing RO, Dempsey EC. Divergent contractile and structural responses of the murine PKC-epsilon null pulmonary circulation to chronic hypoxia. Am J Physiol Lung Cell Mol Physiol. 2005; 289:L1083–1093. 00472.2004 [pii] 10.1152/ajplung.00472.2004. [PubMed: 16085670]

169. Long L, MacLean MR, Jeffery TK, Morecroft I, Yang X, Rudarakanchana N, Southwood M, James V, Trembath RC, Morrell NW. Serotonin increases susceptibility to pulmonary

hypertension in BMPR2-deficient mice. Circ Res. 2006; 98:818–827. 01.RES.0000215809.47923.fd [pii] 10.1161/01.RES.0000215809.47923.fd. [PubMed: 16497988]

170. Ludatscher RM. Fine structure of the muscular wall of rat pulmonary veins. J Anat. 1968; 103:345–357. [PubMed: 4879653]
171. Luts A, Sundler F. Peptide-containing nerve fibers in the respiratory tract of the ferret. Cell Tissue Res. 1989; 258:259–267. [PubMed: 2582477]
172. Mackay EH, Banks J, Sykes B, Lee G. Structural basis for the changing physical properties of human pulmonary vessels with age. Thorax. 1978; 33:335–344. [PubMed: 684670]
173. Macklin CC. Evidences of increase in the capacity of the pulmonary arteries and veins of dogs, cats and rabbits during inflation of the freshly excised lung. Rev Can Biol. 1946; 5:199–232. [PubMed: 20983227]
174. Magee F, Wright JL, Wiggs BR, Pare PD, Hogg JC. Pulmonary vascular structure and function in chronic obstructive pulmonary disease. Thorax. 1988; 43:183–189. [PubMed: 3406902]
175. Maina JN. The morphology and morphometry of the adult normal baboon lung (Papio anubis). J Anat. 1987; 150:229–245. [PubMed: 3654336]
176. Maina JN, van Gils P. Morphometric characterization of the airway and vascular systems of the lung of the domestic pig, Sus scrofa: comparison of the airway, arterial and venous systems. Comp Biochem Physiol A Mol Integr Physiol. 2001; 130:781–798. S1095-6433(01)00411-1 [pii]. [PubMed: 11691614]
177. Mandache E, Popescu LM, Gherghiceanu M. Myocardial interstitial Cajal-like cells (ICLC) and their nanostructural relationships with intercalated discs: shed vesicles as intermediates. J Cell Mol Med. 2007; 11:1175–1184. JCMM117 [pii] 10.1111/j.1582-4934.2007.00117.x. [PubMed: 17979892]
178. Martling CR, Matran R, Alving K, Hokfelt T, Lundberg JM. Innervation of lower airways and neuropeptide effects on bronchial and vascular tone in the pig. Cell Tissue Res. 1990; 260:223–233. [PubMed: 1694104]
179. Masani F. Node-like cells in the myocardial layer of the pulmonary vein of rats: an ultrastructural study. J Anat. 1986; 145:133–142. [PubMed: 3429299]
180. Mastin JP, Shelburne JD, Thet LA. Subcellular changes in capillary endothelial cells during repair of hyperoxic lung injury. J Appl Physiol. 1988; 64:689–696. [PubMed: 3372427]
181. Mayhew TM, Muhlfeld C, Vanhecke D, Ochs M. A review of recent methods for efficiently quantifying immunogold and other nanoparticles using TEM sections through cells, tissues and organs. Ann Anat. 2009; 191:153–170. S0940-9602(08)00157-X [pii] 10.1016/j.aanat.2008.11.001. [PubMed: 19135344]
182. Mays PK, McAnulty RJ, Campa JS, Laurent GJ. Age-related changes in collagen synthesis and degradation in rat tissues. Importance of degradation of newly synthesized collagen in regulating collagen production. Biochem J. 1991; 276(Pt 2):307–313. [PubMed: 2049064]
183. Mazzone RW. Influence of vascular and transpulmonary pressures on the functional morphology of the pulmonary microcirculation. Microvasc Res. 1980; 20:295–306. [PubMed: 7207223]
184. Mazzone RW, Durand CM, West JB. Electron microscopy of lung rapidly frozen under controlled physiological conditions. J Appl Physiol. 1978; 45:325–333. [PubMed: 681218]
185. McAnulty RJ, Laurent GJ. Collagen synthesis and degradation in vivo. Evidence for rapid rates of collagen turnover with extensive degradation of newly synthesized collagen in tissues of the adult rat. Coll Relat Res. 1987; 7:93–104. [PubMed: 3497767]
186. McLaughlin RF Jr. Tyler WS, Canada RO. A study of the subgross pulmonary anatomy in various mammals. Am J Anat. 1961; 198:149–165.
187. McLaughlin RF Jr. Tyler WS, Canada RO. Subgross pulmonary anatomy of the rabbit, rat, and guinea pig, with additional notes on the human lung. Am Rev Respir Dis. 1966; 94:380–387. [PubMed: 5918216]
188. McNiff JM, Gil J. Secretion of Weibel-Palade bodies observed in extra-alveolar vessels of rabbit lung. J Appl Physiol. 1983; 54:1284–1286. [PubMed: 6863088]
189. Melnyk P, Ehrlich JR, Pourrier M, Villeneuve L, Cha TJ, Nattel S. Comparison of ion channel distribution and expression in cardiomyocytes of canine pulmonary veins versus left atrium.

Cardiovasc Res. 2005; 65:104–116. S0008-6363(04)00380-3 [pii] 10.1016/j.cardiores.2004.08.014. [PubMed: 15621038]

190. Mercer RR, Crapo JD. Spatial distribution of collagen and elastin fibers in the lungs. J Appl Physiol. 1990; 69:756–765. [PubMed: 2228886]
191. Mercer RR, Russell ML, Crapo JD. Alveolar septal structure in different species. J Appl Physiol. 1994; 77:1060–1066. [PubMed: 7836104]
192. Merklinger SL, Wagner RA, Spiekerkoetter E, Hinek A, Knutsen RH, Kabir MG, Desai K, Hacker S, Wang L, Cann GM, Ambartsumian NS, Lukanidin E, Bernstein D, Husain M, Mecham RP, Starcher B, Yanagisawa H, Rabinovitch M. Increased fibulin-5 and elastin in S100A4/Mts1 mice with pulmonary hypertension. Circ Res. 2005; 97:596–604. 01.RES.0000182425.49768.8a [pii] 10.1161/01.RES.0000182425.49768.8a. [PubMed: 16109920]
193. Meyrick B. Structure function correlates in the pulmonary vasculature during acute lung injury and chronic pulmonary hypertension. Toxicol Pathol. 1991; 19:447–457. [PubMed: 1813988]
194. Meyrick B, Hislop A, Reid L. Pulmonary arteries of the normal rat: the thick walled oblique muscle segment. J Anat. 1978; 125:209–221. [PubMed: 624674]
195. Meyrick B, Reid L. The effect of continued hypoxia on rat pulmonary arterial circulation. An ultrastructural study. Lab Invest. 1978; 38:188–200. [PubMed: 146763]
196. Meyrick B, Reid L. Hypoxia-induced structural changes in the media and adventitia of the rat hilar pulmonary artery and their regression. Am J Pathol. 1980; 100:151–178. [PubMed: 7395963]
197. Meyrick B, Reid L. Intra-alveolar wall nerve in rat lung: an electron-microscopic study. J Physiol. 1971; 214:6P–7P.
198. Meyrick B, Reid L. Nerves in rat intra-acinar alveoli: an electron microscopic study. Respir Physiol. 1971; 11:367–377. [PubMed: 5552773]
199. Meyrick B, Reid L. Normal postnatal development of the media of the rat hilar pulmonary artery and its remodeling by chronic hypoxia. Lab Invest. 1982; 46:505–514. [PubMed: 7078094]
200. Meyrick B, Reid L. Ultrastructural features of the distended pulmonary arteries of the normal rat. Anat Rec. 1979; 193:71–97. 10.1002/ar.1091930106. [PubMed: 104638]
201. Meyrick B, Reid L. Ultrastructural findings in lung biopsy material from children with congenital heart defects. Am J Pathol. 1980; 101:527–542. [PubMed: 7446706]
202. Michel RP. Arteries and veins of the normal dog lung: qualitative and quantitative structural differences. Am J Anat. 1982; 164:227–241. 10.1002/aja.1001640304. [PubMed: 7124654]
203. Michel RP, Gordon JB, Chu K. Development of the pulmonary vasculature in newborn lambs: structure-function relationships. J Appl Physiol. 1991; 70:1255–1264. [PubMed: 2032991]
204. Michel RP, Hakim TS. Increased resistance in postobstructive pulmonary vasculopathy: structure-function relationships. J Appl Physiol. 1991; 71:601–610. [PubMed: 1938734]
205. Michel RP, Hu F, Meyrick BO. Myoendothelial junctional complexes in postobstructive pulmonary vasculopathy: a quantitative electron microscopic study. Exp Lung Res. 1995; 21:437–452. [PubMed: 7621779]
206. Michelakis ED, Weir EK, Wu X, Nsair A, Waite R, Hashimoto K, Puttagunta L, Knaus HG, Archer SL. Potassium channels regulate tone in rat pulmonary veins. Am J Physiol Lung Cell Mol Physiol. 2001; 280:L1138–1147. [PubMed: 11350792]
207. Miller AA, Hislop AA, Vallance PJ, Haworth SG. Deletion of the eNOS gene has a greater impact on the pulmonary circulation of male than female mice. Am J Physiol Lung Cell Mol Physiol. 2005; 289:L299–306. 00022.2005 [pii] 10.1152/ajplung.00022.2005. [PubMed: 15821017]
208. Millino C, Sarinella F, Tiveron C, Villa A, Sartore S, Ausoni S. Cardiac and smooth muscle cell contribution to the formation of the murine pulmonary veins. Dev Dyn. 2000; 218:414–425. 10.1002/1097-0177(200007)218:3<414::AID-DVDY1002>3.0.CO;2-H [pii] 10.1002/1097-0177(200007)218:3<414::AID-DVDY1002>3.0.CO;2-H. [PubMed: 10878607]
209. Mitani Y, Maruyama K, Sakurai M. Prolonged administration of L-arginine ameliorates chronic pulmonary hypertension and pulmonary vascular remodeling in rats. Circulation. 1997; 96:689–697. [PubMed: 9244244]

210. Miyamoto Y, Moll W. Measurements of dimensions and pathway of red cells in rapidly frozen lungs in situ. Respir Physiol. 1971; 12:141–156. [PubMed: 5568458]

211. Miyata M, Sakuma F, Ito M, Ohira H, Sato Y, Kasukawa R. Athymic nude rats develop severe pulmonary hypertension following monocrotaline administration. Int Arch Allergy Immunol. 2000; 121:246–252. iaa21246 [pii]. [PubMed: 10729784]

212. Molthen RC, Karau KL, Dawson CA. Quantitative models of the rat pulmonary arterial tree morphometry applied to hypoxia-induced arterial remodeling. J Appl Physiol. 2004; 97:2372–2384. 10.1152/japplphysiol.00454.2004 00454.2004 [pii]. [PubMed: 15333611]

213. Mommersteeg MT, Brown NA, Prall OW, de Gier-de Vries C, Harvey RP, Moorman AF, Christoffels VM. Pitx2c and Nkx2-5 are required for the formation and identity of the pulmonary myocardium. Circ Res. 2007; 101:902–909. CIRCRESAHA.107.161182 [pii] 10.1161/CIRCRESAHA.107.161182. [PubMed: 17823370]

214. Morel E, Meyronet D, Thivolet-Bejuy F, Chevalier P. Identification and distribution of interstitial Cajal cells in human pulmonary veins. Heart Rhythm. 2008; 5:1063–1067. S1547-5271(08)00346-9 [pii] 10.1016/j.hrthm.2008.03.057. [PubMed: 18598966]

215. Morrell NW, Morris KG, Stenmark KR. Role of angiotensin-converting enzyme and angiotensin II in development of hypoxic pulmonary hypertension. Am J Physiol. 1995; 269:H1186–1194. [PubMed: 7485548]

216. Mueller-Hoecker J, Beitinger F, Fernandez B, Bahlmann O, Assmann G, Troidl C, Dimomeletis I, Kaab S, Deindl E. Of rodents and humans: a light microscopic and ultrastructural study on cardiomyocytes in pulmonary veins. Int J Med Sci. 2008; 5:152–158. [PubMed: 18612369]

217. Mühlfeld C, Nyengaard JR, Mayhew TM. A review of state-of-the-art stereology for better quantitative 3D morphology in cardiac research. Cardiovasc Pathol. 2010; 19:65–82. S1054-8807(08)00161-0 [pii] 10.1016/j.carpath.2008.10.015. [PubMed: 19144544]

218. Mühlfeld C, Weibel ER, Hahn U, Kummer W, Nyengaard JR, Ochs M. Is length an appropriate estimator to characterize pulmonary alveolar capillaries? A critical evaluation in the human lung. Anat Rec (Hoboken). 2010; 293:1270–1275. 10.1002/ar.21158. [PubMed: 20583281]

219. Nathan H, Eliakim M. The junction between the left atrium and the pulmonary veins. An anatomic study of human hearts. Circulation. 1966; 34:412–422. [PubMed: 5922708]

220. Nathan H, Gloobe H. Myocardial atrio-venous junctions and extensions (sleeves) over the pulmonary and caval veins. Anatomical observations in various mammals. Thorax. 1970; 25:317–324. [PubMed: 5452285]

221. Nishi Y, Kitamura N, Otani M, Hondo E, Taguchi K, Yamada J. Distribution of capsaicin-sensitive substance P- and calcitonin gene-related peptide-immunoreactive nerves in bovine respiratory tract. Ann Anat. 2000; 182:319–326. [PubMed: 10932322]

222. Nohr D, Eiden LE, Weihe E. Coexpression of vasoactive intestinal peptide, calcitonin gene-related peptide and substance P immunoreactivity in parasympathetic neurons of the rhesus monkey lung. Neurosci Lett. 1995; 199:25–28. 030439409512001K [pii]. [PubMed: 8584218]

223. Nohr D, Weihe E. Tachykinin-, calcitonin gene-related peptide-, and protein gene product 9.5-immunoreactive nerve fibers in alveolar walls of mammals. Neurosci Lett. 1991; 134:17–20. 0304-3940(91)90498-I [pii]. [PubMed: 1840000]

224. Nyengaard JR, Gundersen HJ. Direct and efficient stereological estimation of total cell quantities using electron microscopy. J Microsc. 2006; 222:182–187. JMI1586 [pii] 10.1111/j.1365-2818.2006.01586.x. [PubMed: 16872417]

225. Ochs M. A brief update on lung stereology. J Microsc. 2006; 222:188–200. JMI1587 [pii] 10.1111/j.1365-2818.2006.01587.x. [PubMed: 16872418]

226. Ofori-Acquah SF, King J, Voelkel N, Schaphorst KL, Stevens T. Heterogeneity of barrier function in the lung reflects diversity in endothelial cell junctions. Microvasc Res. 2008; 75:391–402. S0026-2862(07)00122-7 [pii] 10.1016/j.mvr.2007.10.006. [PubMed: 18068735]

227. Ohar JA, Waller KS, Williams TJ, Luke DA, Demello DE. Computerized morphometry of the pulmonary vasculature over a range of intravascular pressures. Anat Rec. 1998; 252:92–101. 10.1002/(SICI)1097-0185(199809)252:1<92::AID-AR8>3.0.CO;2-G [pii]. [PubMed: 9737746]

228. Ohtani O. Microvasculature of the rat lung as revealed by scanning electron microscopy of corrosion casts. Scan Electron Microsc. 1980:349–356. [PubMed: 7414275]

229. Oldmixon EH, Hoppin FG Jr. Distribution of elastin and collagen in canine lung alveolar parenchyma. J Appl Physiol. 1989; 67:1941–1949. [PubMed: 2600027]

230. Paes de Almeida O, Bohm CM, de Paula Carvalho M, Paes de Carvalho A. The cardiac muscle in the pulmonary vein of the rat: a morphological and electrophysiological study. J Morphol. 1975; 145:409–433. 10.1002/jmor.1051450403. [PubMed: 1127702]

231. Palade GE, Simionescu M, Simionescu N. Structural aspects of the permeability of the microvascular endothelium. Acta Physiol Scand Suppl. 1979; 463:11–32. [PubMed: 382743]

232. Parker JC, Stevens T, Randall J, Weber DS, King JA. Hydraulic conductance of pulmonary microvascular and macrovascular endothelial cell monolayers. Am J Physiol Lung Cell Mol Physiol. 2006; 291:L30–37. 291/1/L30 [pii] 10.1152/ajplung.00317.2005. [PubMed: 16760315]

233. Peao MN, Aguas AP, de Sa CM, Grande NR. Identification of vascular sphincters at the junction between alveolar capillaries and pulmonary venules of the mouse lung. Anat Rec. 1995; 241:383–390. 10.1002/ar.1092410313. [PubMed: 7755178]

234. Perez-Lugones A, McMahon JT, Ratliff NB, Saliba WI, Schweikert RA, Marrouche NF, Saad EB, Navia JL, McCarthy PM, Tchou P, Gillinov AM, Natale A. Evidence of specialized conduction cells in human pulmonary veins of patients with atrial fibrillation. J Cardiovasc Electrophysiol. 2003; 14:803–809. 03075 [pii]. [PubMed: 12890038]

235. Perkett EA, Brigham KL, Meyrick B. Continuous air embolization into sheep causes sustained pulmonary hypertension and increased pulmonary vasoreactivity. Am J Pathol. 1988; 132:444–454. [PubMed: 3414777]

236. Pietra GG, Szidon JP, Leventhal MM, Fishman AP. Hemoglobin as a tracer in hemodynamic pulmonary edema. Science. 1969; 166:1643–1646. [PubMed: 5360588]

237. Plato M, Kummer W, Haberberger RV. Structural and neurochemical comparison of vagal and spinal afferent neurons projecting to the rat lung. Neurosci Lett. 2006; 395:215–219. S0304-3940(05)01261-9 [pii] 10.1016/j.neulet.2005.10.078. [PubMed: 16309834]

238. Plopper CG, Dungworth DL, Tyler WS. Morphometric evaluation of pulmonary lesions in rats exposed to ozone. Am J Pathol. 1973; 71:395–408. [PubMed: 4577265]

239. Popescu LM, Gherghiceanu M, Cretoiu D, Radu E. The connective connection: interstitial cells of Cajal (ICC) and ICC-like cells establish synapses with immunoreactive cells. Electron microscope study in situ. J Cell Mol Med. 2005; 9:714–730. 009.003.19 [pii]. [PubMed: 16202219]

240. Pump KK. The circulation in the peripheral parts of the human lung. Dis Chest. 1966; 49:119–129. [PubMed: 5907968]

241. Qi JG, Ding YG, Tang CS, Du JB. Chronic administration of adrenomedullin attenuates hypoxic pulmonary vascular structural remodeling and inhibits proadrenomedullin N-terminal 20-peptide production in rats. Peptides. 2007; 28:910–919. S0196-9781(06)00571-7 [pii] 10.1016/j.peptides.2006.12.008. [PubMed: 17267073]

242. Rabinovitch M, Haworth SG, Castaneda AR, Nadas AS, Reid LM. Lung biopsy in congenital heart disease: a morphometric approach to pulmonary vascular disease. Circulation. 1978; 58:1107–1122. [PubMed: 709766]

243. Racke K, Matthiesen S. The airway cholinergic system: physiology and pharmacology. Pulm Pharmacol Ther. 2004; 17:181–198. 10.1016/j.pupt.2004.03.001 S1094-5539(04)00023-9 [pii]. [PubMed: 15219263]

244. Randell SH, Mercer RR, Young SL. Neonatal hyperoxia alters the pulmonary alveolar and capillary structure of 40-day-old rats. Am J Pathol. 1990; 136:1259–1266. [PubMed: 2356858]

245. Rannels DE, Stockstill B, Mercer RR, Crapo JD. Cellular changes in the lungs of adrenalectomized rats following left pneumonectomy. Am J Respir Cell Mol Biol. 1991; 5:351–362. [PubMed: 1910820]

246. Ray L, Mathieu M, Jespers P, Hadad I, Mahmoudabady M, Pensis A, Motte S, Peters IR, Naeije R, McEntee K. Early increase in pulmonary vascular reactivity with overexpression of endothelin-1 and vascular endothelial growth factor in canine experimental heart failure. Exp Physiol. 2008; 93:434–442. expphysiol.2007.040469 [pii] 10.1113/expphysiol.2007.040469. [PubMed: 17993509]

247. Reeves JT, Leathers JE, Quigley MB. Microradiography of pulmonary arterioles, capillaries, and venules of the rabbit. Anat Rec. 1965; 151:531–545. [PubMed: 14326982]

248. Rehan VK, Sugano S, Wang Y, Santos J, Romero S, Dasgupta C, Keane MP, Stahlman MT, Torday JS. Evidence for the presence of lipofibroblasts in human lung. Exp Lung Res. 2006; 32:379–393. G3M48045202Q730P [pii] 10.1080/01902140600880257. [PubMed: 17090478]

249. Reid A, Heard BE. Preliminary studies of human pulmonary capillaries by India ink injection. Med Thorac. 1962; 19:215–219. [PubMed: 13973741]

250. Reid L. The angiogram and pulmonary artery structure and branching (in the normal and with reference to disease). Proc R Soc Med. 1965; 58:681–684. [PubMed: 4220448]

251. Reid L, Meyrick B. Microcirculation: definition and organization at tissue level. Ann N Y Acad Sci. 1982; 384:3–20. [PubMed: 6953826]

252. Reid LM. Structure and function in pulmonary hypertension. New perceptions. Chest. 1986; 89:279–288. [PubMed: 3510824]

253. Rendas A, Branthwaite M, Lennox S, Reid L. Response of the pulmonary circulation to acute hypoxia in the growing pig. J Appl Physiol. 1982; 52:811–814. [PubMed: 7085412]

254. Rendas A, Branthwaite M, Reid L. Growth of pulmonary circulation in normal pig--structural analysis and cardiopulmonary function. J Appl Physiol. 1978; 45:806–817. [PubMed: 730578]

255. Rhodin JA. Microscopic anatomy of the pulmonary vascular bed in the cat lung. Microvasc Res. 1978; 15:169–193. [PubMed: 661610]

256. Ricci A, Mariotta S, Greco S, Pallone G, Papale M, Bisetti A. Age-related changes of the noradrenergic innervation of rat tracheo-bronchial tree and pulmonary vasculature. Mech Ageing Dev. 1997; 99:245–255. S004763749700105X [pii]. [PubMed: 9483496]

257. Richardson JB. The innervation of the lung. Eur J Respir Dis Suppl. 1982; 117:13–31. [PubMed: 6954075]

258. Richardson JB. Recent progress in pulmonary innervation. Am Rev Respir Dis. 1983; 128:S65–68. [PubMed: 6881712]

259. Ritman EL. Micro-computed tomography of the lungs and pulmonary-vascular system. Proc Am Thorac Soc. 2005; 2:477–480. 2/6/477 [pii] 10.1513/pats.200508-080DS. [PubMed: 16352751]

260. Rosenberg HC, Rabinovitch M. Endothelial injury and vascular reactivity in monocrotaline pulmonary hypertension. Am J Physiol. 1988; 255:H1484–1491. [PubMed: 3144186]

261. Rosenberg HG, Williams WG, Trusler GA, Higa T, Rabinovitch M. Structural composition of central pulmonary arteries. Growth potential after surgical shunts. J Thorac Cardiovasc Surg. 1987; 94:498–503. [PubMed: 3657252]

262. Said SI, Hamidi SA, Dickman KG, Szema AM, Lyubsky S, Lin RZ, Jiang YP, Chen JJ, Waschek JA, Kort S. Moderate pulmonary arterial hypertension in male mice lacking the vasoactive intestinal peptide gene. Circulation. 2007; 115:1260–1268. CIRCULATIONAHA.106.681718 [pii] 10.1161/CIRCULATIONAHA.106.681718. [PubMed: 17309917]

263. Saldana M, Arias-Stella J. Studies on the strcture of the pulmonary trunk. I. Normal changes in the elastic configuration of the human pulmonary trunk at different ages. Circulation. 1963; 27:1086–1093. [PubMed: 13991048]

264. Saldana M, Arias-Stella J. Studies on the structure of the pulmonary trunk. II. The evolution of the elastic configuration of the pulmonary trunk in people native to high altitudes. Circulation. 1963; 27:1094–1100. [PubMed: 13991049]

265. Schneeberger EE. Structure of intercellular junctions in different segments of the intrapulmonary vasculature. Ann N Y Acad Sci. 1982; 384:54–63. [PubMed: 6953838]

266. Schneeberger EE. Ultrastructural basis for alveolar-capillary permeability to protein. Ciba Found Symp. 1976:3–28. [PubMed: 181220]

267. Schneeberger EE. Ultrastructure of intercellular junctions in the freeze fractured alveolar-capillary membrane of mouse lung. Chest. 1977; 71:299–300. [PubMed: 836379]

268. Schneeberger EE, Lynch RD. Structure, function, and regulation of cellular tight junctions. Am J Physiol. 1992; 262:L647–661. [PubMed: 1616050]

269. Schneeberger EE, Lynch RD. Tight junctions. Their structure, composition, and function. Circ Res. 1984; 55:723–733. [PubMed: 6388896]

270. Schnittler HJ. Structural and functional aspects of intercellular junctions in vascular endothelium. Basic Res Cardiol. 1998; 93(Suppl 3):30–39. [PubMed: 9879442]

271. Schraufnagel DE, Agaram NP, Faruqui A, Jain S, Jain L, Ridge KM, Sznajder JI. Pulmonary lymphatics and edema accumulation after brief lung injury. Am J Physiol Lung Cell Mol Physiol. 2003; 284:L891–897. 10.1152/ajplung.00333.2002 00333.2002 [pii]. [PubMed: 12547731]

272. Schraufnagel DE, Malik R, Goel V, Ohara N, Chang SW. Lung capillary changes in hepatic cirrhosis in rats. Am J Physiol. 1997; 272:L139–147. [PubMed: 9038913]

273. Schraufnagel DE, Patel KR. Sphincters in pulmonary veins. An anatomic study in rats. Am Rev Respir Dis. 1990; 141:721–726. [PubMed: 2310100]

274. Shapiro SD, Endicott SK, Province MA, Pierce JA, Campbell EJ. Marked longevity of human lung parenchymal elastic fibers deduced from prevalence of D-aspartate and nuclear weapons-related radiocarbon. J Clin Invest. 1991; 87:1828–1834. 10.1172/JCI115204. [PubMed: 2022748]

275. Shaw AM, Bunton DC, Fisher A, McGrath JC, Montgomery I, Daly C, MacDonald A. V-shaped cushion at the origin of bovine pulmonary supernumerary arteries: structure and putative function. J Appl Physiol. 1999; 87:2348–2356. [PubMed: 10601188]

276. Shelton DM, Keal E, Reid L. The pulmonary circulation in chronic bronchitis and emphysema. Chest. 1977; 71:303–306. [PubMed: 137801]

277. Sheppard MN, Polak JM, Allen JM, Bloom SR. Neuropeptide tyrosine (NPY): a newly discovered peptide is present in the mammalian respiratory tract. Thorax. 1984; 39:326–330. [PubMed: 6377561]

278. Shi W, Cernacek P, Hu F, Michel RP. Endothelin reactivity and receptor profile of pulmonary vessels in postobstructive pulmonary vasculopathy. Am J Physiol. 1997; 273:H2558–2564. [PubMed: 9435587]

279. Shi W, Giaid A, Hu F, Michel RP. Increased reactivity to endothelin of pulmonary arteries in long-term post-obstructive pulmonary vasculopathy in rats. Pulm Pharmacol Ther. 1998; 11:189–196. S1094-5539(98)90136-5 [pii] 10.1006/pupt.1998.0136. [PubMed: 9918754]

280. Shi W, Hu F, Kassouf W, Michel RP. Altered reactivity of pulmonary vessels in postobstructive pulmonary vasculopathy. J Appl Physiol. 2000; 88:17–25. [PubMed: 10642357]

281. Shi W, Wang CG, Dandurand RJ, Eidelman DH, Michel RP. Differential responses of pulmonary arteries and veins to histamine and 5-HT in lung explants of guinea-pigs. Br J Pharmacol. 1998; 123:1525–1532. 10.1038/sj.bjp.0701759. [PubMed: 9605557]

282. Shifren A, Durmowicz AG, Knutsen RH, Faury G, Mecham RP. Elastin insufficiency predisposes to elevated pulmonary circulatory pressures through changes in elastic artery structure. J Appl Physiol. 2008; 105:1610–1619. 90563.2008 [pii] 10.1152/japplphysiol.90563.2008. [PubMed: 18772328]

283. Short AC, Montoya ML, Gebb SA, Presson RG Jr. Wagner WW Jr. Capen RL. Pulmonary capillary diameters and recruitment characteristics in subpleural and interior networks. J Appl Physiol. 1996; 80:1568–1573. [PubMed: 8727541]

284. Simionescu, M. Lung endothelium: structure-function correlates.. In: Crystal, RC.; West, JB.; Barnes, PJ.; Weibel, ER., editors. The lung: Scientific foundations. Lippincott-Raven Publishers; Philadelphia: 1997. p. 615-628.

285. Simons P, Reid L. Muscularity of pulmonary artery branches in the upper and lower lobes of the normal young and aged lung. Br J Dis Chest. 1969; 63:38–44. [PubMed: 4180005]

286. Singhal S, Henderson R, Horsfield K, Harding K, Cumming G. Morphometry of the human pulmonary arterial tree. Circ Res. 1973; 33:190–197. [PubMed: 4727370]

287. Sirianni FE, Chu FS, Walker DC. Human alveolar wall fibroblasts directly link epithelial type 2 cells to capillary endothelium. Am J Respir Crit Care Med. 2003; 168:1532–1537. 10.1164/rccm.200303-371OC 200303-371OC [pii]. [PubMed: 14551162]

288. Smith P, Heath D, Mooi W. Observations on some ultrastructural features of normal pulmonary blood vessels in collapsed and distended lungs. J Anat. 1979; 128:85–96. [PubMed: 422487]

289. Snow RL, Davies P, Pontoppidan H, Zapol WM, Reid L. Pulmonary vascular remodeling in adult respiratory distress syndrome. Am Rev Respir Dis. 1982; 126:887–892. [PubMed: 7149455]

290. Sobin SS, Chen PC. Ultrastructural changes in the pulmonary arterioles in acute hypoxic pulmonary hypertension in the rat. High Alt Med Biol. 2000; 1:311–322. 10.1089/15270290050502381. [PubMed: 11256467]

291. Sobin SS, Tremer HM, Fung YC. Morphometric basis of the sheet-flow concept of the pulmonary alveolar microcirculation in the cat. Circ Res. 1970; 26:397–414. [PubMed: 4906258]

292. Soufan AT, van den Hoff MJ, Ruijter JM, de Boer PA, Hagoort J, Webb S, Anderson RH, Moorman AF. Reconstruction of the patterns of gene expression in the developing mouse heart reveals an architectural arrangement that facilitates the understanding of atrial malformations and arrhythmias. Circ Res. 2004; 95:1207–1215. 01.RES.0000150852.04747.e1 [pii] 10.1161/01.RES.0000150852.04747.e1. [PubMed: 15550689]

293. Spencer H, Leof D. The innervation of the human lung. J Anat. 1964; 98:599–609. [PubMed: 14229991]

294. Springall DR, Bhatnagar M, Wharton J, Hamid Q, Gulbenkian S, Hedges M, Meleagros L, Bloom SR, Polak JM. Expression of the atrial natriuretic peptide gene in the cardiac muscle of rat extrapulmonary and intrapulmonary veins. Thorax. 1988; 43:44–52. [PubMed: 2965426]

295. Staub NC. The interdependence of pulmonary structure and function. Anesthesiology. 1963; 24:831–854. [PubMed: 14071417]

296. Staub NC, Schultz EL. Pulmonary capillary length in dogs, cat and rabbit. Respir Physiol. 1968; 5:371–378. [PubMed: 4879179]

297. Stenmark KR, Frid MG. Smooth muscle cell heterogeneity: role of specific smooth muscle cell subpopulations in pulmonary vascular disease. Chest. 1998; 114:82S–90S. [PubMed: 9676647]

298. Stevens T. Molecular and cellular determinants of lung endothelial cell heterogeneity. Chest. 2005; 128:558S–564S. 128/6_suppl/558S [pii] 10.1378/chest.128.6_suppl.558S. [PubMed: 16373825]

299. Stevens T, Phan S, Frid MG, Alvarez D, Herzog E, Stenmark KR. Lung vascular cell heterogeneity: endothelium, smooth muscle, and fibroblasts. Proc Am Thorac Soc. 2008; 5:783–791. 5/7/783 [pii] 10.1513/pats.200803-027HR. [PubMed: 18757318]

300. Stone KC, Mercer RR, Freeman BA, Chang LY, Crapo JD. Distribution of lung cell numbers and volumes between alveolar and nonalveolar tissue. Am Rev Respir Dis. 1992; 146:454–456. [PubMed: 1489139]

301. Su C, Bevan RD, Duckles SP, Bevan JA. Functional studies of the small pulmonary arteries. Microvasc Res. 1978; 15:37–44. [PubMed: 634155]

302. Tachihara A, Jin E, Matsuoka T, Ghazizadeh M, Yoshino S, Takemura T, W DT, Kawanami O. Critical roles of capillary endothelial cells for alveolar remodeling in nonspecific and usual interstitial pneumonias. J Nippon Med Sch. 2006; 73:203–213. JST.JSTAGE/jnms/73.203 [pii]. [PubMed: 16936446]

303. Tan AY, Li H, Wachsmann-Hogiu S, Chen LS, Chen PS, Fishbein MC. Autonomic innervation and segmental muscular disconnections at the human pulmonary vein-atrial junction: implications for catheter ablation of atrial-pulmonary vein junction. J Am Coll Cardiol. 2006; 48:132–143. S0735-1097(06)00918-1 [pii] 10.1016/j.jacc.2006.02.054. [PubMed: 16814659]

304. Taylor AE, Granger DN. Equivalent pore modeling: vesicles and channels. Fed Proc. 1983; 42:2440–2445. [PubMed: 6840295]

305. Taylor, AE.; Granger, DN. Exchange of macromolecules across the microcirculation.. In: Renkin, EM.; Michel, CC., editors. Handbook of Physiology Section 2: The cardiovascular system. American Physiological Society; Bethesda: 1984. p. 467-520.

306. Taylor, AE.; Parker, JC. Pulmonary interstitial spaces and lymphatics.. In: Fishman, AP.; Fisher, AB., editors. Handbook of Physiology Section 3: The respiratory system. American Physiological Society; Bethesda: 1985. p. 167-230.

307. Thet LA, Law DJ. Changes in cell number and lung morphology during early postpneumonectomy lung growth. J Appl Physiol. 1984; 56:975–978. [PubMed: 6725076]

308. Toshima M, Ohtani Y, Ohtani O. Three-dimensional architecture of elastin and collagen fiber networks in the human and rat lung. Arch Histol Cytol. 2004; 67:31–40. [PubMed: 15125021]

309. Toshimori H, Nakazato M, Toshimori K, Asai J, Matsukura S, Oura C, Matsuo H. Distribution of atrial natriuretic polypeptide (ANP)-containing cells in the rat heart and pulmonary vein.

Immunohistochemical study and radioimmunoassay. Cell Tissue Res. 1988; 251:541–546. [PubMed: 2966675]

310. Townsley MI, Fu Z, Mathieu-Costello O, West JB. Pulmonary microvascular permeability. Responses to high vascular pressure after induction of pacing-induced heart failure in dogs. Circ Res. 1995; 77:317–325. [PubMed: 7614719]
311. Townsley MI, Snell KS, Ivey CL, Culberson DE, Liu DC, Reed RK, Mathieu-Costello O. Remodeling of lung interstitium but not resistance vessels in canine pacing-induced heart failure. J Appl Physiol. 1999; 87:1823–1830. [PubMed: 10562627]
312. Tozzi CA, Thakker-Varia S, Yu SY, Bannett RF, Peng BW, Poiani GJ, Wilson FJ, Riley DJ. Mast cell collagenase correlates with regression of pulmonary vascular remodeling in the rat. Am J Respir Cell Mol Biol. 1998; 18:497–510. [PubMed: 9533937]
313. Tsukimoto K, Mathieu-Costello O, Prediletto R, Elliott AR, West JB. Ultrastructural appearances of pulmonary capillaries at high transmural pressures. J Appl Physiol. 1991; 71:573–582. [PubMed: 1718936]
314. Tucker A, McMurtry IF, Alexander AF, Reeves JT, Grover RF. Lung mast cell density and distribution in chronically hypoxic animals. J Appl Physiol. 1977; 42:174–178. [PubMed: 138666]
315. Tucker A, McMurtry IF, Reeves JT, Alexander AF, Will DH, Grover RF. Lung vascular smooth muscle as a determinant of pulmonary hypertension at high altitude. Am J Physiol. 1975; 228:762–767. [PubMed: 234690]
316. Uddman, R.; Sundler, R.; Cardell, L-O.; Luts, A. Neuropeptides in the lung.. In: Crystal, RC.; West, JB.; Weibel, ER.; Barnes, PJ., editors. The Lung: Scientific Foundations. Lippincott-Raven Publishers; Philadelphia: 1997. p. 103-115.
317. Vaccaro C, Brody JS. Ultrastructure of developing alveoli. I. The role of the interstitial fibroblast. Anat Rec. 1978; 192:467–479. 10.1002/ar.1091920402. [PubMed: 736269]
318. Vaccaro CA, Brody JS. Structural features of alveolar wall basement membrane in the adult rat lung. J Cell Biol. 1981; 91:427–437. [PubMed: 7198126]
319. Vaitkevicius R, Saburkina I, Rysevaite K, Vaitkeviciene I, Pauziene N, Zaliunas R, Schauerte P, Jalife J, Pauza DH. Nerve supply of the human pulmonary veins: an anatomical study. Heart Rhythm. 2009; 6:221–228. S1547-5271(08)01052-7 [pii] 10.1016/j.hrthm.2008.10.027. [PubMed: 19187915]
320. Verheule S, Wilson EE, Arora R, Engle SK, Scott LR, Olgin JE. Tissue structure and connexin expression of canine pulmonary veins. Cardiovasc Res. 2002; 55:727–738. S000863630200490X [pii]. [PubMed: 12176122]
321. Verity MA, Bevan JA. Fine structural study of the terminal effecror plexus, neuromuscular and intermuscular relationships in the pulmonary artery. J Anat. 1968; 103:49–63. [PubMed: 5691966]
322. Vermeersch P, Buys E, Pokreisz P, Marsboom G, Ichinose F, Sips P, Pellens M, Gillijns H, Swinnen M, Graveline A, Collen D, Dewerchin M, Brouckaert P, Bloch KD, Janssens S. Soluble guanylate cyclase-α1 deficiency selectively inhibits the pulmonary vasodilator response to nitric oxide and increases the pulmonary vascular remodeling response to chronic hypoxia. Circulation. 2007; 116:936–943. CIRCULATIONAHA.106.677245 [pii] 10.1161/CIRCULATIONAHA.106.677245. [PubMed: 17679618]
323. von Hayek, H. The human lung. Hafner Publishing Co., Inc.; New York: 1960.
324. Wagenseil JE, Mecham RP. Vascular extracellular matrix and arterial mechanics. Physiol Rev. 2009; 89:957–989. 89/3/957 [pii] 10.1152/physrev.00041.2008. [PubMed: 19584318]
325. Wagenvoort CA. Morphologic changes in intrapulmonary veins. Hum Pathol. 1970; 1:205–213. [PubMed: 5521723]
326. Wagenvoort CA, Dingemans KP. Pulmonary vascular smooth muscle and its interaction with endothelium. Morphologic considerations. Chest. 1985; 88:200S–202S. [PubMed: 4042723]
327. Walch L, Taisne C, Gascard JP, Nashashibi N, Brink C, Norel X. Cholinesterase activity in human pulmonary arteries and veins. Br J Pharmacol. 1997; 121:986–990. 10.1038/sj.bjp.0700158. [PubMed: 9222557]

328. Walker DC, Behzad AR, Chu F. Neutrophil migration through preexisting holes in the basal laminae of alveolar capillaries and epithelium during streptococcal pneumonia. Microvasc Res. 1995; 50:397–416. S0026-2862(85)71067-9 [pii] 10.1006/mvre.1995.1067. [PubMed: 8583953]

329. Walker DC, MacKenzie A, Hosford S. The structure of the tricellular region of endothelial tight junctions of pulmonary capillaries analyzed by freeze-fracture. Microvasc Res. 1994; 48:259–281. S0026-2862(84)71054-5 [pii] 10.1006/mvre.1994.1054. [PubMed: 7731392]

330. Walker DC, MacKenzie AL, Wiggs BR, Montaner JG, Hogg JC. Assessment of tight junctions between pulmonary epithelial and endothelial cells. J Appl Physiol. 1988; 64:2348–2356. [PubMed: 3403419]

331. Ward SM, Sanders KM, Hirst GD. Role of interstitial cells of Cajal in neural control of gastrointestinal smooth muscles. Neurogastroenterol Motil. 2004; 16(Suppl 1):112–117. 10.1111/j.1743-3150.2004.00485.x NMO485 [pii]. [PubMed: 15066015]

332. Watanabe N, Horie S, Michael GJ, Keir S, Spina D, Page CP, Priestley JV. Immunohistochemical co-localization of transient receptor potential vanilloid (TRPV)1 and sensory neuropeptides in the guinea-pig respiratory system. Neuroscience. 2006; 141:1533–1543. S0306-4522(06)00569-0 [pii] 10.1016/j.neuroscience.2006.04.073. [PubMed: 16765524]

333. Weibel, ER. Lung cell biology.. In: Fishman, AP., editor. Handbook of Physiology Section 3: The Respiratory System. American Physiological Society; Bethesda: 1985. p. 47-91.

334. Weibel ER. Morphological basis of alveolar-capillary gas exchange. Physiol Rev. 1973; 53:419–495. [PubMed: 4581654]

335. Weibel ER. On pericytes, particularly their existence on lung capillaries. Microvasc Res. 1974; 8:218–235. [PubMed: 4140459]

336. Weibel, ER.; Crystal, RC. Organization of the lung interstitium.. In: Crystal, RC.; West, JB.; Barnes, PJ.; Weibel, ER., editors. The lung: Scientific foundations. Lippincott-Raven Publishers; Philadelphia: 1997. p. 685-695.

337. Weibel ER, Hsia CC, Ochs M. How much is there really? Why stereology is essential in lung morphometry. J Appl Physiol. 2007; 102:459–467. 00808.2006 [pii] 10.1152/japplphysiol.00808.2006. [PubMed: 16973815]

338. Weibel ER, Palade GE. New cytoplasmic components in arterial endothelia. J Cell Biol. 1964; 23:101–112. [PubMed: 14228505]

339. Welle M. Development, significance, and heterogeneity of mast cells with particular regard to the mast cell-specific proteases chymase and tryptase. J Leukoc Biol. 1997; 61:233–245. [PubMed: 9060446]

340. Wessler I, Kirkpatrick CJ. Acetylcholine beyond neurons: the non-neuronal cholinergic system in humans. Br J Pharmacol. 2008; 154:1558–1571. bjp2008185 [pii] 10.1038/bjp.2008.185. [PubMed: 18500366]

341. Winkler GC, Cheville NF. Morphometry of postnatal development in the porcine lung. Anat Rec. 1985; 211:427–433. 10.1002/ar.1092110409. [PubMed: 3993992]

342. Wu DX, Weibel ER, Bachofen H, Schurch S. Lung lesions in experimental hydrostatic pulmonary edema: an electron microscopic and morphometric study. Exp Lung Res. 1995; 21:711–730. [PubMed: 8556990]

343. Yan X, Bellotto DJ, Foster DJ, Johnson RL Jr. Hagler HK, Estrera AS, Hsia CC. Retinoic acid induces nonuniform alveolar septal growth after right pneumonectomy. J Appl Physiol. 2004; 96:1080–1089. 10.1152/japplphysiol.00771.2003 00771.2003 [pii]. [PubMed: 14617528]

344. Yeh HI, Lai YJ, Lee YN, Chen YJ, Chen YC, Chen CC, Chen SA, Lin CI, Tsai CH. Differential expression of connexin43 gap junctions in cardiomyocytes isolated from canine thoracic veins. J Histochem Cytochem. 2003; 51:259–266. [PubMed: 12533535]

345. Yeh HI, Rothery S, Dupont E, Coppen SR, Severs NJ. Individual gap junction plaques contain multiple connexins in arterial endothelium. Circ Res. 1998; 83:1248–1263. [PubMed: 9851942]

346. Yen RT, Sobin SS. Elasticity of arterioles and venules in postmortem human lungs. J Appl Physiol. 1988; 64:611–619. [PubMed: 3372419]

347. Yen RT, Zhuang FY, Fung YC, Ho HH, Tremer H, Sobin SS. Morphometry of cat pulmonary venous tree. J Appl Physiol. 1983; 55:236–242. [PubMed: 6885576]

348. Yen RT, Zhuang FY, Fung YC, Ho HH, Tremer H, Sobin SS. Morphometry of cat's pulmonary arterial tree. J Biomech Eng. 1984; 106:131–136. [PubMed: 6738017]

349. Yoneda K. Regional differences in the intercellular junctions of the alveolar-capillary membrane in the human lung. Am Rev Respir Dis. 1982; 126:893–897. [PubMed: 7149456]

350. Zaidi SH, You XM, Ciura S, Husain M, Rabinovitch M. Overexpression of the serine elastase inhibitor elafin protects transgenic mice from hypoxic pulmonary hypertension. Circulation. 2002; 105:516–521. [PubMed: 11815437]

351. Zeltner TB, Bertacchini M, Messerli A, Burri PH. Morphometric estimation of regional differences in the rat lung. Exp Lung Res. 1990; 16:145–158. [PubMed: 2328712]

352. Zeltner TB, Burri PH. The postnatal development and growth of the human lung. II. Morphology. Respir Physiol. 1987; 67:269–282. [PubMed: 3575906]

353. Zeltner TB, Caduff JH, Gehr P, Pfenninger J, Burri PH. The postnatal development and growth of the human lung. I. Morphometry. Respir Physiol. 1987; 67:247–267. [PubMed: 3575905]

354. Zhou C, Chen H, King JA, Sellak H, Kuebler WM, Yin J, Townsley MI, Shin HS, Wu S. The α_{1G} T-type calcium channel selectively regulates P-selectin surface expression in pulmonary capillary endothelium. Am J Physiol Lung Cell Mol Physiol. 2010 ajplung.00331.2009 [pii] 10.1152/ajplung.00331.2009.

355. Zhuang FY, Yen MR, Fung YC, Sobin SS. How many pulmonary alveoli are supplied by a single arteriole and drained by a single venule? Microvasc Res. 1985; 29:18–31. [PubMed: 3982283]

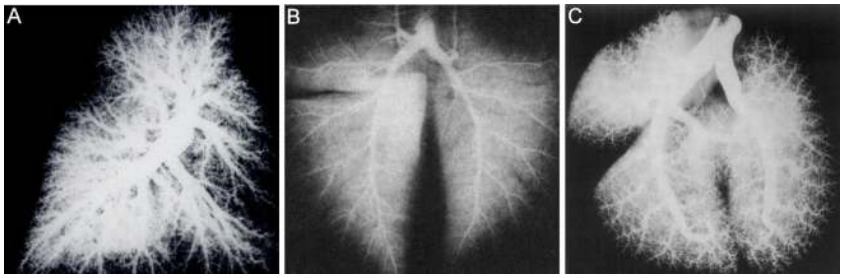

Figure 1.

Contrast arteriograms of the pulmonary arterial tree. The extensive branching of distal pulmonary arteries contributes to the space-filling nature of the pulmonary arterial tree. Contrast arteriograms of lungs from adult human (**A**, from Reid (252), with permission), neonatal pig (**B**, from Rendas *et al.* (254), with permission), and adult rat (**C**, from Jones *et al.* (141), with permission) were prepared with a barium-gelatin mixture. Even though gelatin does not penetrate into the capillary network, the background haze generated by filling of distal arterial branches < 200 μm in diameter highlights the density of the arterial tree (141). Some major branches extend nearly to the pleural surface.

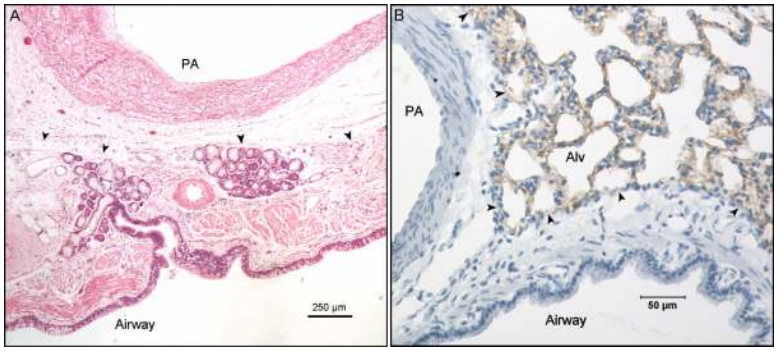

Figure 2.

The adventitial sheath of the bronchovascular bundle tethers to the adjacent airway or to alveolar septal networks. A section of human lung stained with hematoxylin and eosin (**A**) shows the adventitia of the pulmonary artery abutting the submucosa of the adjacent airway. Bronchial vessels (bv), the vasa vasorum of the pulmonary artery wall (v), and submucosal glands are visible. The section from rat lung (**B**) was probed using immunohistochemistry for the adhesion molecule ICAM-1, with hematoxylin counterstaining. In this micrograph, a portion of the arterial wall is seen to be tethered to surrounding alveolar septal walls. Adventitial borders are pinpointed with arrowheads.

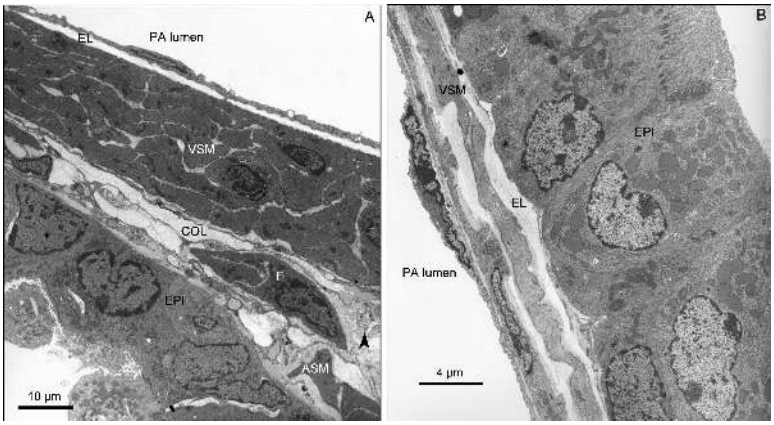

Figure 3.

Proximity of muscular pulmonary arteries to airway epithelium. Transmission electron micrographs from rat (**A**) and mouse (**B**) lung illustrate the proximity of small pulmonary arteries to airway epithelium. In **A**, the basal aspect of the airway epithelium lies within 10 μm of the arterial adventitia-media border. Elastic lamina (EL) are situated at both borders of the media and intercalated between the vascular smooth cell (VSM) layers. Collagen bundles (COL), a fibroblast (F) and a nerve bundle (arrowhead) can be seen in the adventitia. Smooth muscle associated with the airway (ASM) is also present. In the more distal artery shown in panel **B**, the basal aspect of the airway epithelium is only several microns distant from the endothelial cell in the vessel intima.

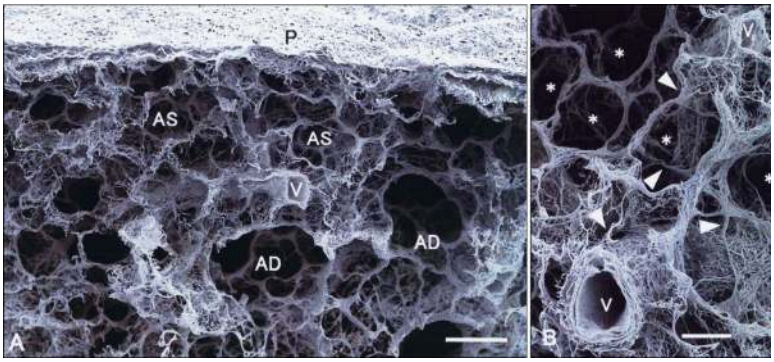

Figure 4.

The elastin fiber scaffold in human lung. After selective maceration of fixed human lung, the elastin fiber network in human lung was visualized with scanning electron microscopy. In panel **A** (scale 200 μm) elastic fibers in the outermost lamina of small extra-alveolar vessels (V) of human lung are seen to be continuous with elastin fibers in alveolar septal walls and the pleura (P). Alveolar sacs (AS) and ducts (AD) are noted. At higher magnification (**B**, scale 100 μm) the elastic lamina in the wall of the extra-alveolar vessel (v) are apparent. Further, the continuity between elastin fibers at the adventitial surface of the vessel and those in the alveolar septal network (arrowheads) is clear. The elastin network is particularly dense around the entrance to alveoli (*). From Toshima *et al.* (308), with permission.

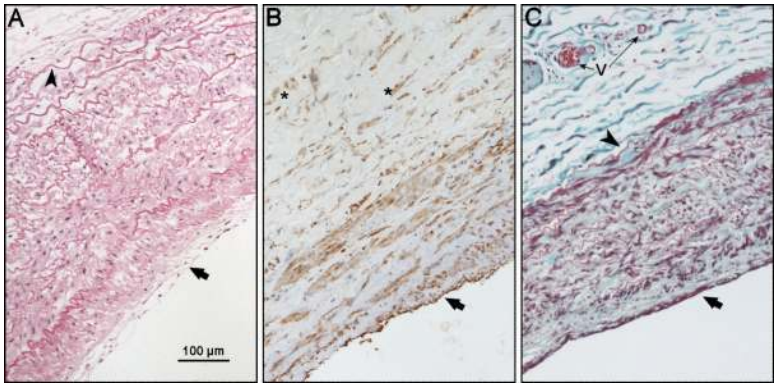

Figure 5.

Layers of the arterial wall in human lung. Sections from proximal pulmonary arteries of human lung show portions of the adventitia, a thick media containing numerous elastic lamina and a thin intima. The numerous, wavy elastic lamina (**A**, hematoxylin and eosin) create a layered-like structure in the arterial media, though the lamina are incomplete. The distribution of smooth muscle in the media is highlighted by immunohistochemistry for α-smooth muscle actin (**B**). Note that there are some α-smooth muscle actin positive cells in the adventitia. Collagen bundles in the adventitia and media are more clearly visualized with trichrome stain, where collagen appears blue (**C**, trichrome). Although there is substantial collagen in the adventitia in this artery, collagen can also be seen broadly distributed within the arterial media. Small blood vessels in the adventitial space are components of the vasa vasorum. Arrows point to the lumenal surface of the intima; arrowheads highlight elastic lamina at the adventitia-media border. All micrographs were captured at the same magnification (10x).

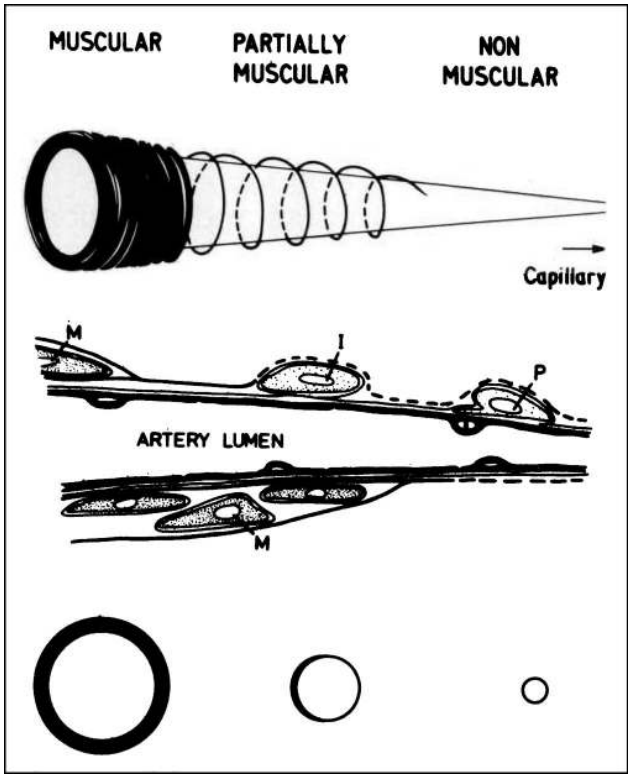

Figure 6.
Schematic showing the graded structural changes in the media of the pulmonary arterial wall, moving from muscular arteries to precapillary non-muscular vessels. The top panel illustrates the gradual loss of musculature. The middle panel shows the transition from vascular smooth muscle cells (M) to intermediate cells (I) and finally to pericytes (P). The bottom panel represents cross-sections, highlighting the partial circumferential coverage of the media. From Reid *et al.* (252), with permission.

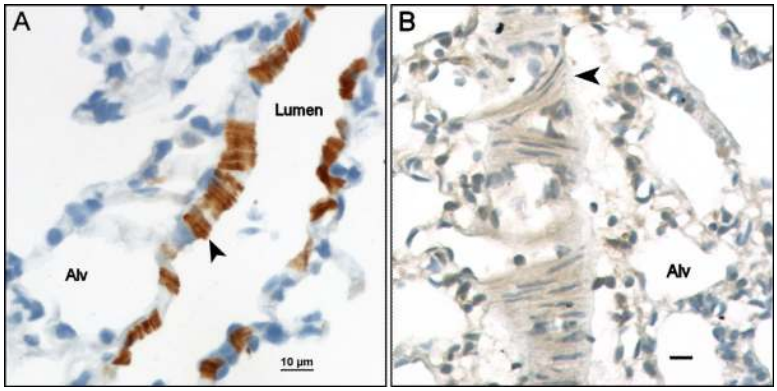

Figure 7.

Organization of vascular smooth muscle in small partially muscular vessels elucidated with immunohistochemistry. In light micrographs of rat lung (5 μm sections, hematoxylin counterstain), vascular smooth muscle can be seen to partially cover the vascular wall. Smooth muscle cells staining positive for CD40, seen in cross-section (**A**), cover ~ 50% of the vessel wall perimeter. Similar coverage is seen in a more superficial section immunostained for vascular cell adhesion molecule or VCAM (**B**). In the latter image, some broad bands of smooth muscle cells are organized in a spiral (arrowhead), rather than circumferential, fashion over the wall surface. Scale 10 μm in both panels.

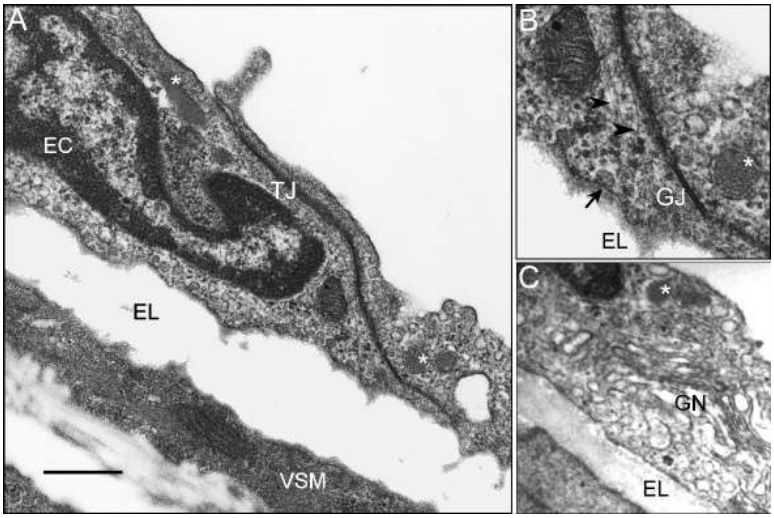

Figure 8.

Endothelial ultrastructure in the arterial wall. Endothelial cells (**A**, scale 500 nm, rat lung) connected by a long tight junctional complex (TJ) are situated on a broad elastic lamina which separates the intima of this vessel from vascular smooth muscle cells (VSM) in the media. Numerous vesicles and caveolae, as well as mitochondria and Weibel-Palade bodies (*) are present. In an enlarged section from this image (**B**), microtubules (arrowheads) and a Weibel-Palade body (*) can be seen adjacent to the interendothelial cell tight junction. The very dense, laminated appearance of the junctional complex at the basal cell border denotes a gap junction (GJ). A small Golgi network (GN) sits adjacent to the nucleus (**C**, mouse lung).

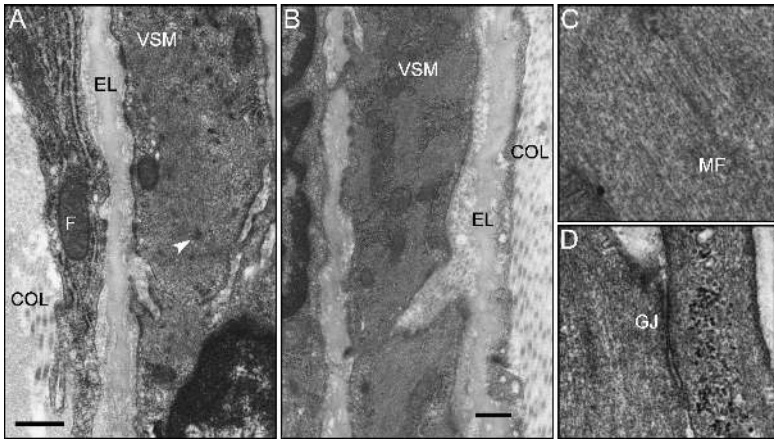

Figure 9.

Ultrastructure of vascular smooth muscle. Two micrographs from mouse lung show smooth muscle cells in the arterial wall with myofibrils along the long-axis of the cell (**A**, 500 nm scale) and when the cell is sectioned perpendicular to this plane (**B**, 500 nm scale). In the latter view, myofibrils appear as lighter clumps surrounded by mitochondria and rough endoplasmic reticulum. At the media-adventitia border (**A**), a fibroblast (F) containing an extensive rough endoplasmic reticulum network and the vascular smooth muscle cell (VSM) lie on either side of the external elastic lamina (EL). Bundles of fibrillar collagen (COL) are seen in the adventitia as well. Numerous dense bodies (**A**, arrowhead) are evident in the smooth muscle cell. A higher resolution image (**C**) shows the fine structure of an extensive parallel array of myofibrils (MF) in a smooth muscle cell. Panel **D** shows a gap junction (GJ) connecting two smooth muscle cells in mouse pulmonary artery.

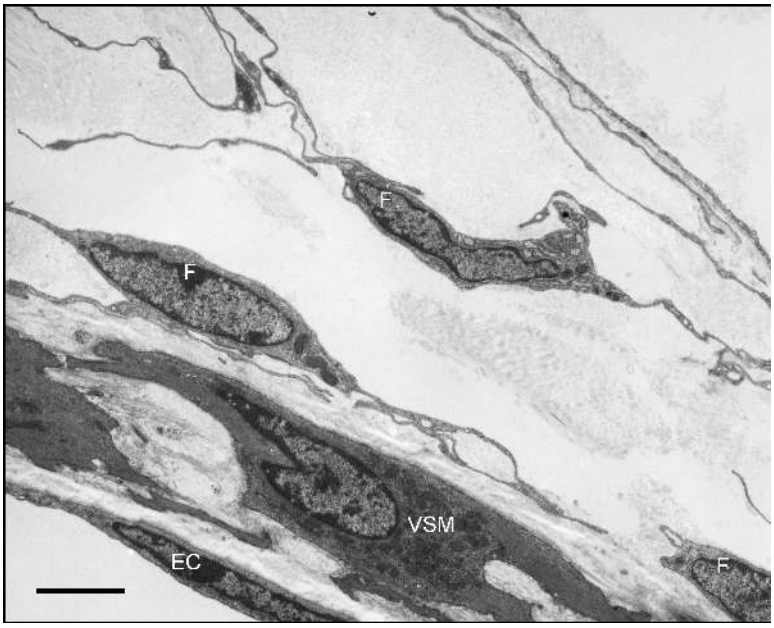

Figure 10.
Stellate fibroblasts in the vascular wall. The stellate nature and extensive cytoplasmic projections of adventitial fibroblasts are better appreciated in the adventitia of an extra-alveolar vessel from edematous mouse lung.

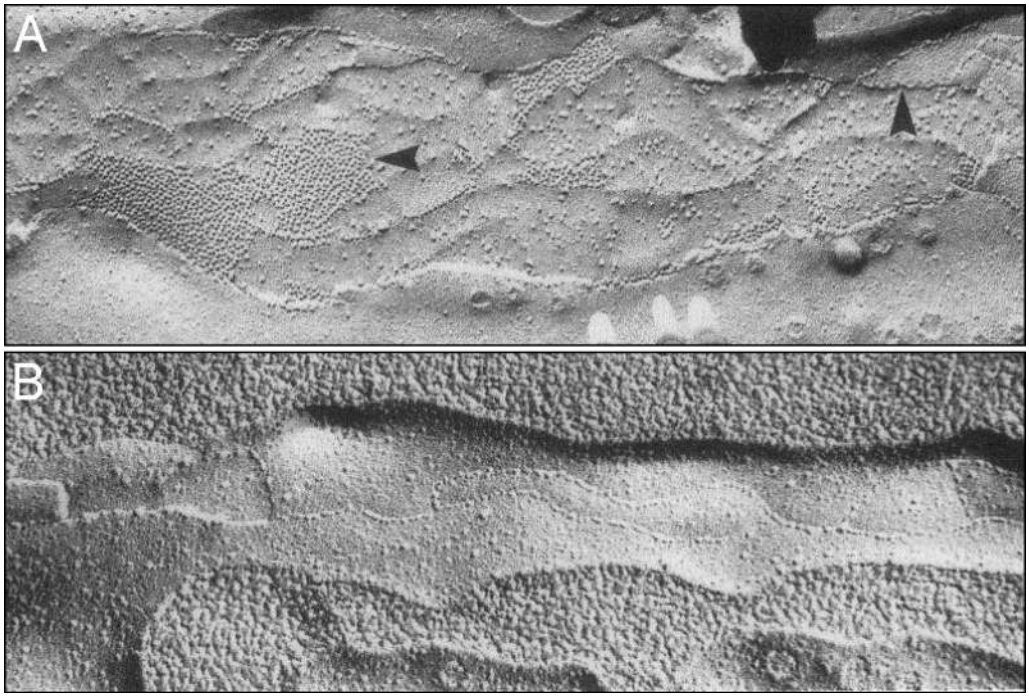

Figure 11.
Freeze-fracture of inter-endothelial junctions. Freeze-fracture replicas of endothelium from a small intra-acinar pulmonary artery (**A**) and a pulmonary capillary (**B**). In the artery, packed clusters of gap junction particles (arrowheads) lie embedded between junctional strands. In contrast, the inter-endothelial junction in the capillary is much simpler, comprised of only 1-2 junctional strands. From Schneeberger and Lynch (268), with permission.

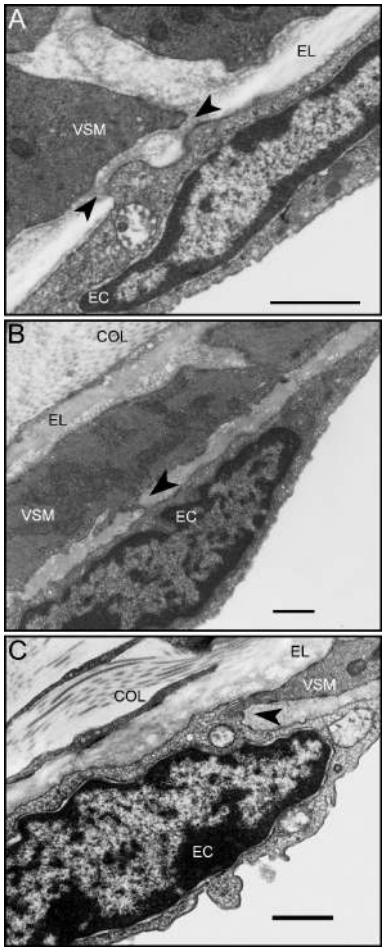

Figure 12.
Myoendothelial junctions in the pulmonary vasculature. Various morphologies in myoendothelial junctions (arrowheads) can be found in rat (**A** and **B**) or mouse (**C**) lung. Either the endothelial cell or the smooth muscle cell (or both) sends a projection through a focal discontinuity in the internal elastic lamina, allowing contact. VSM, vascular smooth muscle; EL, elastic lamina; COL, collagen fibrils. Scales are 1 μm.

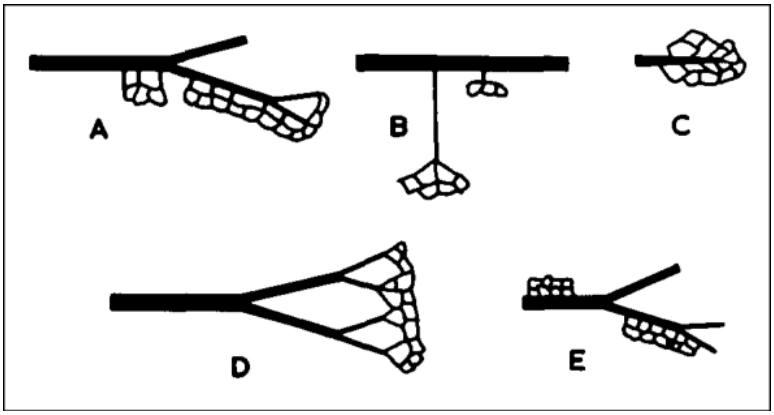

Figure 13.
Variable origin of pulmonary capillary networks. Precapillary arteries may branch at right angles from a small parent artery then give rise to a capillary network after some distance (**A** and **B**). Alternatively small arteries may abruptly end in a capillary network (**C** and **D**). Capillary networks may also emerge directly from the parent artery (**E**). In human and rat lung, extra-alveolar pulmonary arteries 100 μm or more in diameter may give rise directly to capillary networks (119, 137). From Horsfield, with permission (119).

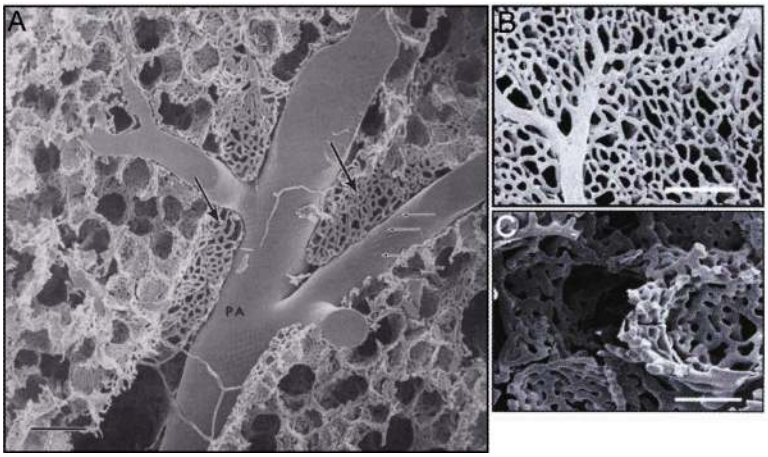

Figure 14.

Capillary density differs in perivascular and pleural networks versus that in the alveolar septal wall. Vascular corrosion casting of rat lung has elucidated variability in capillary density in the distal lung. Low density networks are present adjacent to extra-alveolar vessels (**A**) and on the pleural surface (**B**); scale bars are 100 μm. In contrast, high density capillary networks populate alveolar septal walls (**C**, scale 50 μm). Panel **A** from Guntheroth *et al.* (98), with permission.

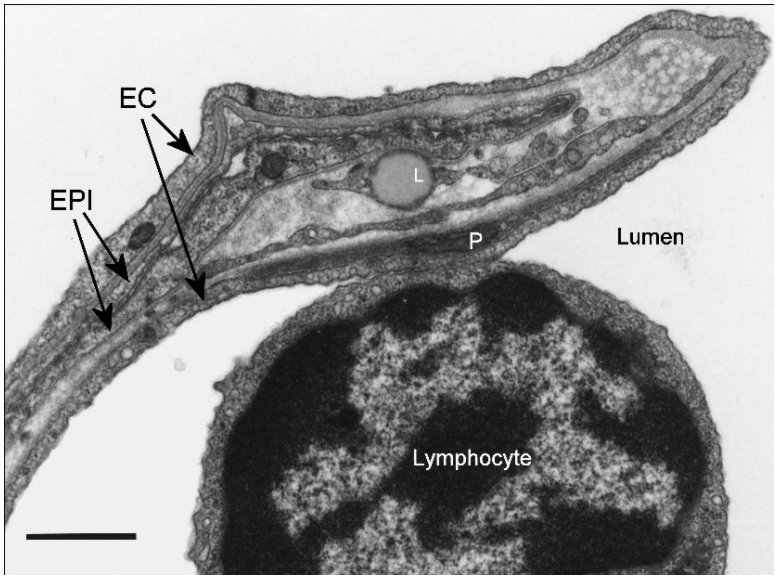

Figure 15.

Endothelium in alveolar capillaries can be extremely attenuated. In this section from rat lung, the thin side of the septal wall is shown for a capillary running across a septal wall fold. No alveolar space can be seen. Both the endothelium (EC) and the type I alveolar epithelium (EPI) are extremely attenuated, with few organelles present other than vesicles and an occasional mitochondria. Through much of this section the basement membranes of these layers appear fused, except at the tip of the fold (upper right). While interstitium is quite thin, nonetheless several interstitial cells are apparent. A pericyte (P) lies adjacent to the endothelium and is enveloped by the endothelial basement membrane. Attenuated cytoplasmic processes of several interstitial fibroblasts are present, one containing a lipid droplet (L). Scale 1 μm.

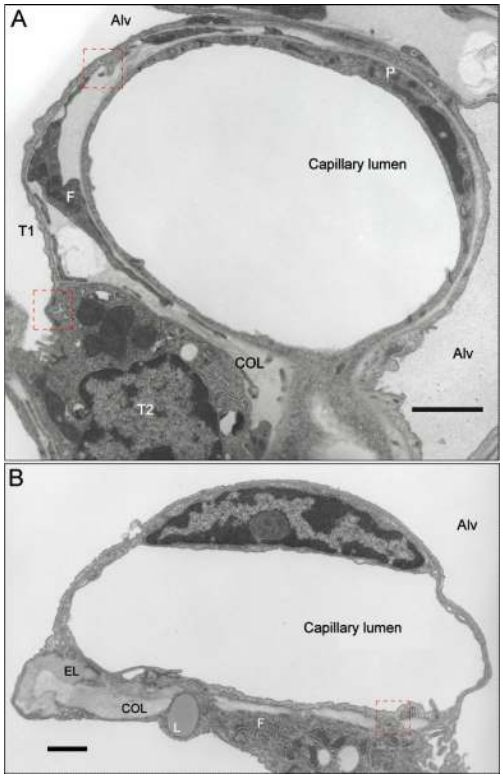

Figure 16.

Capillary ultrastructure in rat and mouse lung. In cross section, the very attenuated endothelial cells comprising the capillary can be seen (**A**, scale 2 μm, from rat lung). In this section, portions of three cells can be identified. For the most part, the perinuclear region typically evident on the thick side of the septal wall remains out of the section plane for this capillary. While the presence of edema in the septal wall is not normal, this image does allow clear visualization of collagen fibers (COL) and interstitial cells, including fibroblasts (F). Long, thin cytoplasmic extensions of the fibroblast wrap around nearly half of the capillary circumference. In addition, a pericyte (P) can be seen closely adherent to the basal aspect of one endothelial cell. The attenuated type I alveolar epithelial cells (T1) and a type II epithelial cell (T2) complete the septal wall facing the alveolus (Alv). The capillary shown in panel **B** (scale 1 μm) is situated at the tip of a septal wall, where typically bundles of collagen (COL) and elastin (EL) fibers provide support at the entrance ring to the alveolus. In this view, thick and thin sides of the alveolar septal wall are more clearly delineated. A fibroblast (F) containing an extensive rough endoplasmic reticulum and lipid droplets (L) is present within the interstitium. In panels **A** and **B**, red dashed boxes that highlight inter-cellular connections in the septal wall are enlarged in **Figure 17**.

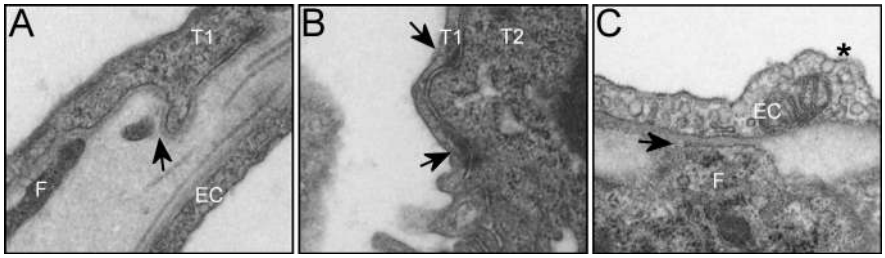

Figure 17.

Intercellular connections in the alveolar septal wall. Boxed areas from **Figure 16** are enlarged here. In panel **A**, the thin cytoplasmic extension of a interstitial fibroblast (F) approaches the alveolar type I epithelium (T1). Panel **B** shows tight junctions between type I and type II (T2) alveolar epithelial cells. Finally, panel **C** shows the close apposition between an interstitial fibroblast and the capillary endothelium (EC). Arrows show points of cell-cell contact. Similar interconnectedness has been documented in human lung (287); see **Figure 18** for more detail.

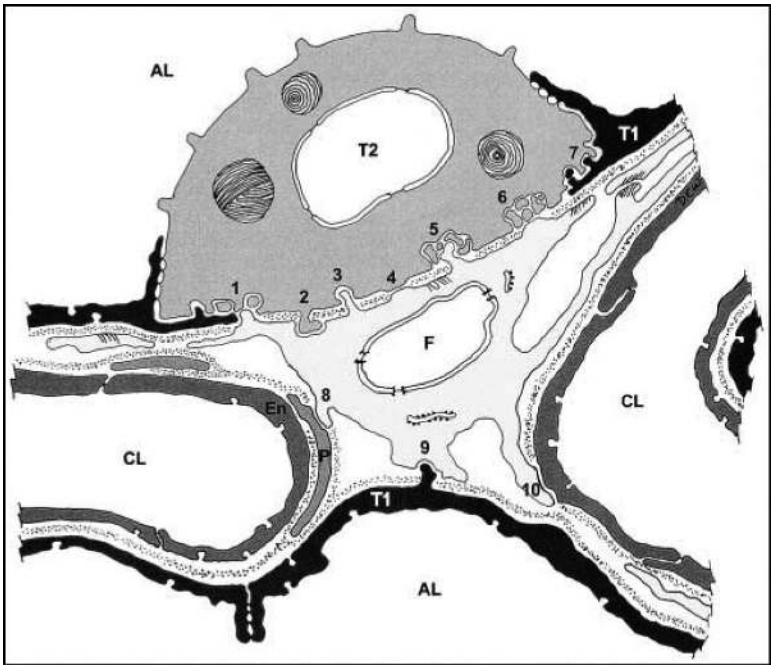

Figure 18.
Model of intercellular connections in the alveolar septal wall. This model of the alveolar septal wall was developed using serial sections of human lung, visualized with transmission electron microscopy. Type I (T1) and type II (T2) alveolar epithelial cells interdigitate at the lateral borders of the type II cell (sites 1 and 7). Intercellular connections between the type II cell and fibroblasts (F) in the alveolar septal wall take on numerous morphologies (sites 2-6), enabled by focal discontinuities in the type II cell basement membrane. Fibroblasts also connect with pericytes (P, site 8), type I cells (site 9), and capillary endothelial cells (En, site 10). From Sirianni *et al.* (287), with permission.

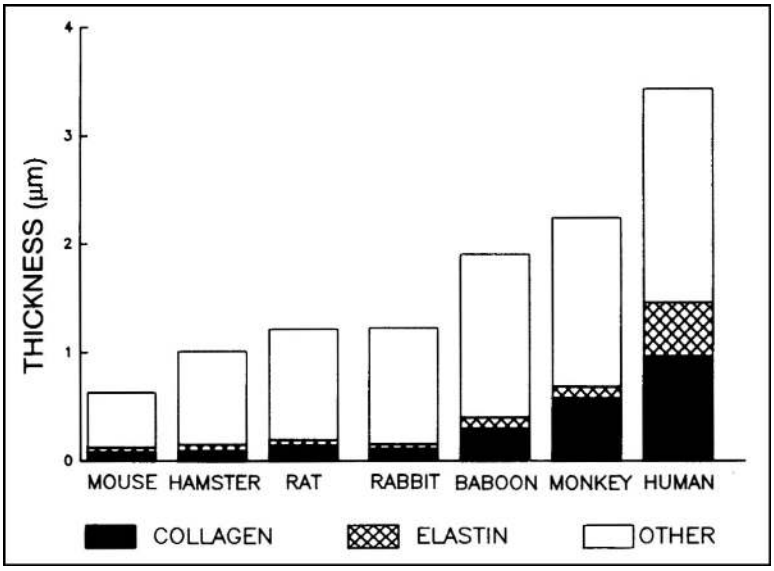

Figure 19.

Thickness and composition of the alveolar septal wall interstitium. The total thickness of the alveolar septal wall in adult mammals scales with body size (and alveolar curvature, not shown), although the slope of the relationship is relatively shallow. In addition, the relative contributions of collagen and elastin in the septal wall interstitium also increase with body size and scale with alveolar curvature. “Other” includes cellular elements, basement membrane and other non-collagen/non-elastin areas within the interstitial compartment. Note that these data were calculated for the whole width of the alveolar septum, thus the measures of interstitial thickness shown here are 2-fold higher that measured as the arithmetic mean interstitial thickness (see **Table 3**). From Mercer *et al.*, with permission (191).

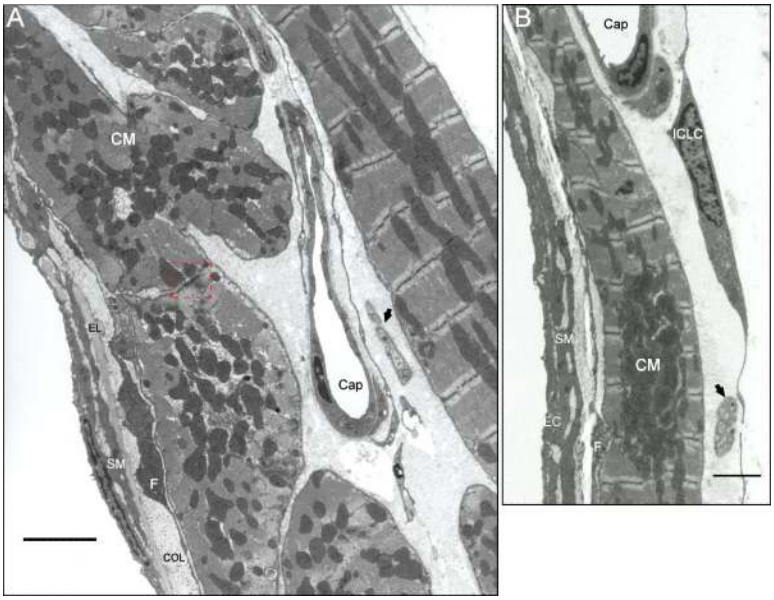

Figure 20.

Ultrastructure of pulmonary veins in rat and mouse. The wall of a large intrapulmonary vein from rat lung (Panel **A**, scale 3 μm) includes the endothelium (EC), scant smooth muscle (SM), fibroblasts (F), nerves (arrow) and abundant striated cardiac myocytes (CM). The pulmonary myocardium can be oriented in a circumferential or longitudinal pattern (or both as shown here). When multiple layers exist, they are much more loosely organized than are layers of smooth muscle cells in pulmonary arteries. Capillaries lie within the myocardial layer. In a pulmonary vein from mouse (panel **B**, scale 2 μm), an additional cell is present: the interstitial Cajal-like cell (ICLC).

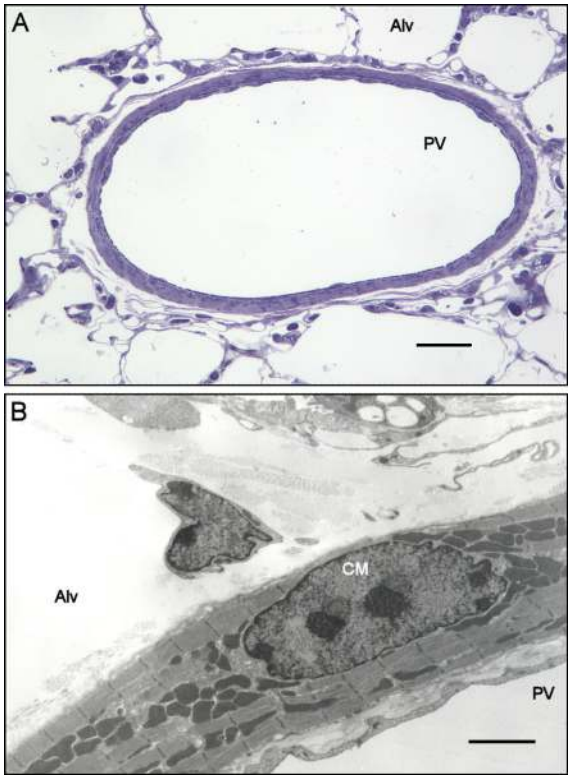

Figure 21.
Resolution of the pulmonary venous myocardium. With light microscopy, a myocardial sleeve in intrapulmonary veins can appear similar to smooth muscle, unless smooth muscle-specific probes are utilized. Light (**A**, scale 25 μm) and electron (**B**, scale 2 μm) micrographs of a small pulmonary vein (lumen diameter ~ 100 μm) from the same block of rat lung highlight this point. For light microscopy, a 1 μm section of plastic embedded glutaraldehyde-fixed lung prepared for transmission electron microscopy was stained with toluidine blue. The media in this image is notable only by its relative thickness and density. A transmission electron micrograph of an 80 nm section from the same block elucidated the presence of a cardiac myocyte rather than smooth muscle in the media. PV, lumen of the pulmonary vein; Alv, alveolar space.

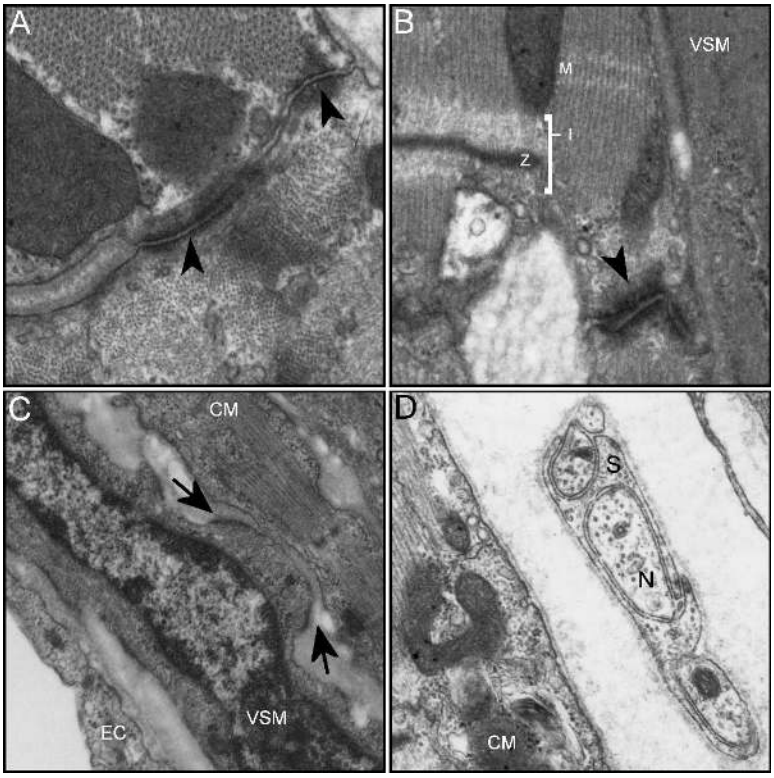

Figure 22.

High resolution ultrastructure of pulmonary vein in rat and mouse lung. Panels **A** and **B** show myocytes in the venous myocardium cut through the short or long axis, respectively. Panel A shows desmosomes (arrowhead), seen as dense laminated junctional complexes structures, joining lateral borders of adjacent myocardial cells. In the long axis view (panel **B**), intercalated discs that connect myocytes end-to-end are apparent (arrowhead). The well-organized contractile apparatus, including clear I, Z and M bands, can be clearly seen in this image. Panel **C** shows dense segments of the plasmalemmal membrane (arrows) in a pulmonary vein smooth muscle cell adjoining a small tapered striated myocyte, which suggests the potential for gap junction communication. Finally, panel **D** shows a small nerve bundle (N) in the adventitia of pulmonary veins, adjacent to striated myocytes. The axons are enclosed in Schwann cells (S). EC, endothelial cell; VMS, vascular smooth muscle cell; CM, cardiac myocyte. Scale 1 μm.

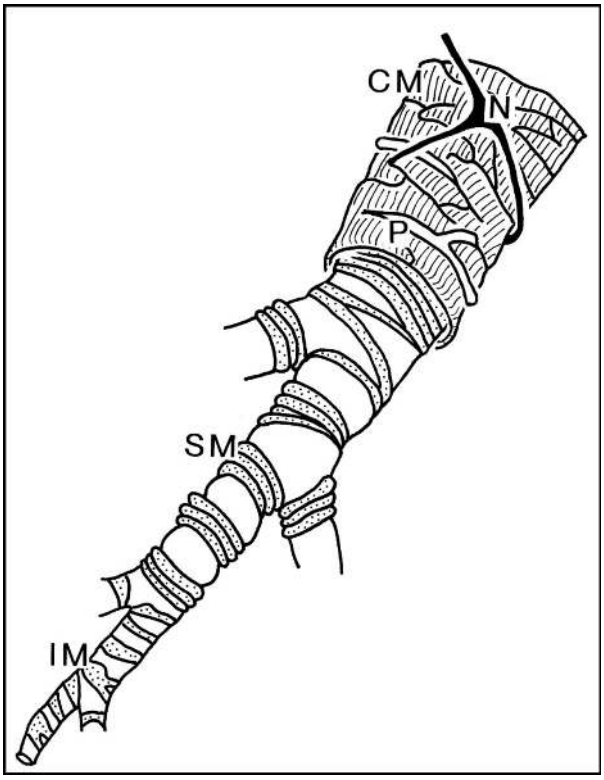

Figure 23.

Model of pulmonary vein structure. Using a combination of light and scanning EM, Hashizume and colleagues developed a model of the pulmonary vein (106). After capillaries coalesce into small non-muscular pulmonary veins, several compartments appear sequentially in the venous tree. These include 1) partially muscular pulmonary veins populated by intermediate (IM) and vascular smooth muscle cells (SM) and 2) muscular veins, where a sleeve of striated cardiac myocytes (CM) may overlay the smooth muscle. This model has general utility for understanding structure in pulmonary veins, with the caveat that in large mammals, myocardial sleeves only appear in large extra-pulmonary veins (107, 117, 216, 219, 220, 320). In contrast, in rat and mouse, the musculature of even small muscular intrapulmonary veins is comprised of smooth muscle and a sleeve of striated myocardium (151, 170, 206, 216, 230). When present, the myocardium is overlaid (and intertwined) with a capillary network and nerve fibers. From Hashizume *et al.* (106), with permission.

Table 1

Branching pattern and dimensions of extra-alveolar arteries and veins

Species	Lung studied	Total # orders	Order	# Branches	Branch ratio	Diameter (mm)	Diameter ratio	Length (mm)	Length ratio	Reference
					Pulmonary Arteries					
Human	W	17	17 1	1 7.29×10^7	3.11[a]	30 0.015	1.60[a]	90.5 0.13	1.46[a]	(119, 286)
	W Angiography Proximal arteries only	6	6 1	-	-	27.5 1.2	1.87[a]	-	-	(121)
	L	15	15 1	2 5.12×10^7	3.33	15.1 0.020	1.56	10.1 0.2	1.49	(127)
	LLL only	11	11 1	-	-	1.7 0.019	1.55[a]	-	-	(346)
Pig	*R*	*22* *Generations*	*1* *21* *22*	-	-	*22.3* *0.85* *0.71*	-	*9.0* *4.5* -	-	*(176)*
Dog	R	12	12 1	1 3.98×10^6	3.69[a]	11.1 0.028	1.67[a]	49.2 0.34	1.52[a]	(80)
Cat	R	11	11 10 1	1 4 3.00×10^5	3.58	5.5 2.7 0.021	1.72	- 11.9 0.12	1.81	(348)
Rat	L	11	11 1	1 6.40×10^4	2.76	1.6 0.013	1.58	2.3 0.04	1.60	(135)
					Pulmonary Veins					
Human	W	15	1 15	7.29×10^7 4	-	0.013 13.9	-	0.13 36.7	-	(120)
	R	15	1 15	3.98×10^7 2	3.33	0.018 13.0	1.58	0.12 35.7	1.50	(127)
Pig	*R*	*23* *Generations*	*23* *1*	-	-	*0.77* *14.8*	-	*3.92* *10.8*	-	*(176)*
Dog	W	11	1 11	2.48×10^6 2	3.76	0.029 8.5	1.70	0.41 34.4	1.56	(79)
Cat	R	11	1 11	2.83×10^5 1	3.52	0.022 4.6	1.73	0.087 19.2	1.53*	(78, 347)

W, whole lung; L, left lung; R, right lung.

*Orders 4-10 only

[a]calculated from data provided by authors.

Table 2

Muscularity of extra-alveolar pulmonary vessels

Species		Fixation	Location or type	External diameter (μm)	Medial thickness	% Muscularized			Other notes	Reference
						M	PM	NM		
				Pulmonary Arteries						
Human	-	Immersion Airway	M	100-1000	2-6.9 % 2.8-3.1 %	-	-	-		(19)
	SE	Immersion	-	>1000 501-1000 201-500 101-200 51-100 25-50	4.0 ± 1.4 % 6.2 ± 2.3 % 6.5 ± 1.3 % 6.4 ± 1.9 % 3.4 ± 1.3 % -	-	-	-		(33)
	-	Airway	-	<500	2.5-10 %	-	-	-		(101)
	SD	Airway	-	501-1000 401-500 301-400 201-300 101-200 51-100 <50	7.6 ± 1.7 % 6.4 ± 1.5 % 5.8 ± 1.2 % 5.8 ± 1.5 % 7.2 ± 1.8 % 7.4 ± 2.5 % 9.6 ± 3.4 %	-	-	-	0.3-9 yo	(108)
			TB RB AD	75-445 50-300 35-175	-	- 94 73	- 6 24	- 0 3	9-14 yo	
	SD	Airway/G	-	>200 85-200 50	2.4 ± 0.7 % 4.8 ± 1.3 % 10 %	-	-	-	19-35 yo	(285)
			-	>200 85-200	4.6 ± 1.4 % 6.6 ± 2.3 %	-	-	-	67-76 yo	
	SE	Airway/G	M PM NM	259 ± 23 75 ± 9 38 ± 5	-	-	-	-		(289)
	- -	Immersion	AD	80 100 120	-	0 17 30	-	-	2yo 6yo adult	(242)
Monkey	-	Immersion	M	30-80	5.1-13.6 %	-	-	-		(19)
Cow	-	Immersion	M	30-90	5.0-22.6 %	-	-	-		(19)
Sheep	-	Immersion	M	30-200	5.2-11.8 %	-	-	-		(19)
	-	Airway/G	RB	-	-	39	31	30		(193)

Species		Fixation	Location or type	External diameter (μm)	Medial thickness	% Muscularized			Other notes	Reference
						M	PM	NM		
	-	Airway/G	-	1000 250 74 25	0.7 % 1.9 % 3.1 % 4.8 %	-	-	-		(235)
			RB AD AW			56 10 0	23 29 0	22 61 100		
	SE	Airway	RB/AD	30-100	5.0 ± 0.5 %	-	-	-		(315)
Yak	SE	Perfusion	M NM	100-300 <100	4.1 ± 0.1 %	-	-	-		(62)
Llama	-	Airway	M	28-233 35-198	4.9 % 3.8 %	-	-	-	Male Femaie	(111)
Goat	-	Airway	M	100-300	2.2-4.0 %	-	-	-		(19)
Pig	-	Immersion	M	25-70	7.4-17.6 %	-	-	-		(19)
	SE	Airway/G	M	>500 350 150 25	2.2 ± 0.3 % 2.5 ± 0.5 % 2.7± 0.2 % 7.8± 0.3 %	-	-	-		(253)
	SE	Airway	RB/AD	30-100	6.0 ± 0.4 %	-	-	-		(315)
Dog	-	Immersion Airway	M	30-120	3.9-11.7 % 1.8-3.8 %	-	-	-		(19)
	-	Airway/G	RB AD AW	-	-	44 24 2	22 22 2	33 54 96		(52)
	SE	Airway	-	601-800 401-600 201-400 101-200 51-100 25-50	7.0 ± 0.4 % 8.0 ± 0.4 % 8.0± 0.4 % 8.4 ± 0.4 % 9.1 ± 0.5 % 9.3 ± 0.4 %	-	-	-		(153)
	SE	Airway/G	-	>1000 51-100 <50	8.2 ± 1.5 % 17.3 ± 2.3 % 33.6 ± 11.0 %	36 56 15	0 29 13	0 15 72		(202)
	SE	Airway	-	>1000 100-200 51-100 <50	3.0 ± 0.8 % - - 8.5 ± 5.6 %	36 56 12 5	0 40 37 7	0 4 51 88		(204)
			RB AD AW			72 40 5	24 38 16	2 22 79		

Species		Fixation	Location or type	External diameter (μm)	Medial thickness	% Muscularized			Other notes	Reference
						M	PM	NM		
	SE	nr	-	>400 201-400 101-200 50-100 <50	27.8 ± 3.5 % 21.7 ± 1.1 % 20.7± 1.1 % 21.8± 0.9 % 33.8 ± 1.6 %	-	-	-		(246)
	SE	Airway	-	> 400 201-400 101-200 51-100 21-50	35.1 ± 3.2 μm 19.5 ± 1.5 μm 27.8 ± 11.6 μm 9.8 ± 1.4 μm 7.3 ± 0.5 μm	-	-	-	Medial thickness includes intima	(311)
	SE	Airway	RB/AD	30-100	3.6 ± 0.2 %	-	-	-		(315)
Rabbit	-	Immersion	M	40-150	3.8-10.6 %	-	-	-		(19)
	-	Airway/G	TB RB AD/AW	155-429 110-222 52-110	-	-	-	-		(227)
	SE	Airway	RB/AD	30-100	5.1 ± 0.3 %	-	-	-		(315)
Guinea pig	SE	Immersion	-	522 ± 23	56 ± 3 μm	-	-	-		(281)
	SE	Immersion	-	524 ± 49 666 ± 40 546 ± 31	53 ± 3 μm 48 ± 2 μm 47 ± 3 μm	-	-	-	1 mo 3 mo 10 mo	(280)
	SE	Airway	RB/AD	30-100	4.3 ± 0.2 %	-	-	-		(315)
Rat	-	Airway/G	TB RB AD AW	-	-	58 10 0 0	3-4 38 13 7	8 52 87 93	WKY	(2)
			TB RB AD AW			40 4 0 0	50 24 11 3	10 79 89 97	F344	
	-	Immersion	M	25-300	2.6-26.0 %	-	-	-		(19)
	SE	Immersion	-	1574 1317	25.7 ± 2.0 μm 26.6 ± 1.1 μm	-	-	-		(39)
	SE	Airway/G	-	101-200 50-100	3.2 ± 1.5 % 8.0 ± 2.2 %	-	-	-		(42)
	SE	Immersion	M NM	69 ± 4 38 ± 3	-	-	-	-		(51)
	-	Airway/G	TB RB AD	-	-	54 6 0	46 59 17	0 35 83		(115)
	SD	nr	-	100-150	11.9 ± 0.6 μm	-	-	-	Wistar	(134)

Species	Fixation	Location or type	External diameter (μm)	Medial thickness	% Muscularized			Other notes	Reference
					M	PM	NM		
-	Airway/G	BR	128-2040	-	95	5	0	CD	(141)
		TB	106-237		67	33	0		
		RB	15-208		45	48	7		
		AD	29-147		11	32	57		
		AW	22-131		0	7	93		
SE	Airway/G	BR-M	663 ±115	13.5 ± 6.9 μm	45	55	0	% Musclarized represent average of all at each airway level	(140)
		-PM	271 ± 22	2.7 ± 0.3 μm					
		TB -M	174 ± 27	3.3± 1.0 μm	20	75	5		
		-PM	166 ± 19	2.4± 0.3 μm					
		-NM	160 ± 6						
		RB -M	157	1.5 μm	8	92	0		
		-PM	113 ± 17	2.1 ± 0.4 μm					
		AD -PM	88 ± 1	1.8 ± 0.1 μm	0	50	50		
		-NM	64 ± 2						
		AW -PM	76 ± 5	1.7 ± 0.2 μm	0	19	81		
		-NM	52 ± 2	-					
SE	Airway/G	AD-PM	79 ± 5	-	-	-	-		(139)
		-NM	54 ± 3						
		AW-PM	86 ± 8						
		-NM	51 ± 3						
-	Airway	AD	-	-	0	36	64		(138)
		AW			0	15	85		
		αSM actin + cells	15-25	-		0	-	M+PM	
			26-50			15			
			51-75			16			
			76-100			6			
SE	Airway	-	401-600	5.0± 0.6 %	-	-	-		(154)
			201-400	4.6 ± 0.4 %					
			101-200	6.1± 0.5 %					
			51-100	6.8 ± 0.6 %					
			25-50	7.8 ± 0.6 %					
		TB	65 ± 12	-	-	-	-		
		RB	50 ± 10						
		AW	57 ± 9						
		M	226 ± 21	-	-	-	-		
		PM	82 ± 8						
		NM	54 ± 6						
-	Airway/G	AD	-	-	1	30	69		(167)
SE	Airway/G	AD	-	-	5	-	-		(209)
		AW			5	-	-		
		-	100-200	3.2± 0.2 %	-	-	-		
			50-100	3.3± 0.1%					

Species		Fixation	Location or type	External diameter (μm)	Medial thickness	% Muscularized			Other notes	Reference
						M	PM	NM		
	-	Airway/G	AD	-	-	0	6	94		(215)
			AW			0	0	100		
	SD	Airway/G	-	50-150	16.7 ± 5.2 %	13	20	67		(241)
				15-50	9.8 ± 1.4 %					
	SE	Immersion	-	619 ± 49	44 ± 4 μm	-	-	-		(279)
	SE	Immersion	-	557 ± 17	44 ± 1 μm	-	-	-		(278)
	SE	Airway	RB/AD	30-100	4.6 ± 0.3 %	-	-	-		(315)
Mouse	-	Immersion	M	20-300	4.4-11.7 %					(19)
	SE	Airway & Perfusion	-	>100	10.9 ± 0.7 %	96	-	-		(34)
				51-100	15.0± 0.4 %	84	-	-		
				25-50	20.1± 0.3 %	74	-	-		
				<25	23.5 ± 1.2 %	57	-	-		
		Airway/G	αSM actin + cells	10-50	-		23	-	M+PM	
	-	Airway/G	TB/RB	75 ± 9	-		20	-	M+PM	(66)
	SE	Airway	-	50-125	9.4 ± 0.6 %	-	-	-		(168)
				10-50	-	13	-	-		
	SE	Airway	TB	-	5.7 ± 0.4 %	-	-	-		(169)
			AD		-	21	-	-		
	SE	Airway	TB	63 ± 2	20.0 ± 1.7 %	-	-	-	male	(207)
			RB	45 ± 1	18.8 ± 1.7 %	-	-	-		
			AD	44 ± 1	12.7 ± 0.9 %	-	-	-		
			AW	-	-	-	-	73		
			TB	56 ± 2	21.9 ± 1.8 %	-	-	-	female	
			RB	43 ± 1	19.5 ± 1.7 %	-	-	-		
			AD	37 ± 1	10.9 ± 0.6 %	-	-	-		
			AW	-	-	-	-	68		
	SE	Airway/G	RB	-	1.1 ± 0.1 μm	-	-	-		(192)
			AD			30	-	-		
	SD	Airway	TB		5.9 ± 0.6 μm	-	-	-		(262)
				48 ± 4						
	-	Airway	-	15-50	-	27	-	-		(282)
	-	Airway	-	15-80	-	23	21	56		(322)
	-	Perfusion	AD	-	-		15	-	M+PM	(350)
					Pulmonary Veins					
Sheep	SE	Airway/G	-	25-74	-	0	2	98		(136)
				75-124	3.4 ± 2.6 %	0	5	95		
				125-249	-	4	5	91		
				>250	0.5 ± 0.2 %	20	22	58		

Species		Fixation	Location or type	External diameter (μm)	Medial thickness	% Muscularized			Other notes	Reference
						M	PM	NM		
Dog	SE	Airway/G	-	<50	15.7 ± 0 %	0	5	95		(202)
				51-100	11.5 ± 2.0 %	10	51	38		
				>1000	2.8 ± 0 %	100	0	0		
	SE	Airway	-	21-50	6.6 ± 0.3 μm	-	-	-	includes intimal thickness	(311)
				51-100	9.5 ± 0.8 μm					
				101-200	11.3 ± 0.9 μm					
				201-400	11.1 ± 1.6 μm					
				> 400	17.5 ± 5.1 μm					
Guinea pig	SE	Immersion	-	323 ± 18	47 ± 3 μm	-	-	-		(281)
	SE	Immersion	-	361 ± 12	44 ± 3 μm	-	-	-	1 mo	(280)
				487 ± 35	41 ± 3 μm				3 mo	
				414 ± 24	39 ± 4 μm				10 mo	
Rat	SE	Airway/G	NM	44 ± 2	-	-	-	-		(126)
			PM	69 ± 6	2.2 ± 0.1 μm					
			M	168 ± 16	7.7 ± 0.7 μm					
			-	20	-	0	0	100		
				25		2	3	95		
				50		18	11	72		
				100		65	11	24		
				>150		100	0	0		
	SE	Immersion	-	458 ± 35	15 ± 1 μm	-	-	-		(279)
	SE	Immersion	-	352 ± 26	17 ± 2 μm	-	-	-		(278)

Summary data are means ± either SD or SE. nr, fixation strategy not reported; EL, elastic; M, muscular; PM, partially muscular; NM, non-muscular.

Table 3

Morphometry of alveolar septal wall components

Species	SD SE	Endothelium				Interstitium	Epithelium	Notes	Reference
		Thickness (μm)	Volume (μm^3)	Surface Area (μm^2)	Cell Number	Thickness (μm)	Thickness (μm)		
Human	SE	0.48 ± 0.05	632 ± 64	1353 ± 67	30.2 ± 2.4%	-	0.36 ± 0.02 5.02 ± 0.55	Type I epithelium Type II epithelium	(44)
	SE	0.47 ± 0.05	-	-	-	1.63 ± 0.16	0.36 ± 0.01 5.02 ± 0.55	Type I epithelium Type II epithelium	(47)
	SE	0.42 ± 0.02	-	-	-	1.24 ± 0.15	0.61 ± 0.05		(84)
		-	-	-	-	1.72	-		(191)
Horse	SE	0.45 ± 0.04	-	-	-	0.65 ± 0.02	0.33 ± 0.01		(85)
Baboon	SE	-	351 ± 57	-	39.0%	-	-		(38)
		0.35	284 ± 10	971 ± 90	35.9%	0.85	0.38		(45)
	SE	0.36 ± 0.04	365 ± 61	1040 ± 209	36.3 ± 2.4%	0.85 ± 0.14	0.31 ± 0.02 1.84 ± 0.14	Type I epithelium Type II epithelium	(47)
	SE	-	303 ± 26	-	-	-	-		(74)
		-	-	-	-	0.95	-		(191)
Pig	SE	0.42 ± 0.02	-	-	-	1.00 ± 0.16	0.37 ± 0.01		(341)
Dog	SD	0.34 ± 0.06 0.33 ± 0.03	-	-	-	0.42 ± 0.23 0.53 ± 0.02	0.31 ± 0.01 0.39 ± 0.07	Hilar capillaries Peripheral capillaries	(18)
	SD	0.12 ± 0.02 0.15 ± 0.01	-	-	-	-	-	Thin side Thick side	(55)
	SE	0.31 ± 0.02	343 ± 19	1137 ± 127	45.7 ± 0.8%	0.66 ± 0.03	0.33 ± 0.04 4.14 ± 0.34	Type I epithelium Type II epithelium	(47)
	SD	0.27 ± 0.05	-	-	-	0.63 ± 0.15	-		(56)
	SE	0.20 ± 0	-	-	-	0.22 ± 0.01	0.23 ± 0.01		(310)
Rabbit	SD	0.19 ± 0.02	-	-	39%	-	0.15 ± 0.01		(93)
		-	-	-	-	-	-		(191)
Guinea pig	SE	0.47 ± 0.01	-	-	-	0.26 ± 0.04	0.40 ± 0.02		(72)
Rat	SE	0.36 ± 0.03	387 ± 30	1105 ± 72	46%	0.62	0.50 ± 0.03		(43)
	SE	-	275 ± 25	1121 ± 95	51.1 ± 1.7%	0.72 ± 0.02			(47)
	SD	0.10 ± 0.02 0.12 ± 0.02	-	-	-	-	--	Alveolar: thin side thick side	(57)
	SD	0.10 ± 0.01	-	-	-		--	Subpleural: thin side	(57)

Species	SD SE	Endothelium				Interstitium	Epithelium	Notes	Reference
		Thickness (μm)	Volume (μm^3)	Surface Area (μm^2)	Cell Number	Thickness (μm)	Thickness (μm)		
		0.15 ± 0.02						thick side	
	SE	-	336 ± 35	946 ± 103	43.0%	-	-		(100)
	SE	0.36 ± 0.03	-	-	46.0%	0.69 ± 0.06	0.50 ± 0.03		(109)
	SE	-	-	*1642 ± 186 cm^2 per LL*	*1.60 ± 0.09 ×10^8 per LL*	-	-		(122)
	-	0.30	-	-	-	0.55	0.65		(156)
	SE	-	407 ± 65	-	-	-	-		(180)
		-	-	-	-	0.62	-		(191)
	SE	0.27 ± 0.02	-	-	-	0.41 ± 0.02	0.28 ± 0.02		(245)
	SD	0.43 ± 0.04	-	-	-	0.56 ± 0.07	0.28 ± 0.07 0.12 ± 0.02	Type I epithelium Type II epithelium	(238)
	SE	-	-	*2853 ± 123 cm^2 per RL*	*2.01 ± 0.11 ×10^8 per RL*	-	-		(307)
Mouse	SE	0.19 ± 0.01	-	-	-	0.58 ± 0.04	0.17 ± 0.02		(40)
		-	-	-	-	0.33	-		(191)

Data were derived utilizing morphometric techniques. Mean data and either standard deviations (SD) or errors (SE) are shown. LL, left lung; RL, right lung.